INVESTIGATIONS ON NONLINEAR AND RADIATIVE PROPERTIES OF CERTAIN PHOTONIC MATERIALS

Thesis submitted
in partial fulfilment of the requirements
for the degree of
DOCTOR OF PHILOSOPHY

Geetha K Varier

International School of Photonics
Cochin University of Science & Technology
Cochin 682 022, INDIA
April, 1998

Light from the beacon flashes the truth-
boats are made to sail.
I learned it from my wonderful parents
To them I dedicate this.

Cochin University of Science & Technology
International School of Photonics
A centre of higher learning dedicated to the Science & Technology of Photonics
Cochin 682 022, INDIA

Dr. V P N Nampoori
Professor

April 28, 1998

CERTIFICATE

This is to certify that the work presented in the thesis entitled *Investigations on Nonlinear and Radiative Properties of Certain Photonic Materials* is based on the bonafide research work carried out by Ms. Geetha K Varier under my guidance at the International School of Photonics, Cochin University of Science & Technology, Cochin 682 022 and that no part thereof has been included in any other thesis submitted previously for the award of any degree.
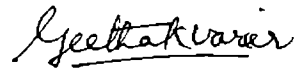
V P N Nampoori

(Supervising guide)

DECLARATION

Certified that the work presented in this thesis entitled **Investigations on Nonlinear and Radiative Properties of Certain Photonic Materials** is based on original work carried out by me under the guidance of Dr. V P N Nampoori, Professor, International School of Photonics, Cochin University of Science & Technology, Cochin-682 022 and that no part thereof has been included in any other thesis submitted previously for the award of any degree.

Geetha K Varier

Cochin-22
28th April, 1998

ACKNOWLEDGMENTS

adequately express my deep gratitude to all the people who have contributed to my overall development. Here I thank them all.

I am forever indepted to my family, my grandparents for their love and affection, and my parents who taught me to set high goals and achieve it by sheer will.

Finally to HIM who has given me so much.

<div align="right">Geetha K Varier</div>

PREFACE

Light in its physical and philosophical sense has captured the imagination of human mind right from the dawn of civilization. The invention of lasers in the 60's caused a renaissance in the field of optics. This intense, monochromatic, highly directional radiation created new frontiers in science and technology. The strong oscillating electric field of laser radiation creates a polarisation response that is nonlinear in character in the medium through which it passes and the medium acts as a new source of optical field with alternate properties. It was in this context, that the field of optoelectronics which encompasses the generation, modulation, transmission etc. of optical radiation has gained tremendous importance. Organic molecules and polymeric systems have emerged as a class of promising materials of optoelectronics because they offer the flexibility, both at the molecular and bulk levels, to optimize the nonlinearity and other suitable properties for device applications. Organic nonlinear optical media, which yield large third-order nonlinearities, have been widely studied to develop optical devices like high speed switches, optical limiters etc.

Transparent polymeric materials have found one of their most promising applications in lasers, in which they can be used as active elements with suitable laser dyes doped in it. The solid-matrix dye lasers make possible combination of the advantages of solid state lasers with the possibility of tuning the radiation over a broad spectral range. The polymeric matrices impregnated with organic dyes have not yet widely used because of the low resistance of the polymeric matrices to laser damage, their low dye photostability, and low dye stability over longer time of operation and storage.

In this thesis we investigate the nonlinear and radiative properties of certain organic materials and doped polymeric matrix and their possible role in device development.

The thesis contains eight chapters, of which Chapter I gives a general introduction to different materials whose nonlinear and radiative properties we have studied. These materials include dye doped polymers, metallo-phthalo, naphthalocyanines, fullerenes and chlorophyll.

In Chapter II the basic experimental setup and the details of the instruments used for the studies are described. Nd:YAG, Ar$^+$, and He-Ne laser systems were used as

pumping source. The observed phenomena were measured using photodiode, powermeters, monochromator, photomultiplier tubes, digital storage oscilloscope etc.. A brief account of the working of these instruments along with the different experimental techniques like the amplified spontaneous emission studies, Z scan, limiting etc. are given in this chapter.

Chapter III gives the details of the studies done on dye doped polymers. By investigating the amplified spontaneous emission characteristics of the laser dye rhodamine 6G impregnated in transparent polymer, polyacrylamide, we evaluated the single pass peak gain coefficient and the conversion efficiencies. The present studies show that by properly controlling the pump intensity and concentration of the dye molecules, polyacrylamide-rhodamine 6G system can be used as the active medium for solid state lasers. The dye degradation due to aging found in other polymeric hosts such as polymethylmethacrylate is absent due to the porous nature of polyacrylamide.

In the application of polymers as host-matrix, the resistance to laser damage is of special importance. We have used the photothermal phase shift spectroscopy (PTPS) to study the damage threshold of the matrices. The principle of PTPS is simple: A laser beam (pump beam) passing through the medium causes heating of the medium of interest. The heating modifies the refractive index of the laser irradiated region. The change in the refractive index of the medium is detected by a low power laser beam. Its basic element is a Michelson Interferometer (MI) with He-Ne laser beam as the light source (probe beam). The refractive index change of the medium introduced into one of the arms of the MI causes a change in optical pathlength of the probe beam which can be detected as fringe shift. In Chapter IV, using PTPS, the damage threshold of the polymers polymethyl methacrylate and polyacrylamide were studied.

Phthalocyanines have emerged as a novel class of materials for optical, electronic and photovoltaic applications. They are chemically stable and also offer the advantages of architectural flexibility, ease of fabrication and tailoring for synthetic engineering. There are two types of charge-transfer transitions: metal-to-ligand and ligand-to-metal. The metal ligand bonding plays an important role in displaying large molecular hyperpolarizability due to the transfer of electron density between the metal atom and the conjugated ligand systems. In Chapter IV the nonlinear properties of phthalo and napthalo cyanines with Europium as central metal atom was studied using Z-scan

technique. Z-scan is a single beam, highly sensitive technique to study the third order nonlinearity of materials. It was found that reverse saturable absorption and thermal nonlinearity contribute to the high value of nonlinearity.

Fullerene with the soccer ball structure has highly delocalised π electrons over its nearly spherical surface hence they appear as promising new nonlinear optical materials. Among organics, porphyrins are attracting considerable attention and have been shown to be excellent materials for a variety of second and third order nonlinear optical effects. The nonlinearity of fullerene and chlorophyll a, obtained from tea in organic solution were studied using Z-scan technique and the details of this is given in chapter V.

Chapter VI gives an account of the application of these organic materials for device development. The ability to control the intensity of light in a predetermined manner is one of the important manipulations for different device applications. Significant attention is being focussed on the property of optical limiting because of its application in radiation damage protection of sensitive optical detectors, including the human eye. Optical limiters using nonlinear materials are very fast since the sensing, processing, actuating functions are inherent in them. The strong reverse saturation which is observed in Europium naphthalocyanine is made use of to generate optical switching.

The luminescent solar concentrator (LSC) offers the promise of reducing the cost of photovoltaic energy conversion by the use of high gain concentrators which do not require tracking. The operation of LSC is based on light pipe trapping of luminescence induced by the absorption of solar radiation. Rhodamine 6G doped polyacrylamide, was found to be efficient as luminescent solar concentrator. Irradiation with different wavelengths of Ar^+ produces homogenous emission spectrum which is an essential characteristics of LSC. The same matrix in the wavelength range 440-465 nm acts as reverse saturable absorber, a molecular spatial light modulator has been developed using it.

Chapter VIII gives an overall summary and the conclusion of the work presented in the thesis. We have studied some of the nonlinear and radiative characteristics of certain organic materials, and tried to develop devices which are useful in photonics technology.

The list of papers published in reputed journals and conferences are given below.

[1] Electron density determination of laser induced plasma from Poly Methyl Methacrylate using phaseshift detection technique

G K Varier, S S Harilal, C V Bindhu, R C Issac, V P N Nampoori and C P G Vallabhan, Modern Phys. Letts. B, 10, 235, (1996).

[2] Investigations on laser induced plasma from superconducting $YBa_2Cu_3O_7$ and $NdBa_2Cu_3O_7$ using photothermal phase shift spectroscopy

G K Varier, R C Issac, C V Bindhu, S S Harilal, V P N Nampoori and C P G Vallabhan, Commun. Instru., 4, 15, (1996).

[3] Investigations in nanosecond laser produced plasma in air from $YBa_2Cu_3O_7$

G K Varier, R C Issac, C V Bindhu, S S Harilal, V P N Nampoori and C P G Vallabhan, Spectrochimica Acta B, 52, 657, (1997).

[4] Photoacoustic and optical limiting studies in C_{60}

R C Issac, S S Harilal, G K Varier, C V Bindhu, V P N Nampoori and C P G Vallabhan, Opt. Engg., 36, 332, (1997).

[5] A study of photoacoustic effect and optical limiting in the solution of C_{60} in toluene

R C Issac, C V Bindhu, S S Harilal, G K Varier, V P N Nampoori and C P G Vallabhan, Mod. Phys. Lett. B, 10, 61, (1996).

[6] Anomalous profile of a self reversed resonance line from Ba^+ in a laser produced plasma from $YBa_2Cu_3O_7$

R C Issac, S S Harilal, C V Bindhu, G K Varier, V P N Nampoori and C P G Vallabhan, Spectrochemica Acta B, 52, 1791, (1997).

[7] Dynamics of laser produced silver plasma under film deposition conditions studies using optical emission spectroscopy

R C Issac, K V Pillai, S S Harilal, **G K Varier**, C V Bindhu, Pramod Gopinath, P Radhakrishnan, V P N Nampoori and C P G Vallabhan, Appl. Sur. Sci., (1998).

[8] Pulsed photoacoustic study of toluene

S S Harilal, R C Issac, **G K Varier**, C V Bindhu, V P N Nampoori and C P G Vallabhan, J. Pure Appl. Ultrason., **17**, 72, (1995).

[9] Observation of multiphoton process in liquid CS_2 using pulse photoacoustic technique

S S Harilal, R C Issac, C V Bindhu, **G K Varier**, V P N Nampoori and C P G Vallabhan, Mod. Phys. Letts. B, **9**, 871 (1995).

[10] Measurement of absolute fluorescence quantum yield of rhodamine B solution using dual beam thermal lens technique

C V Bindhu, S S Harilal, R C Issac, **G K Varier**, V P N Nampoori and C P G Vallabhan , J. Phys. D - Appl. Phys., **29**, 1074, (1996).

[11] Thermal lens study of rhodamine B in methanol:Signature of resonance two photon absorption

C V Bindhu, S S Harilal, R C Issac, **G K Varier**, V P N Nampoori and C P G Vallabhan, Mod. Phys. Letts., **9**, 1471, (1995).

[12] Thermooptic effect using phase shift detection

G K Varier, C V Bindhu, S S Harilal, R C Issac, V P N Nampoori and C P G Vallabhan, Proc. Sym. on Mol. Spect. & Laser (BHU Varanasi), 84, (1994).

[13] An interferometric setup for electron density measurements in laser induced plasma

G K Varier, R C Issac, S S Harilal, C V Bindhu, V P N Nampoori and C P G Vallabhan, Internat. Con. on Instrumentation, ICI-1996, (IISc, Bangalore), O17, (1996).

[14] Study of laser induced plasma from super conducting $YBa_2Cu_3O_7$ and $NdBa_2Cu_3O_7$ using photothermal phase shift spectroscopy.

G K Varier, R C Issac, V P N Nampoori, Eight Kerala Sci. Congress, (CUSAT, Kochin), 331, (1996).

[15] Electron density determination of laser induced plasma from PMMA using phase-shift spectroscopy

G K Varier, S S Harilal, C V Bindhu, R C Issac, V P N Nampoori and C P G Vallabhan, Proc. of National Laser Sym., (BARC Bombay), G10 (1996).

[16] Evaluation of nonlinear refractive index of ZnSe using CW laser

G K Varier, R C Issac, Pramod Gopinath, V P N Nampoori and C P G Vallabhan, Proc. of National Laser Sym., (CAT, Indore) 215, (1997).

[17] Studies on amplified emission from polyacrylamide embedded with rhodamine 6G

G K Varier, R C Issac, Pramod Gopinath, V P N Nampoori and C P G Vallabhan, Proc. of National Laser Sym., (PRL, Ahmedabad), 37, (1997).

[18] The observation of optical limiting by C_{70} in toluene

R C Issac, C V Bindhu, S S Harilal, **G K Varier**, V P N Nampoori and C P G Vallabhan, Proc. of National Sym. on Antn. and Progn., (CUSAT Cochin), 228 (1994).

[19] Photoacoustic measurements in C_{60} & C_{70}

R C Issac, **G K Varier**, C V Bindhu, S S Harilal, V P N Nampoori and C P G Vallabhan, Proc. of National Laser Sym., (IRDE Dehradun), 245, (1995).

[20] Nonlinear refractivity in C_{70}-benzene solution using Z-scan technique

R C Issac, S S Harilal, C V Bindhu, **G K Varier**, V P N Nampoori and C P G Vallabhan, Proc. International Conf. on Spectroscopy : Perspectives & Frontiers (INCONS), (BARC Bombay), 140, (1996).

[21] Prompt electron emission and impact ionization of ambient gas molecules during laser metal interaction

R C Issac, Pramod Gopinath, S S Harilal, **G K Varier**, C V Bindhu, V P N Nampoori and C P G Vallabhan, XII National Symposium on Plasma Science & Technology, (IPR Ahmedabad), RSO-03, (1997).

[22] Spatio-temporal evolution of laser ablated SiC plasma

Pramod Gopinath, R C Issac, S S Harilal, **G K Varier**, C V Bindhu, V P N Nampoori, and C P G Vallabhan, XII National Symposium on Plasma Science & Technology, (IPR, Ahmedabad), PPI-07, (1997).

[23] Emission and electrical characteristics of a neon hollow cathode under resonant laser excitation

P R Sasi Kumar, **G K Varier**, V P N Nampoori, C P G Vallabhan, Proc. of National Laser Sym., (C A T , Indore) 147, (1994).

[24] Some features of ASE from rhodamine B laser dye pumped by 532 nm excitation

C V Bindhu, S S Harilal, R C Issac, **G K Varier**, V P N Nampoori and C P G Vallabhan, Proc. of National Laser Sym., (IRDE Dehradun), 247, (1995).

[25] Spectral features of laser induced fluorescence emission from C_{70}

S S Harilal, R C Issac, **G K Varier**, C V Bindhu,V P N Nampoori C P G Vallabhan and M. P. Joshi, Proc. of National Laser Sym., (IRDE Dehradun), 235, (1995).

[26] Laser ablation in liquids using pulsed photoacoustic technique

S S Harilal, R C Issac, C V Bindhu, **G K Varier**, V P N Nampoori and C P G Vallabhan, Proc. of Trombay sym. on Rad. and Photochem., (BARC, Bombay), 191, (1996).

[27] Self-reversal and anomalous line profile of the 4554 Å Ba^+ resonance line in the laser produced plasma of $YBa_2Cu_3O_7$ in air

S S Harilal, R C Issac, C V Bindhu, **G K Varier**, V P N Nampoori and C P G Vallabhan, Proc. of National Laser Sym., (BARC Bombay), 283, (1997).

[28] Studies on amplified emission from polyacrylamide embedded with rhodamine 6G

G K Varier, R C Issac, Pramod Gopinath, V P N Nampoori and C P G Vallabhan, J. Appl. Phys. **(Paper communicated)**

[29] Optical nonlinearity of green tea investigated using optical limiting and photoacoustic techniques

G K Varier, R C Issac, V P N Nampoori and C P G Vallabhan, Appl. Phys. B. **(Paper communicated)**

[30] Z-scan and photoacoustic study of optical nonlinearity of naturally occuring chlorophyll

G K Varier, R C Issac, V P N Nampoori and C P G Vallabhan, J. Opt. Soc. Am. B. **(Paper communicated)**

[31] Optical nonlinearity of Europium phthalocyanine and Europium napthalocyanine studied using Z-scan technique

G K Varier, R C Issac, Jayan Thomas, V P N Nampoori and C P G Vallabhan, J. Por. & Phthal. **(Paper communicated)**

[32] Optical switching observed in Europium napthalocyanine with continous wave excitation

G K Varier, R C Issac, Jayan Thomas, V P N Nampoori and C P G Vallabhan, Opt. Engg. **(Paper communicated)**

CONTENTS

Chapter V
NONLINEAR OPTICAL PROPERTIES OF EUROPIUM PHTHALOCYANINE AND EUROPIUM NAPHTHALOCYANINE

Chapter VI
STUDIES ON OPTICAL NONLINEARITIES OF CHLOROPHYLL AND FULLERENES

Chapter VII
APPLICATIONS OF PHOTONIC MATERIALS

Chapter VIII
GENERAL CONCLUSIONS

CHAPTER I
INTRODUCTION

Abstract

This introductory chapter gives an overview of the ideas and concepts necessary for the study of nonlinear and radiative properties of materials. It also gives the details of the experimental techniques used along with the theoretical background required for the present study. A description of the materials used and their applicability in the field of photonics are given towards the end of the chapter.

1

1.1 Photonics: Technology of the era

For most part of this century, electrons played the lead role in optical-control, computing and communications, while the photon was relegated to play a supporting role, in device applications like indicators, sensors and fiber-data connections. This is because electrons are relatively easy to manipulate whereas light, on the other hand, is fairly tricky to handle, requiring a much deeper understanding before realizing its full potential. Now applied quantum theory and advanced material science have made it possible to handle light with almost the same ease and efficiency as electrons. Solid state lasers, integrated optics and optical amplifiers are beginning to find applications which were deemed unfeasible a decade ago, blurred the line between electrical and optical system design. Thus the term photonics, which was coined in analogy with electronics, has become increasingly popular in recent times[1-6].

Photonics is emerging as a new multidisciplinary frontier of science and technology that is capturing the imagination of scientists and engineers worldwide because of the potential applications to many areas of present and future information and image processing technologies. Photonics owes its origin to three main events that occurred in the latter half of this century. They are the invention of lasers, low loss optical fibers and of semiconductor devices. Diverse fields like non-linear optics, optical fibers and optical communication, integrated optics, optical switches and display devices come under it. Nonlinear optics plays a major role in photonic device construction and hence much research has been going on in understanding its fundamental and advanced realms[7-12]. Devices such as light modulators, optical switches, optical logic gates, optical limiters, frequency mixers etc. are based on the nonlinear effects of the respective medium[13-21].

Optical processing of information i.e. optical computing is one of the most appealing applications of photonics. Photons have very large band width 10^{14}-10^{15} Hz as against 10^{11}-10^{12} Hz for electrons, which reduces interference or cross-talk between adjacent channels[15]. However the speed of these systems are severely limited by the response times of input and output transducers. To fully utilize the all optical processing and computing systems, real-time reusable two-dimensional input transducers or spatial light modulators are useful. Molecular spatial light modulators can be constructed

2

using nonlinear materials. Another of its application is in optical switching, with switching time of the order of femtoseconds, which may provide computing speed that is many orders of magnitude higher than that of electronic processes. This recent expansion of nonlinear application has stimulated an extensive search for materials which satisfy a variety of new physical criteria. There are other potentially interesting applications for nonlinear materials. Among these, optical limiters which protect eye and optoelectronic devices from unwanted or stray sources of laser radiation are very important.

The doped and undoped polymers and other organic materials are increasingly being recognized as suitable photonic materials for the future because their molecular nature combined with the versatility of synthetic chemistry can be used to alter and optimize molecular structure to maximise nonlinear responses and other properties. Organic materials, especially polymers, have high mechanical strength as well as excellent environmental and thermal stability, hence doped with organic dyes they are useful as passive Q-switches, molecular spatial light modulators, active elements in dye lasers, phase conjugators, luminescent solar concentrators etc.[22-36]. The organic molecular materials exhibit the largest optical nonlinearities because of their delocalised π electrons. Phthalocyanines, napthalocyanines, fullerenes and porphyrins are some of them which has been studied and reported here as part of the thesis.

The objective of the present work is a detailed investigation of radiative and nonlinear properties of certain photonic materials. The feasibility of these materials in technological applications like spatial light modulators, optical switching, optical limiters and luminescent solar concentrators are examined. For the thesis to be self contained a brief description of the radiative and nonlinear properties are given in the ensuing sections.

1.2 Radiative processes

When a dye molecule is pumped with an intense light source (flash lamp or laser), it is excited typically to some higher level, from which it relaxes within picoseconds to the upper radiation level. From here it comes down to the ground state by emitting the excess energy as radiation. But there are many nonradiative processes that compete with the light emission and thus reduce the usability of radiative process. The radiative

3

and nonradiative properties are related to the molecular structure of the dyes. In the following sections the characteristic properties of laser dyes, radiative processes fluorescence and amplified spontaneous emission are discussed.

1.2.1 Laser dyes: An overview

Organic dyes, according to accepted notions, include organic compounds which have a strong absorption band from far ultraviolet to near infrared. A peculiarity of the absorption spectra of organic dyes as opposed to atomic and ionic spectra is the width of the absorption bands which usually covers tens of nanometers. Recalling that a typical dye molecule may contain 50 or more atoms giving rise to about 150 normal modes of vibration of the molecular skeleton, this is immediately comprehensible. These vibrations together with their overtones densely cover the spectrum between a few wave numbers to about $3000\,cm^{-1}$. In the general case of a large dye molecule, many normal vibrations of differing frequencies are coupled to the electronic transition. The individual lines of such vibrational series will be broadened by collisional and electrostatic perturbations caused by the surrounding solvent molecules. As a further complication, every vibronic sublevel of electronic states, including the ground state has a ladder of rotationally excited sublevels superimposed on it. These are extremely broadened because of the frequent collisions with solvent molecules which hinder the rotational movement. The population of these levels in contact with the thermalised solvent molecules is determined by a Boltzmann distribution. After an electronic transition leading to a nonequilibrium Franck-Condon state, the approach to thermal equilibrium is very fast in solutions at room temperature. The reason is that a large molecule experiences at least 10^{12} collisions per second with solvent molecules so that equilibrium is reached in a time of the order of picoseconds.

One of the important application of organic dyes is as active elements in dye lasers. Of the thousands of dyes only a few have high conversion efficiencies, low lasing thresholds and high thermal and photochemical stabilities needed for laser dyes. The pioneering studies on laser dyes by Schafer, Drexhage, Pavlopoulos, Rulliere and many others illustrate the extent to which the modification of the molecular structure of the laser dye can produce predictable improvements in the lasing performance[37-40]. However the incorporation of all the desired properties such as: (1) high solubility, (2) near

4

unity fluorescence quantum yield, (3) low singlet-triplet intersystem crossing rate, (4) short triplet state lifetime, (5) stimulated emission cross-section greater than induced absorption cross-section and (6) minimal self absorption of laser emission, presents a great challenge in molecular structure design and synthesis.

Most dye lasers today operate with dyes that belong to the class of xanthene. Their emission is in the wavelength region of 500-700 nm and are generally very efficient. Dyes like rhodamine 6G, rhodamine B and fluorescein come under the class of xanthene dyes. The structure of rhodamine 6G which is studied here in polymer hosts is shown in Fig.1.1.
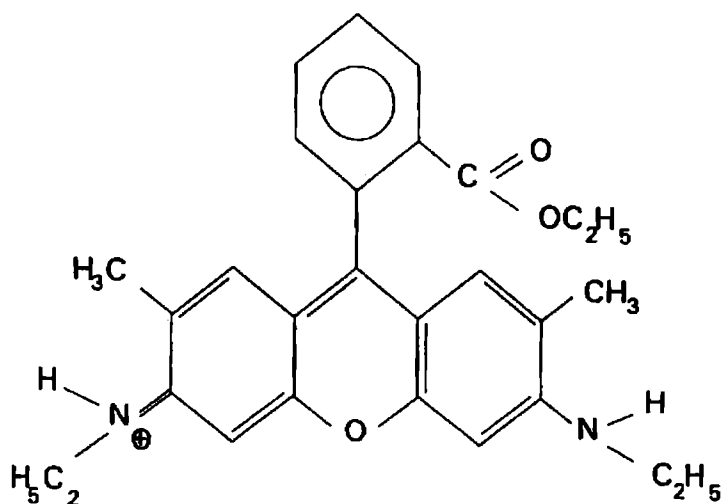
Fig.1.1 The structure of rhodamine 6G laser dye

The xanthene dyes are soluble in water, but they tend to form aggregates in water. The absorption maximum of the rhodamines vary in different solvents[41]. The fluorescence spectra of xanthene dyes closely resemble the mirror image of the long-wavelength absorption band. Several factors such as temperature and viscosity of the solvents affect the fluorescence efficiency.

1.2.2 Theoretical model for absorption of light

The light absorption of dyes can be understood on a semi quantitative basis using

a highly simplified quantum-mechanical model such as the free electron gas model[42]. This model takes into account the planarity of the dye molecules with all atoms of the conjugated chain lying in a common plane and linked by σ bonds. The π electrons will form a charge cloud above and below this plane along the conjugated chain. The centers of the upper and lower lobes of the π electron cloud are about one half bond length away from the molecular plane. Hence the electrostatic potential for any single π electron moving in the field of the rest of the molecule may be considered constant, provided all bond lengths and atoms are the same. The energy E_n of the nth eigen state of this electron is given by

$$E_n = \frac{h^2\,n^2}{8mL^2} \tag{1}$$

where h is the Planck's constant, m is the mass of the electron, n is the quantum number giving the number of antinodes of the eigen function along the chain and L is the length of the conjugated chain. Thus if there are N electrons, the lower $1/2$ N states will be filled with two electrons each according to Pauli's exclusion principle while all higher states are empty. The longest wavelength absorption band then corresponds to a transition from the higher occupied to the lowest empty state with

$$\Delta E_{min} = \frac{h^2}{8mL^2}(N+1) = \frac{hC_0}{\lambda_{max}} \tag{2}$$

where $\lambda_{max} = \frac{8mC_0\,L^2}{h(N+1)}$. This indicates that to a first approximation the position of the absorption band is determined only by the chain length and by the number of π electrons N. This simple formula predicts the absorption wavelength of many symmetrical cyanine dyes satisfactorily[43]. A perturbation treatment applied to the above theory makes it useful for analysing molecules with non identical atoms and variable bond lengths along the conjugated chain as well. The oscillator strength of the absorption bands can also be calculated using the free electron model.

1.2.3 Jablonski diagram

The absorption and emission of light can be illustrated using an energy level diagram[44] as shown in Fig.1.2. The ground, first and the second electronic states are depicted by S_0 , S_1 , S_2 respectively. Vibrational sub-levels of each electronic level is depicted as

0,1,2, etc. The transition between various electronic levels occurs in about 10^{-15} sec, a time too short for significant displacement of nuclei, i.e., Frank-Condon principle is valid.
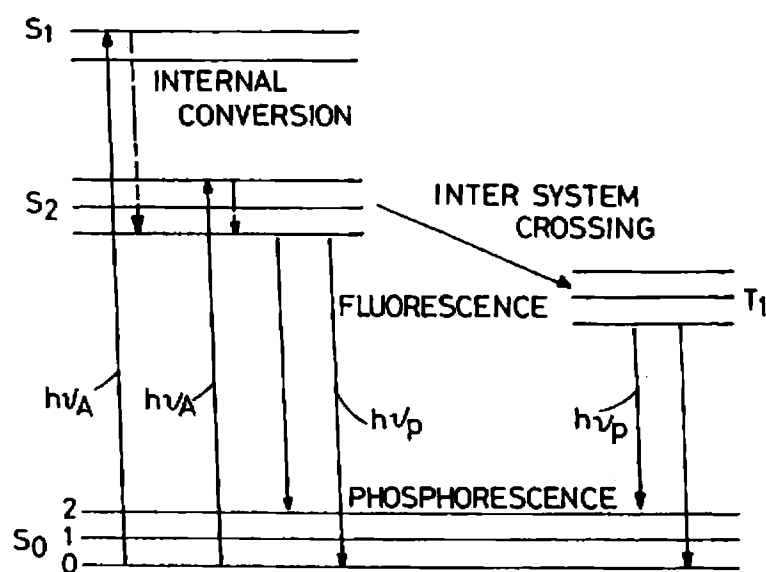
Fig.1.2 Jablonski diagram

Light absorption is followed by several processes such as (a) Vibrational relaxation, (b) Internal conversion, (c) Intersystem crossing and Phosphorescence and (d) Fluorescence which are also depicted in the Fig. 1.2.

(a) Vibrational relaxation: The molecules are usually excited to some higher vibrational levels of S_1 or S_2. In most cases the molecules rapidly relax to the lowest vibrational level of S_1 without changing the electronic energy and generally this occurs in 10^{-12} sec. Since fluorescence life times are typically of the order of 10^{-8} sec, internal conversion is generally complete prior to emission. The mechanism of this process is a collision-like interaction in liquid phase and occurs as a result of excited molecules attaining thermal equilibrium with the environment.

(b) Internal conversion: A nonradiative transition between states of the same multiplicity is described as the internal conversion. The nonradiative decay of the lowest excited singlet state S_1 directly to the ground state S_0 is mostly responsible for the loss

of fluorescence efficiency in laser dyes. Depending on the molecular structure of the dye and the properties of the solvent, the rate of relaxation can vary by many orders of magnitude. It has been known that a rigid, planar molecular structure favours high fluorescence efficiency[45,46].

(c) Intersystem crossing and phosphorescence: A nonradiative transition between states of different multiplicity is described as intersystem crossing. This process is generally forbidden. This occurs through spin-orbit coupling in which states with different spin angular momenta and orbital angular momenta mix slightly because they have the same total angular momentum. The intersystem crossing rate, intrinsic to the chromophore can be greatly enhanced if the dye is substituted with heavy elements which increase the spin-orbit coupling[47,48]. The dye molecule in the lowest triplet state may relax down to the ground state through a radiative process known as phosphorescence. Since the emission is from a metastable state, phosphorescence life times are very large compared to fluorescence.

(d) Fluorescence: The emission of optical radiation which results in a transition of the molecule from an excited state, usually the first excited singlet S_1 to the singlet ground state S_0 is called fluorescence. This occurs typically with a lifetime of 10^{-9} to 10^{-8} sec.

For an ideal laser dye both internal conversion and intersystem crossing should be negligible so that the quantum yield of fluorescence has the highest possible value of 100%. Also an efficient laser dye in its first excited singlet state should have a negligible absorption at the pump wavelength. Otherwise losses would occur, as in triplet-triplet absorption, because the decay to the first excited singlet or triplet states from higher levels is nonradiative. The laser dye should have an absorption spectrum such that it fully matches with the spectral distribution of the pump source. In order to achieve a broad tuning range dyes should have a wide fluorescence band. Since fluorescence is of utmost importance in lasing action a description of its unique characteristics is appropriate at this juncture.

1.2.4 Fluorescence characteristics

When molecules in the ground state are pumped by an optical source they are excited to the singlet manifold, from where they relax within picoseconds to the lowest vi-

bronic level of the first excited singlet state S_1 . Fluorescence emission is a quantum mechanically allowed transition since there is no change in spin orientation during the transition and has an emissive rate of 10^8 sec^{-1}. These high emissive rates result in a fluorescence life time of the order of 10 ns. In the following sections a brief discussion of the important aspects of fluorescence is given[49,50].

1.2.4.1 Stokes shift

The emission spectrum shows a shift to the higher wavelength (i.e., a loss of energy) of the emission compared to that of absorption. This is called Stoke's shift[44]. One common cause of Stoke's shift is the rapid decay to the lowest vibrational levels of S_1. Furthermore, the molecules generally decay to the excited vibrational levels of S_0, resulting in further loss of vibrational energy. Further stokes shift can arise due to solvent effects and excited state reactions.

1.2.4.2 Mirror image rule
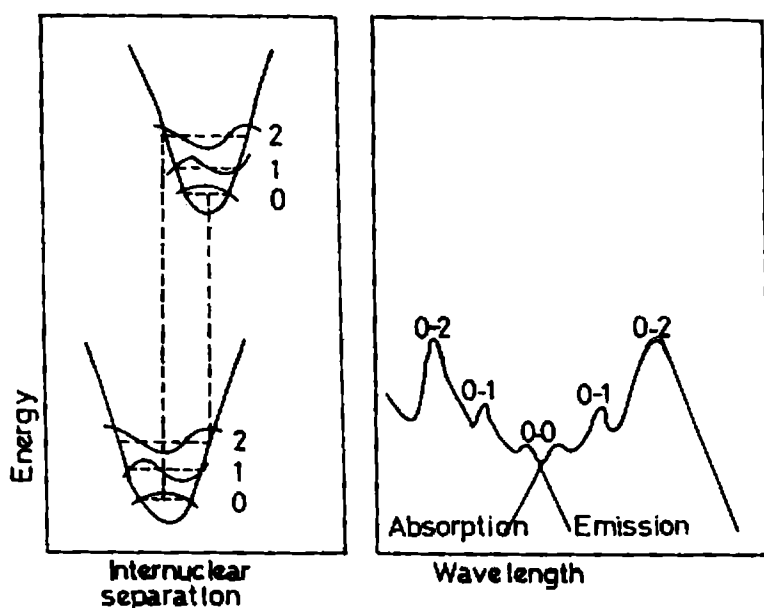
Fig.1.3 Mirror image rule and Franck-Condon factors.

The fluorescence spectrum appears to be a mirror image of the absorption spectrum. The symmetric nature of these spectra is a result of the same transitions being involved

9

in both absorption and emission and the similarities among the vibrational levels of S_0 and S_1. According to Franck-Condon, principle since the time required for an electronic transition is negligible compared with nuclear motion, the most probable transition is one which involves no change in the nuclear co-ordinates. This is referred to as Franck-Condon maxima and represents a vertical transition on the potential energy diagram as shown in Fig.1.3.

1.2.4.3 Invariance of the emission spectrum with excitation wavelength

The same fluorescence spectrum is generally observed irrespective of the excitation wavelength. Upon excitation into higher vibrational and electronic levels the excess energy is quickly dissipated in less than 10^{-12} sec leaving the molecule in the lowest vibrational level of upper electronic level. Because of this rapid relaxation, emission spectra are usually independent of the excitation wavelength.

1.2.4.4 Fluorescence lifetimes and Quantum yields

Using a modified Jablonski diagram shown in Fig.1.4 the basic parameters such as fluorescence quantum yield and fluorescence life time can be illustrated. From the upper electronic level the molecules relax to the ground state either radiatively or nonradiatively. Let the emissive rate of fluorescent molecule be Γ and rate of all possible radiationless decay k. The fluorescence quantum yield is the ratio of the number of photons emitted to the number of photons absorbed. The depopulation from the excited state can occur either radiatively or nonradiatively. The fraction of molecules that decay through emission and hence the quantum yield is given by

$$Q = \frac{\Gamma}{\Gamma + k} \tag{3}$$

The quantum yield can be close to unity if the rate of nonradiative deactivation is much smaller than the rate of radiative decay. But fluorescence yield is always less than unity because of Stoke's losses. The lifetime of the excited state is defined as the average time that the molecule spends in the excited state prior to return to the ground state. Generally the fluorescence lifetimes are near 10 ns for a typical laser dye and is defined as

$$\tau = \frac{1}{\Gamma + k} \qquad (4)$$

The fluorescence is a random process, and a few molecules emit the photons at t = τ. The lifetime of the molecule in the absence of nonradiative processes is called the intrinsic lifetime and is given by,

$$\tau_0 = 1/\Gamma \qquad (5)$$

This gives the relation between quantum yield and lifetime as

$$Q = \tau/\tau_0 \qquad (6)$$
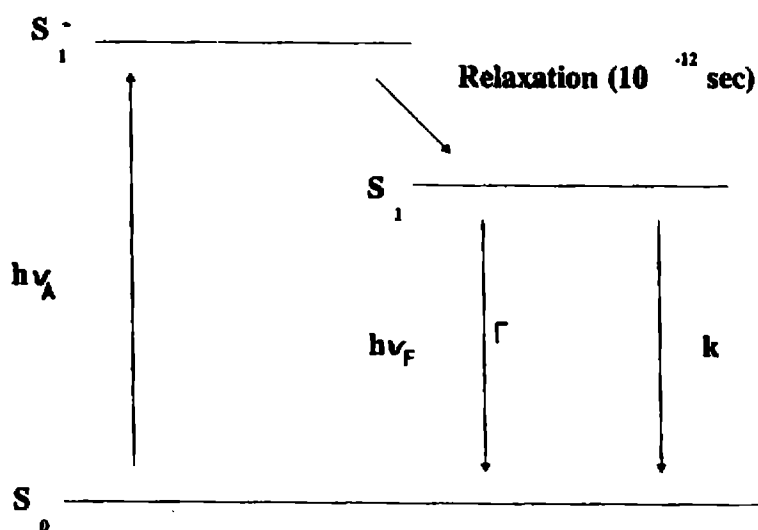
Fig.1.4 Modified Jablonski diagram

1.2.4.5 Fluorescence anisotropy

The fluorophores preferentially absorb photons whose electric vectors are aligned parallel to the transition moment of the molecule. The transition moment has a defined orientation in the fluorophore. In an isotropic solution fluorophores are molecules oriented randomly. Upon excitation with polarised light one selectively excites those fluorophore molecules whose absorption transition dipole is parallel to the electric vector

of the excitation. This selective excitation of a partially oriented population of fluorophores results in partially polarised fluorescence emission. The transition moments for absorption and emission have fixed orientations within each fluorophore and the relative angles between these moments determines the maximum measured anisotropy.

The fluorescence anisotropy r and polarisation P are defined by

$$r = \frac{I_{\parallel} - I_{\perp}}{I_{\parallel} + 2I_{\perp}} \tag{7}$$

and

$$P = \frac{I_{\parallel} - I_{\perp}}{I_{\parallel} + I_{\perp}} \tag{8}$$

respectively, where $I_{\parallel}$ and $I_{\perp}$ are the fluorescence intensities of the parallel ($\parallel$) and perpendicularly ($\perp$) polarised emission. The measurements on polarisation or anisotropy reveal the average angular displacement of the fluorophore which occurs between absorption and subsequent emission of a photon. This angular displacement is dependent upon the rate and extent of rotational diffusion during the lifetime of excited state. These diffusive motion in turn depends on the viscosity of the medium.

1.2.5 Factors affecting radiative properties of dye molecules

Depending on the molecular structure of the dye molecules the rate of nonradiative processes can vary by many orders of magnitude. There are many instances when the surroundings of the dye molecules affect the rate of nonradiative processes to a degree that cannot be neglected. For instance, if a part of the dye molecule is strongly electron donating or electron withdrawing, a reversible charge transfer may occur between this group and the excited chromophore resulting in the loss of electronic excitation[51]. Likewise, a substituent with a low-lying singlet or triplet state may quench the fluorescence via energy transfer[48]. Furthermore, heavy-atom solvents are not well suited for lasing solutions owing to the increased triplet build-up[46-48].

The tendency to form dimers and higher aggregates is a major problem in dye solutions. The dimers usually have a strong absorption band at shorter wavelengths than the monomer and often an additional weaker band at the long-wavelength side of the monomer band[52-55]. Dimers are generally weakly fluorescent or not at all.

The equilibrium between monomers and dimers shifts to the side of the latter with increasing concentration and decreasing temperature. A number of factors have been suggested as responsible for the aggregation of organic dyes. It has been assumed that an attractive dispersion force between the highly polarizable dye chromophores plays an important role while the high dielectric constant of water reduces the coulombic repulsion between the identically charged molecules [56]. It has also been suggested that hydrogen bonding between the dye molecules and an interaction with the accompanying anions may be responsible for the dimerization in certain cases. While aggregation in water is a common phenomenon with most organic dyes, it is usually much less in organic solvents even at very high concentrations[57,58].

1.2.6 Laser action of fluorescent dye solutions

From the spectroscopic properties of dyes it can be concluded that for constructing a laser either phosphorescence or fluorescence emission from the dye can be utilized. Eventhough the long lifetime of the triplet state makes phosphorescence more attractive a high concentration of the active species is required to obtain an amplification factor large enough to overcome the inevitable cavity losses. Since the transition is strongly forbidden the triplet-triplet absorption bands are broad and diffuse and overlap the phosphorescence band there by increasing the losses.

If the fluorescence band of a dye solution is utilized for the operation of a dye laser, the allowed transition from the lowest vibronic level of the first excited state will give a high amplification factor even at low dye concentrations. The main complication in these systems is the existence of the lower lying triplet states. The intersystem crossing rate to the lowest triplet state is high enough in most molecules to reduce the quantum yield of fluorescence to values substantially below unity. Because of this intersystem crossing the excited singlet level population decreases and the lower triplet level population increases, enhancing triplet-triplet absorption. This intersystem crossing can be reduced by using giant pulse laser as pump source which have a pulse width of few nanoseconds[59].

1.2.7 Amplified spontaneous emission

An amplifier can amplify not only the input field from a laser oscillator or another

amplifier but also the spontaneous radiation emitted by the excited molecules of the amplifier itself. It can be seen that spontaneously emitted photons at one end of an amplifier which is directed along the amplifier axis or close to that direction, can stimulate the emission of more photons and lead to substantial output radiation at the other end of the amplifier. This radiation is called Amplified Spontaneous Emission (ASE)[60-67].

It is clear that many of the properties of ASE has resemblance to laser radiation. In particular, it is narrow-band in frequency and also highly directional. For these reasons, high-gain systems emitting ASE are referred to as mirrorless lasers. For a quantitative description of ASE, the effect of spontaneous emission also must be added to the steady state equation for the propagation of intensity in an amplifying medium,

$$\frac{dI}{dz} = gI + A_{21}N_2 h\nu(\Omega/4\pi) \qquad (9)$$

where g is the gain coefficient. The second term is the contribution to dI/dz from spontaneous emission of photons of energy $h\nu$ by N_2 excited molecules per unit volume with spontaneous emission rate A_{21} . Since spontaneous emission is isotropic, a factor of $\Omega/4\pi$, where Ω is an appropriate solid angle which accounts for the fact that only a fraction $\Omega/4\pi$ of spontaneously emitted photons are emitted in directions for which amplification can occur. In the simplest approximation Ω is taken to be A/L^2, where A is the cross-sectional area of the amplifier and L is the length.

In the small-signal regime in which g and N_2 are independent of I, the solution of the above equation becomes

$$I(z) \simeq \frac{h\nu A_{21}}{4\pi} \frac{\Omega N_2}{g} e^{gz} \qquad (10)$$

for $\exp(gz) >> 1$. If it is assumed that the lower-level population of the amplifying transition is negligible, so that $g = \sigma N_2$, where σ is the stimulated emission cross-section. For a homogeneously broadened transition having a Lorentzian lineshape of full width at half-maximum $\Delta\nu$, the stimulated emission crosssection is given by

$$\sigma = \frac{\lambda^2 A_{21}}{4\pi^2 c\Delta\lambda} \qquad (11)$$

14

where $\Delta\lambda = (c/\nu^2)\Delta\nu$ is the width in the emission wavelength $\lambda = c/\nu$. In this case the eq. 10 becomes

$$I(z) = \frac{\pi\ hc^2\Omega}{\lambda^2}\Delta\lambda e^{gz} \tag{12}$$

for the growth of intensity with propagation in the amplifier.

ASE radiation can have spatial coherence comparable to true laser radiation. The bandwidth of ASE is typically a few times smaller than the gain linewidth $\Delta\nu$. An understanding of the gain of the active medium can be obtained by studying the amplified spontaneous emission.

1.3 Nonlinear processes

1.3.1 Introduction

Nonlinear optics is a field that involves the study of modification of a suitable optical system by the presence of intense electromagnetic radiation. At low intensities of light that normally occur in nature, the optical properties of materials are quite independent of the intensity of illumination. However if the illumination is made sufficiently intense, the optical properties begin to depend on the intensity and other characteristics of the light. The light waves may then interact with each other as well as with the medium. This is the realm of nonlinear optics. For observing this type of phenomenon, high intensities obtained by lasers are necessary. Such behaviour provides an insight into the structure and properties of matter. This effect can be utilized in optical devices and techniques which have important applications in many branches of science and engineering.

1.3.2 Theoretical description of optical nonlinearities

When an electric field is applied to a material, the positive charges tend to move in the direction of the field while the negative charges in the opposite direction. In conductors, the charged particles can move as long as the electric field is applied. In a dielectric medium the charges are displaced slightly from their usual positions. This small movement results in a collection of induced electric dipolemoments. In other words the electric field on a dielectric medium induces polarisation.

15

Since the positively charged ion cores have much higher mass than negatively charged electrons, it is the motion of electrons that is more significant in an electric field. The response of an electron to the electromagnetic field is that of a particle in an anharmonic potential well. This model was used by Bloembergen, Garret and Robinson to estimate the second and third order nonlinear susceptibilities of dielectric materials[68,69].

Suppose that the electron has a mass m and charge -e and is attached to the ion core, then motion of the electron in a time dependent electric field E(t) is governed by the equation of motion for an oscillator,

$$m\left[\frac{d^2x}{dt^2} + 2\Gamma\frac{dx}{dt} + \Omega^2 x - (\xi^{(2)}x^2 + \xi^{(3)}x^3 + ...)\right] = -eE(t) \tag{13}$$

where x is the displacement from the mean position, Ω is the resonance frequency, and Γ is a damping constant. The term on the right hand side represents the force exerted on the electron by the applied field, $E(t) = \frac{1}{2}E_0\left[\exp(-i\omega t) + \exp(i\omega t)\right]$, where ω is the optical frequency which drives the oscillations.

The solution of the equation if the anharmonic terms are not taken into consideration is

$$x = \frac{-eE_0}{2m}\frac{\exp(-i\omega t)}{\Omega^2 - 2i\Gamma\omega - \omega^2} + c.c \tag{14}$$

where c.c is the complex conjugate.

If there are N electric dipoles per unit volume, the polarisation induced in the medium is P = -Nex. The linear dependence of the polarisation P on the field E in terms of the susceptibility χ as

$$P = \frac{1}{2}\epsilon_0\chi E_0\exp(-i\omega t) + c.c \tag{15}$$

where

$$\chi = \frac{Ne^2}{\epsilon_0 m}\frac{1}{\Omega^2 - 2i\Gamma\omega - \omega^2}$$

and ϵ_0 is the free space permittivity.

The electric dipoles (and hence the polarisation) therefore oscillate at the same frequency as the incident optical field. They radiate into the medium and modify the

wave propagation. Since the electric displacement $D = \epsilon_0 E + P$, the dielectric constant is $1+\chi$ and the refractive index is $(1+\chi)^{1/2}$. Losses in the medium is denoted by the imaginary part of χ.

When the anharmonic terms are included, there is nonexact solution for the equation of motion, viz. eq.13. However if the anharmonic terms are small compared with the harmonic one, the equation can be solved by expressing x as a power series in E. Equivalently, the polarisation P can be written in the form,

$$P = \epsilon_0(\chi^{(1)}E + \chi^{(2)}E^2 + \chi^{(3)}E^3 + ...)$$ (16)

where $\chi^{(1)}$ denotes the linear susceptibility and $\chi^{(2)}$, $\chi^{(3)}$, ... are called the nonlinear susceptibilities of the medium.
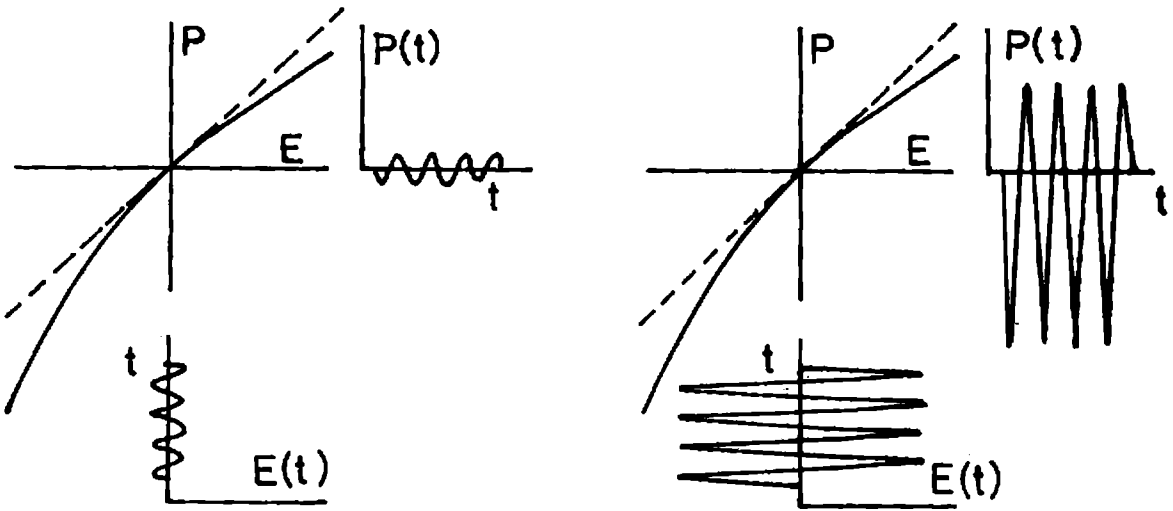

Fig.1.5 The effect of a nonlinear dependence of the polarisation P on the electric field E is shown. For small input fields (a), P does not depart significantly from the linear dependence (dashed lines). At larger fields (b), the polarisation has a distorted waveform which contains significant components at harmonic frequencies

17

The quadratic polarisation, $P^{(2)} = \epsilon_0\chi^{(2)}E^2$, gives rise to effects which are basically all mixing phenomena, involving the generation of sum and difference frequencies, but takes a variety of forms. Examples are electrooptic effect, second harmonic generation, parametric amplification, etc.

The cubic polarisation, $P^{(3)} = \epsilon_0\chi^{(3)}E^3$, gives rise to third harmonic generation and related mixing phenomena. The most important of all third-order processes is the intensity-dependent refractive index. An optical field passing through the nonlinear medium induces a cubic polarisation which is proportional to the optical intensity. It is this effect which is involved in processes like self focussing and self defocussing of laser beams, self phase and frequency modulation, soliton pulse propagation and phase conjugate reflection. The intensity dependent refractive index is, in many cases, the key nonlinear effect used in optical switching and signal-processing devices.

1.3.3 Physical origin of third order nonlinear optical response

Different nonlinear mechanisms contribute to the third order susceptibility viz, molecular orientation, electrostriction, atomic alignment, change in population equilibrium and electronic excitation. In this thesis the third order optical response of certain nonlinear organic materials are explored and a detailed description of the phenomena involved is given below.

1.3.3.1 Self focussing

Self focussing occurs as a combined effect of a positive n_2 and a spatial profile of the laser beam intensity which is usually a Gaussian. This results in a larger refractive index of the nonlinear medium in the center of the beam which is analogous to a positive lens and hence the beam tends to focus to a point. As the beam focuses, the strength of the nonlinear lens increases causing stronger focussing and increasing the strength of the lens further. This results in catastrophic focusing into a small spot.

Self focussing occur in many materials but the exact mechanism causing the phenomena varies from one material to another. In solids and in some gases the nonlinear index is due to the interaction with the electronic energy levels which causes a distortion of the electron cloud resulting in an increase in the refractive index of the medium. In materials such as molecular liquids with anisotropic molecules the nonlinear index arises

from orientation of the molecules so that their axis of easy polarisation is aligned more closely along the polarisation vector of the incident field. In such materials since the molecules are randomly arranged, refractive index is isotropic. But when the molecules line up along the optical field, the polarizability increases in that direction, resulting in different refractive index for light polarized in the direction of the incident field and perpendicular to it, resulting in birefringence. This effect is termed as optical Kerr effect. Self focussing is observed most commonly in these materials. Electrostriction, in which the molecules of the medium move into the most intense regions of the electric field, also results in optical field induced refractive index variation. Here the increase in density causes an increase in the refractive index near the regions of intense fields. Because of the relatively slow response time of moving molecules, electrostriction has a longer time constant than molecular orientation and is important for pulses that lasts several tens to hundreds of nanoseconds or longer.

1.3.3.2 Self-defocusing

Self-defocusing happens when the nonlinear refractive index, n_2, is negative and the beam profile maximum intensity is at the center than at the edge. This causes refractive index minimum in the center, i.e., the medium acts as a negative lens and the beam defocuses. A common source of self-defocusing is thermal self-defocusing or as it is commonly called thermal blooming which occurs in materials that are absorbing. The energy that is absorbed from the light wave heats the medium reducing its density and hence its refractive index, in the most intense regions of the beam. When the beam intensity is more intense at the center than at the edge, the medium acts as a negative lens and the beam diverges.

1.3.4 Measuring techniques for third order susceptibilities

There are many techniques to measure the third-order nonlinear susceptibility or polarisation of the third order materials. But it is difficult to compare the nonlinearity measured with different techniques. First of all the laser wavelength is very important, especially at wavelengths close to the resonance absorption enhancement. The repetition frequency and pulse duration of the laser are also of equal importance.

Usually $\chi^{(3)}$ measurements are done by observing (1) Third-harmonic generation

19

(2) Electric field-induced second-harmonic generation (3) Degenerate four-wave mixing (4) Optical Kerr-effect and (5) Self-focussing and defocusing[73-83]. Of these five techniques, we have concentrated mainly on the measurements based on self-focussing and defocusing, which are special cases of self action originating from the intensity dependent refractive index of the medium.

The various types of self action effects depend on whether the susceptibility is real or imaginary and on the temporal and spatial distribution of the incident light. The real part of the nonlinear susceptibility gives rise to spatial effects of self-focussing and self-defocussing. The imaginary part of the susceptibility is responsible for nonlinear absorption.

1.3.5 Z-Scan Technique

1.3.5.1 Introduction

The third order susceptibility $\chi^{(3)}$ is normally measured from the nonlinear transmission of laser beam through the medium or using Z-scan technique[18,83,84]. In 1989, Sheik-Bahae et al.[84] developed the sensitive Z-scan measurement technique that involves focusing a laser beam through a thin sample and detecting the light transmitted through a small aperture in the far field for nonlinear refractive measurement. For nonlinear absorption measurements the total transmitted intensity is measured. The transmittance is measured for a constant laser input as the sample is scanned along the z-direction through the focus of the lens. The laser intensity at the sample is varied by moving the sample along a focussed laser beam (i.e., Z-direction), Hence this method of measurement is known as Z-scan technique. The experimental setup for Z-scan is shown in Fig.1.6.

Consider the example of a material with negative nonlinear refractive index and thickness smaller than the diffraction length of the focused beam (thin medium). When the sample is far away from the focus (negative z), the beam irradiance is low and negligible nonlinear refraction occurs; hence, the transmittance remains relatively constant. As the sample is brought closer to the focus, the beam irradiance increases leading to self lensing in the sample. A negative self-lensing prior to focus will tend to collimate the beam causing a beam narrowing at the aperture in the far field which results in an increase in the measured transmittance.

20

$Z < 0$
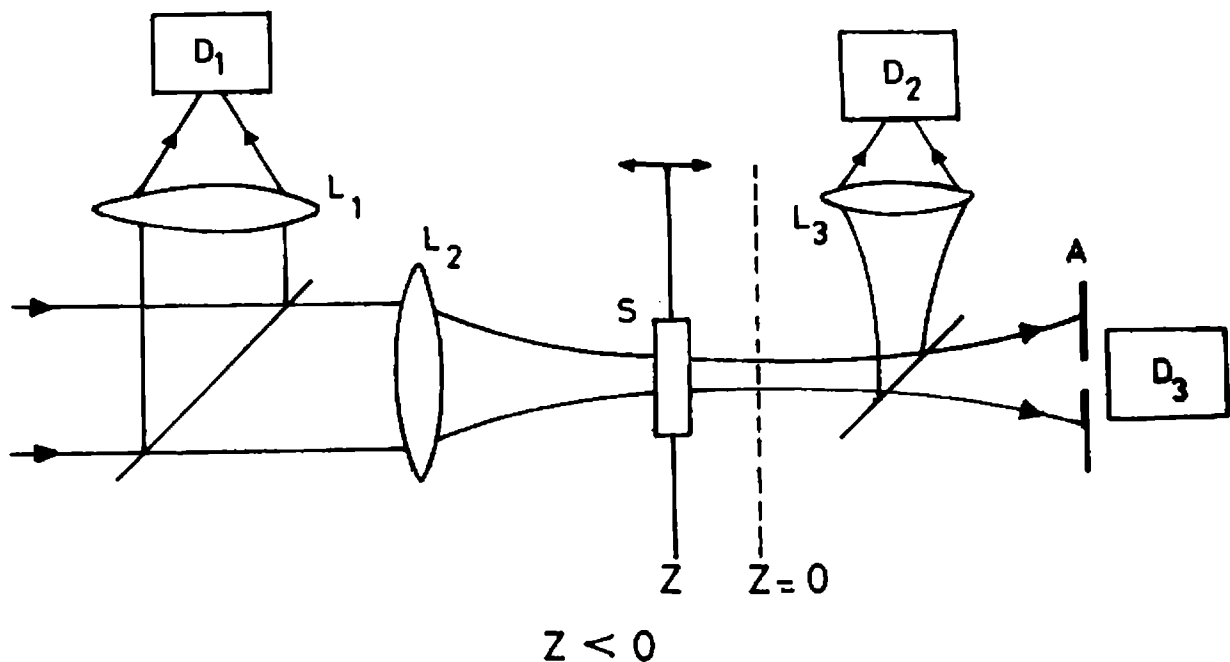
D$_1$, D$_2$, D$_3$-Detectors, L$_1$, L$_2$, L$_3$-Lens, S-Sample, A-Aperture

Fig.1.6 Experimental setup for Z-scan technique.

As the scan in z continues and the sample passes the focal plane to the right (positive z), the same self-defocussing increases the beam divergence, leading to beam broadening at the aperture, and thus a decrease in the transmittance measured at the far field. This suggests that there is a null as the sample crosses the focal plane. This is analogous to placing a thin concave lens at or near the focus, resulting in a minimal change in the far field pattern of the beam. The Z-scan is completed as the sample is moved away from the focus (positive z) such that the transmittance becomes linear since the irradiance is again low.

A prefocal transmittance maximum (peak) followed by a postfocal minimum (valley) is, therefore the Z-scan signature of a negative refractive nonlinearity. Positive nonlinear refraction, following the same analogy, gives rise to a valley-peak configuration. An extremely useful feature of Z-scan method is that the sign of nonlinear index is immediately obvious from the data and the magnitude can be calculated from the analysis of the transmittance curve.

This is the case for an ideally refractive sample. Absorptive nonlinearities changes the signal shape such that multiphoton absorption suppresses the peak and enhances

21

the valley, while saturation produces the reverse effect. The sensitivity to nonlinear refraction is entirely due to the aperture, and the removal of the aperture completely eliminates the effect. In that case Z-scan will be sensitive to nonlinear absorption. Nonlinear absorption coefficient can be extracted from such open aperture experiments.

1.3.5.2 Theory of Z-scan

In a cubic nonlinear medium the index of refraction n is expressed in terms of nonlinear indices n_2 (esu) or γ (m^2 /W) through

$$n = n_0 + \frac{n_2}{2}|E|^2 = n_0 + \gamma I \tag{17}$$

where n_0 is the linear index of refraction, E is the peak electric field, n_2 the intensity dependent refractive index and I denotes the irradiance of the laser beam within the sample. [n_2 and γ are related through the conversion formula n_2(esu) = $(cn_0/40\pi)\gamma$(m^2/W) where c(m/s) is the speed of light in vacuum].

Assume a TEM$_{00}$ beam of waist radius w_0 travelling in the +z direction. E can be written as[84]

$$E(z,r,t) = E_0(t)\frac{w_0}{w(z)}\exp\left[-\frac{r^2}{w^2(z)} - \frac{ikr^2}{2R(z)}\right] e^{-i\phi(z,t)} \tag{18}$$

where $w^2(z) = w_0^2(1+z^2/z_0^2)$ is the beam radius, $R(z) = z(1+z_0^2/z^2)$ is the radius of curvature of the wave front at z, $z_0 = kw_0^2/2$ is the diffraction length of the beam, $k = 2\pi/\lambda$ is the wave vector, and λ is the laser wavelength, all in free space. $E_0(t)$ denotes the radiation electric field at the focus and contains the temporal envelope of the laser pulse. The $e^{-i\phi(z,t)}$ term contains all the radially uniform phase variations. For calculating the radial phase variations $\Delta\phi(r)$, the slowly varying envelope approximation (SVEA) was used and all other phase changes that are uniform in r are ignored, $L \ll z_0/\Delta\phi(0)$, where L is the sample length, the amplitude $\sqrt{I}$ and the phase ϕ of the electric field as a function of z' are now governed in the SVEA by a pair of simple equations:

$$\frac{d\Delta\phi}{dz'} = \Delta n(I)k \tag{19}$$

and

22

$$\frac{dI}{dz'} = -\alpha(I)I \tag{20}$$

where z' is the propagation depth in the sample and $\alpha(I)$, in general includes linear and nonlinear absorption terms.

In the case of cubic nonlinearity and negligible nonlinear absorption, eq. 19 and eq. 20 are solved to give the phase shift $\Delta\phi$ at the exit of the sample is given by,

$$\Delta\phi(z,r,t) = \Delta\phi_0(z,t)\exp\left[-\frac{2r^2}{w^2(z)}\right] \tag{21}$$

with

$$\Delta\phi_0(z,t) = \frac{\Delta\Phi_0(t)}{1+z^2/z_0^2}$$

$\Delta\Phi_0(t)$, the on-axis phase shift at the focus, is defined as

$$\Delta\Phi_0(t) = k\Delta n_0(t)L_{eff} \tag{22}$$

where $L_{eff} = (1-e^{-\alpha L})/\alpha$, with α the linear absorption coefficient. Here $\Delta n_0 = \gamma I_0(t)$ with $I_0(t)$ being the on-axis irradiance at the focus (i.e., at z = 0).

The complex electric field exiting the sample E_e now contains the nonlinear phase distortion

$$E_e(r,z,t) = E(z,r,t)e^{-\alpha L/2} \, e^{i\Delta\Phi(z,r,t)} \tag{23}$$

By virtue of Huygen's principle, and making use of Gaussian decomposition method[85]one can show that,

$$e^{i\Delta\Phi(z,r,t)} = \sum_{m=0}^{\infty} \frac{\left[i\Delta\phi_0(z,t)\right]^m}{m!} e^{-2mr^2/w^2(z)} \tag{24}$$

After including the initial beam curvature for the focussed beam, the resultant electric field pattern at the aperture is

$$E_a(r,t) = E(z,r=0,t)e^{-\alpha L/2} \sum_{m=0}^{\infty} \frac{\left[i\Delta\phi_0(z,t)\right]^m}{m!} \frac{w_{m0}}{w_m}\exp\left[-\frac{r^2}{w_m^2} - \frac{ikr^2}{2R_m} + i\theta_m\right] \tag{25}$$

23

Defining 'd' as the propagation distance in free space from the sample to the aperture plane and g = 1+d/ R(z), the remaining parameters in Eq. 25 are expressed as

$$w_{mo}^2 = \frac{w^2(z)}{2m+1}$$

$$d_m = \frac{kw_{mo}^2}{2}$$

$$w_m^2 = w_{mo}^2 \left[g^2 + \frac{d^2}{d_m^2}\right]$$

$$R_m = d \left[1 - \frac{g}{g^2+d^2/d_m^2}\right]^{-1} \text{ and}$$

$$\theta_m = \tan^{-1}\left[\frac{d/d_m}{g}\right]$$

where d is the propagation distance in free space for the sample to the aperture plane and g is defined as g = 1+ d /R(z). The expression given in eq. 25 is a general case of that derived by Weaire et al [85]. Gaussian decomposition method is useful for the small phase distortions detected with Z-scan method since only a few terms of the sum in eq. 25 are needed.

The on-axis Z-scan transmittance for cubic nonlinearity and a small phase change can then be derived as follows. The on-axis electric field at the aperture plane can be obtained by letting r = 0 in eq. 25. In the limit of small nonlinear phase change ($|\Delta\Phi_0|$ << 1), only two terms in the sum in eq. 25 needed to be retained. The normalised Z-scan transmittance can be written as

$$T(z, \Delta\Phi_0) = \frac{|E_a(z, r = 0, \Delta\phi_0)|^2}{|E_a(z, r = 0, \Delta\phi_0 = 0)|^2} = \frac{|(g+id/d_0)^{-1} + i\Delta\phi_0(g+id/d_1)^{-1}|^2}{|(g+id/d_0)^{-1}|^2}$$

(26)

The far field condition d>>z_0 can be used to give a geometry -independent normalised transmittance as

$$T(z,\Delta\Phi_0) = 1 - \frac{4\Delta\Phi_0\, x}{(x^2+9)(x^2+1)}$$

(27)

where x = z/z_0 .

The peak and valley of the Z-scan transmittance can be calculated by solving the equation dT(z, $\Delta\Phi_0$)/dz = 0. Solutions to this equation yield

$$x_{p,v} = \pm\sqrt{\left[\frac{\sqrt{52} - 5}{3}\right]} \cong 0.858$$

(28)

24

therefore, we can write the peak-valley separation as

$$\Delta Z_{p\text{-}v} = 1.7z_0 \qquad (29)$$

Also, inserting the x value from eq. 26 and 27, the peak valley transmittance change is

$$\Delta T_{p\text{-}v} = \frac{8|x|_{p,v}}{\left(x_{p,v}^2 + 9\right)\left(x_{p,v}^2 + 1\right)}\Delta\Phi_0 = 0.406\Delta\Phi_0 \qquad (30)$$

This relation is accurate to 0.5% for $|\Delta\Phi_0| \leq \pi$. For larger aperture this equation is modified and is

$$\Delta T_{p\text{-}v} \simeq 0.406(1\text{-}S)^{0.25}|\Delta\Phi_0|, \text{ for}|\Delta\Phi_0| \leq \pi \qquad (31)$$

Thus by measuring the transmitted power in a closed aperture Z-scan, one can obtain the nonlinear refractive index by knowing the value of $\Delta\Phi_0$ from eq.23

1.3.5.3 Effect of nonlinear absorption

The third order susceptibility $\chi^{(3)}$ in general is a complex quantity having both real $\chi_R^{(3)}$ and imaginary $\chi_I^{(3)}$ parts,

$$\chi^{(3)} = \chi_R^{(3)} + i\chi_I^{(3)} \qquad (32)$$

where the imaginary part is related to the 2PA coefficient β through

$$\chi_I^{(3)} = \frac{n_0\epsilon_0 c^2}{\omega}\beta \qquad (33)$$

where and the real part is related to γ through

$$\chi_R^{(3)} = 2n_0^2\epsilon_0 c\gamma \qquad (34)$$

In the low excitation regime, the following substitution was made

$$\alpha(I)=\alpha+\beta I \qquad (35)$$

This modifies the eqs. 19 and 20 and yields the irradiance distribution and phase shift of the beam at the exit surface of the sample as

25

$$I_e(z,r,t) = \frac{I(z,r,t)\,e^{-\alpha L}}{1 + q(z,r,t)} \qquad (36)$$

and

$$\Delta\phi(z,r,t) = \frac{k\gamma}{\beta}\ln[1+q(z,r,t)] \qquad (37)$$

respectively where $q(z,r,t) = \beta I(z,r,t)L_{eff}$ and z is the sample position. Combining eq. 36 and 37, the complex field obtained at the exit surface of the sample is[86],

$$E_e = E(z,r,t)e^{-\alpha L/2}(1+q)^{(ik\gamma/\beta - 1/2)} \qquad (38)$$

In general, zeroth-order Hankel transform of eq. 38 will give the field distribution at the aperture which can then be used to calculate the transmittance. For $|q| < 1$, following a binomial series expansion in powers of q, eq.38 can be expressed as an infinite sum of Gaussian beams.

$$E_e = E(z,r,t)e^{-\alpha L/2}\sum_{m=0}^{\infty}\frac{q(z,r,t)^m}{m!}[\Pi_{n=0}(ik\gamma/\beta - 1/2 - n + 1)] \qquad (39)$$

where the Gaussian spatial profiles are implicit in $q(z,r,t)$ and $E(z,r,t)$. The complex field pattern at the aperture plane is obtained in the same manner.

$$E_a(r,t) = E(z,r = o,t)e^{-\alpha L/2}\sum_{m=0}^{\infty}f_m\frac{w_{m0}}{w_m}\exp\left[-\frac{r^2}{w^2(z)} - \frac{ikr^2}{2R(z)} + i\Phi_m\right] \qquad (40)$$

where

$$f_m = \frac{[i\Delta\phi_0(z,t)]^m}{m!}\Pi_{n=0}^m\left[1 + i(2n\text{-}1)\frac{\beta}{2k\gamma}\right] \qquad (41)$$

with $f_0=1$.

As is evident from eq. 41, the absorptive and refractive contributions to the far field beam profile and hence to the Z-scan transmittance are coupled. When the aperture is removed, the Z-scan transmittance is insensitive to beam distortion and is only a function of nonlinear absorption. The total transmitted fluence in that case $(S = 1)$ can be obtained by spatially integrating eq. 36. The transmitted power $P(z,t)$ is obtained as follows

26

$$P(z,t) = P_i(t)e^{-\alpha L}\frac{\ln[1+q_0(z,t)]}{q_0(z,t)} \tag{42}$$

where $q_0(z,t) = \beta I_0(t) \, L_{eff} \, /(1+z^2/z_0^2)$ and $P_i(t)$ is the instantaneous input power. For a temporally Gaussian pulse, it can be time integrated to give normalised energy transmittance in the summation form as,

$$T(z,S=1) = \sum_{m=0}^{\infty} \frac{[-q_0(z,o)]^m}{(m+1)^{3/2}} \tag{43}$$

for $|q_0| < 1$. Once an open aperture Z-scan (S=1) is performed, nonlinear coefficient β can be unambiguously deduced. With β known, the Z-scan with the aperture in place can be used to extract the coefficient γ by combining the open and closed aperture Z-scan transmittance curves.

1.3.5.4 Merits and defects of Z-scan technique

The most noteworthy advantage of Z-scan technique is its simplicity of experimental setup and data analysis. As a single- beam technique, it has no difficult alignment other than keeping the beam centered on the aperture. Another very important advantage of Z-scan technique is that it can be used to determine both the magnitude and sign of n_2 on a single analysis of the transmittance curve. Under general conditions it is a very effective method for screening new nonlinear materials. By using closed and open Z-scan measurements it is possible to isolate the refractive and absorptive contributions. Thus, unlike most degenerate four wave mixing methods, the Z-scan can determine both the real and imaginary parts of $\chi^{(3)}$ as well as the sign of the nonlinearity. The technique is also highly sensitive, capable of resolving a phase distortion of $\approx \lambda/300$ in samples of high optical quality. Finally Z-scan can also be modified to study nonlinearities in a time resolved manner.

Disadvantages of the technique include the fact that it requires a high quality Gaussian beam for absolute measurements. Sample distortions or wedges or tilting of the sample during translation can cause the beam to walk off the far field aperture. This produces unwanted fluctuations in the signal. Even if these are kept under control, beam jitter will produce the same effect. A second reference arm can be employed to subtract out the effects of beam jitter. The technique cannot be used to measure

off-diagonal elements of the susceptibility tensor except when a second nondegenerate frequency beam is employed. Such a technique is useful for measuring the time dependence of nonlinearities, but this detracts from simplicity and elegance of the method, since it requires careful alignment.

1.4 Photonic materials

The rapidly developing fields of optical image processing, tuned light sources technology, optical telecommunication logic systems and optical and electrooptical sensors create a large demand for highly efficient nonlinear optical materials[87-90]. It is mainly the third order nonlinearity that contributes to device applications. Hence there has been increased interest in the understanding of the fundamentals of third-order optical nonlinear materials. Some organic materials have been reported to posses large optical nonlinearities and fast response times[91-93]. Electronic structural requirement for third-order nonlinear response is delocalised π-electron systems. Conjugated polymers with alternate single and multiple bonds in their backbone structure provide a molecular frame for extensive conjugation and have emerged as the most widely studied group of $\chi^{(3)}$ organic materials. The conjugated π-electron bonding networks found in these molecules are the principal reason for their strong absorption of visible and near IR.

Organic materials have many merits compared with semiconductor nonlinear optical materials. Their low cost combined with the ease of processing, fabrication and integration into devices, high laser damage thresholds, low dielectric constants, fast optical nonlinear response times and off-resonance nonlinear optical susceptibility make them vital candidates as third order nonlinear materials[94-102]. Their chemical structures and absorption wavelengths can be tailored to achieve highly efficient nonlinear optical devices. They have found application in integrated optics such as optical switching and optical data processing.

The theoretical techniques that are used to calculate third-order polarisabilities have already been well documented[103]. Presently, very accurate calculations (i.e., allowing for quantitative estimates) of third order polarisabilities can only be performed on atoms or very small molecules. For the kind of organic molecular or macro molecular compounds which are usually being investigated for actual applications and for which theoretical guidance is highly desirable, the very size of the system precludes

28

the possibility of predicting absolute hyperpolarisability values. Since the stress in the thesis is on the bulk hyperpolarisability measurements a detailed description of the theoretical aspects is not intended here.

Dye doped polyacrylamide, phthalocyanines, napthalocyanines, chlorophyll and fullerene have been studied to elucidate its properties relevant to photonic applications. The following sections give a brief account on these materials.

1.4.1 Polymeric materials

Polymers, because of their cost effectiveness and ease of handling are ideal optical media. They have found important applications in chip to chip communications in optical integrated circuits. Dye embedded polymeric matrices have attracted considerable attention as a gain media for tunable lasers, as radiation converters in phase conjugation and as potential materials for optical information storage via spectral hole burning etc. to mention a few[104-111].

Polymeric materials having large third-order nonlinear optical properties and good processing had been obtained by doping low molecular weight compounds into polymers. These encapsulated molecules can be used to induce new optical properties in the material or to probe the changes at the molecular level which occur during the polymerization, aging and drying of the matrix. Recently these systems have emerged as potential nonlinear optical materials[112]. A variety of nonlinear optical phenomena, including optical phase conjugation[113-116], laser induced grating diffraction[117,118], photoinduced polarisation rotation[119] etc. have been reported in these systems using low power continuous wave lasers. This makes them attractive for implementation of nonlinear optical logic devices and for demonstration of the principles of all optical signal processing and molecular spatial light modulators[120,121].

Optical components fabricated from organic polymers offer several advantages over their silicate glass counterparts. They can be injection molded or cast, which is less expensive than the grinding and polishing procedures usually required with glass. They are also lighter than glass components, which makes them attractive for portable systems and others where total weight is important. Hence they have attracted attention of scientists in recent times[122]. The major advantage of the polymeric media when compared with other transparent dielectrics like crystals and glasses is the higher laser

29

resistance of polymeric surfaces as compared with its volume resistance. This is very important from the practical point of view since it is the surface resistance of transparent dielectrics which usually represents the limiting factor for their application in laser systems[123]. In fact many plastic optical components (lenses, windows, prisms, Q-switches) are now commonly available and are being used in low power optical systems. Plastic Q-switches, for example, are used in commercially available laser range finders.

1.4.2 Dye doped polymer lasers

Dye lasers have been extensively used for a variety of application because of their tunability over a wide wavelength range. Considerable effort has been made in various laboratories for the improvement of their performance with different classes of laser dyes emitting at different wavelength regions[124,125]. Currently suitable solid hosts are being tried out because of its compactness and ease of handling and the ruggedness and reliability which arise from the solid state nature of the lasing medium. Also the problem of solvent evaporation and hence change in concentration encountered in dye solutions is absent in solid state dye lasers.

Various polymers like polymethyl methacrylate (PMMA), modified polymethyl methacrylate, sol-gels, silica gels etc. have been used as host materials[25−29,126−128]. The main problem encountered in solid host dyes is the photobleaching leading to the degradation of dye molecules. In most of the solid host-dye lasers reported so far, the dye molecules are firmly linked to a polymer matrix. This reduces the total degree of freedom for the dye molecules as they cannot move freely inside the matrix. Consequently the interactions of the dye molecules with the matrix lead to product formation and hence easy photodecomposition. But in a porous material there is enough free volume and the matrix influences intrinsic properties of the emitting molecule to a much lesser extent.

In Chapter III lasing characteristics of polyacrylamide doped with rhodamine 6G have been reported. Polyacrylamide is a porous material which is highly transparent in the visible and is widely used in electrophoresis for the separation of biological molecules, especially proteins[129].

30

1.4.3 Organic materials

Conjugated organic molecules are efficient nonlinear materials and there has been a lot of studies going on to identify newer and efficient materials. The materials that have been studied here are phthalocyanines, chlorophyll and fullerene. The description of representative elements in these classes is given below.

1.4.3.1 Phthalocyanine

Macromolecules are examples of large conjugated organic structures with delocalized π-electron systems. One specific example of this class of material is phthalocyanines. The phthalocyanines can be prepared with various substituents on the ring to control solubility and morphology. Furthermore, the central positions of the phthalocyanine moiety can be metal free or substituted by metals like copper, nickel, platinum, europium, cobalt etc. Metal substitution introduces low-lying energy states derived from metal-to-ligand and ligand-to-metal charge transfer which may contribute to optical nonlinearity.
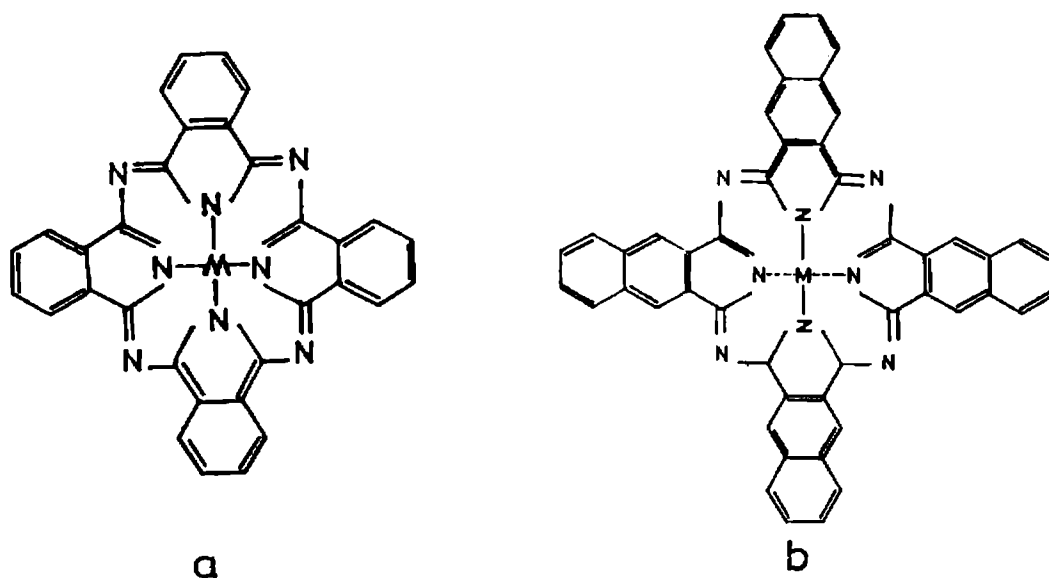

a   b

Fig.1.7 Chemical structure of (a) Phthalocyanine, (b) Napthalocyanine, with central metal atom.

31

Phthalocyanines exhibit strong electronic transitions in the visible region between 600 and 800 nm. This is π-π^* excitation and is called Q-band, the absorption coefficient of which is in excess of 10^4 cm^{-1}. A very important feature of phthalocyanines is their high chemical and thermal stability. No noticeable degradation occurs in air up to 400-500^{0}C. Hence high quality thin films can be prepared by successive sublimation. By appropriate derivatization, many soluble phthalocyanine structures have been synthesized. Some of the soluble phthalocyanines have also been reported to form Langmuir-Blodgett films. These and other unique properties they exhibit have warranted the vast amount of basic and applied research concerning phthalocyanines[130-132]. Industrially, they have been studied for their use as dyes and pigments and for their electrocatalytic activity and suitability for semiconductor devices, gas sensors, optical data storage, rectifying devices, as well as in nonlinear optics[133-149]. Pthalocyanine molecules with benzene ring attached to its four corners form napthalocyanine hence they have more number of conjugated π-electrons.
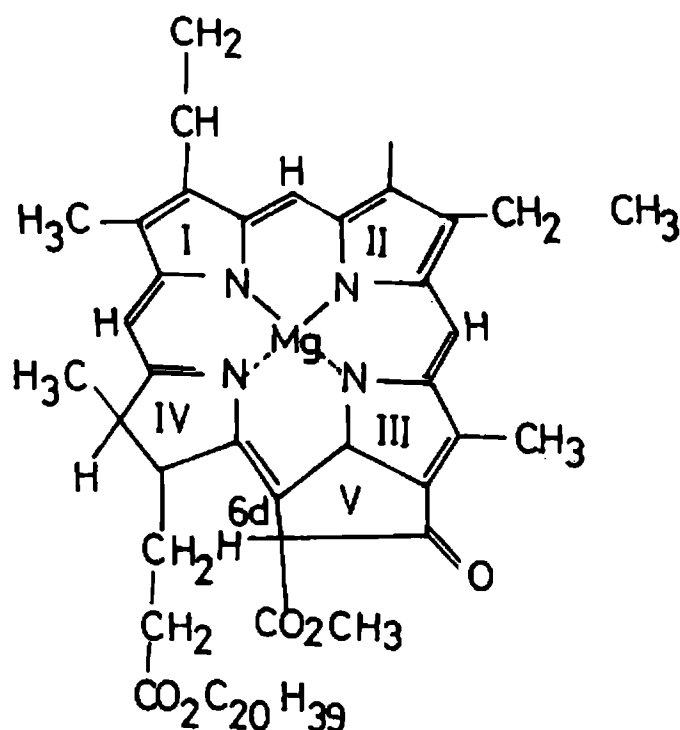
1.4.3.2 Chlorophyll

Fig.1.8 Chemical structure of Chlorophyll

Many studies have been made on the organic and biologic molecules with porphyrin like structures to understand their nonlinear optical properties[150-152]. One of the main member of this family is chlorophyll. In the presence of water it can break CO_2 and liberate oxygen, while fixing carbon as carbohydrates essential for sustaining life. Hence there has been much studies to understand the mechanism of this phenomena. And those in search of materials with large and fast optical nonlinearity found that chlorophyll molecules posses high nonlinear properties. An interesting source of chlorophyll is tea leaves from which chlorophyll can be solvent extracted. Tea extract in organic solvents has been studied to understand the origin of the nonlinearity using different techniques. The solution also shows excellent optical limiting behaviour.

1.4.3.3 Fullerenes

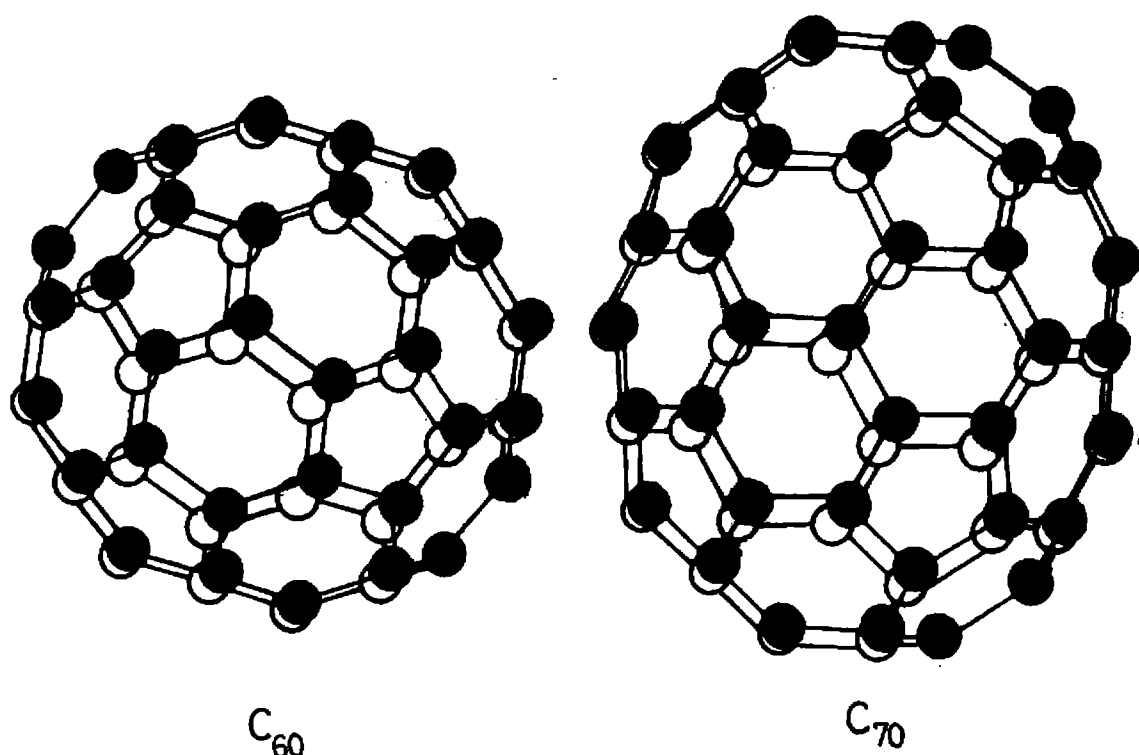Fig.1.9 Chemical structure of the fullerenes C_{60} and C_{70}

The discovery of fullerenes have stirred an enormous scientific interest for a physicist. Fullerenes have attractive truncated icosahedron structure[153,154]. Nonlinear measurements on C_{60} and C_{70} solutions in benzene, toluene and other organic solvents generated much excitement[155-159]. It has been found that fullerenes exhibit optical

nonlinearities leading to second harmonic generation, optical limiting and self defocussing of the laser beams due to its high values of third-order susceptibility[160-165]. The reverse saturable and saturable absorption of this molecule is useful in pulse shaping and optical limiting. These molecules and their derivatives have unique properties like relatively high temperature superconductivity, photovoltaic response, a high degree of hardness, persistent photoconductivity, the ability to trap anions inside the cage, etc.[166-170]. The third order nonlinearities of phthalocyanines, napthalocyanines, chlorophyll and fullerenes have been studied in detail in chapter V and VI.

1.5 Applications of photonic materials

A discussion of the applications is relevant to relate these organic materials to their practical and potential uses. Nonlinear optics is one of the few modern scientific frontiers where the huge surge and recent interest is not only owing to the quest for understanding of new physical phenomena occurring under intense laser fields, but also because of the potential technological applications. The newly emerging technology of photonics utilizes photons instead of electrons to acquire, store, transmit and process information.
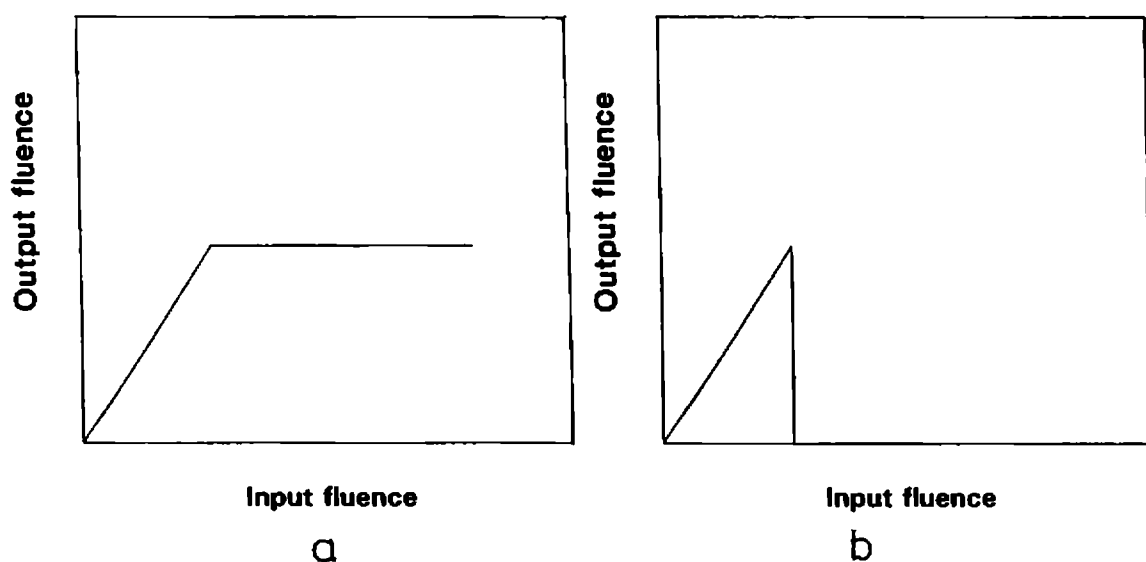

Fig. 1.10 The transmission characteristic of an (a) ideal optical limiter (b) ideal optical switch

Some of the applications, such as optical limiting, optical switching, spatial light modulation etc. utilize nonlinear optical processes to perform the functions mentioned above. The origin of the nonlinear processes are well understood and progress now depends on the development of a materials technology compatible with various device embodiments. Devices based on nonlinear-optical effects utilize two important manifestations: frequency conversion and refractive index modulation. The latter effect provides a mechanism for light control and hence optical switching and optical bistability. The refractive index modulation is induced by a change in intensity of a controlling optical field. In this case light is controlled by light which is inherently faster than the response of electrons to electric fields in conventional electronics.

1.5.1 Light modulation

Light modulation is derived from the change in refractive index of a nonlinear material. The refractive index change can be created by an external control, such as an intense optical field. Light modulators find important applications both in laboratory signal processing as fast optical gates or modulators and in optical signal processing. In relation to optical signal processing and computing, optical modulation devices can be used for beam control and photoaddressing. The principle of optical modulation is the phase shift induced in the propagation of an input optical signal by electric or optical fields, which leads to the modulation of the output optical signal. Numerous device configurations are possible for utilizing this phenomenon to change light intensity, polarisation, frequency and so on. Photochromic spatial light modulators work on the principle of amplitude modulation. Even though different type of electro-optic materials have been used in spatial light modulators, much studies have not been conducted in organic polymeric materials. However, an analysis of the potential advantages was given by Lytel et al[170] in a recent reprint. Since organic materials can be readily fabricated as thin films, and with dielectric constant around 4 at room temperature it seems to be very useful in device applications. Organic materials with their lower dielectric constants and hence capacitance should have considerable advantage in this regard. Since the thermal conductivity of organic materials tends to be low, it will be important to design devices with careful attention to heat sinking and dissipation to make full advantage of their potential benefits.

35

1.5.2 Sensor protection

Optical limiters are materials in which the transmitted intensity is saturated above a threshold laser intensity and they have wide applications in sensor or eye protection to intense light fields. This is also important in the context of nonlethal weapons and military applications.

Fig.1.10 (a) shows the transmission characteristics of an ideal optical limiter which exhibits a linear transmission below threshold, but above threshold its output intensity is constant. All optical limiting devices depend on one or other nonlinear mechanism like nonlinear absorption, nonlinear refraction, induced scattering or even phase transitions. The cause of such nonlinearities vary widely with material properties. Nonlinear absorption may be caused by two-photon absorption, excited state absorption and/or free carrier absorption. But nonlinear refraction arise from molecular reorientation, the electronic Kerr effect, or optically induced heating. Often, more than one of these processes is operative in a given device.

Since all optical nonlinearities can be classified into two groups, instantaneous and accumulative, limiting can also occur in different time scales. In the former, the polarisation density resulting from an applied field occurs instantaneously. In contrast, accumulative nonlinearities arise from interactions with memory, i.e., the polarisation density generated by an applied field either develops or decays on a time scale comparable or longer than the excitation duration. Such interactions are dissipative, and depends on energy density rather than intensity.

Examples of accumulative nonlinearities include process like excited-state absorption, free carrier absorption , optically induced heating etc. Optical limiters which depend on accumulative process are resonant in nature and hence result in devices with narrow bandwidth. By contrast, optical limiters that rely on instantaneous (non-resonant) nonlinearities can be very broad band. These nonlinearities however require high intensities and typically effectively operate only for a very short optical pulses.

In spite of the variety of nonlinearities, materials and device configurations that have been used to implement passive optical limiters, no single device or combination of devices has yet been identified that will protect any given sensor from all potential optical threats[171]. Hence further research is necessary in material and geometry to

expand sensor protection as well as new applications for these devices. The usability of Europium phthalocyanine as an optical limiter is demonstrated.

1.5.3 Optical switching

Photonic switching technology is in a state of emergence with potential to (a) Obviate the need for optical to electronic conversion (b) the ability to route high data rate optical signals (c) possibility of three-dimensional interconnections. Though electronic devices which need less power are more controllable than optical logic devices, they rapidly become slow in operation by electrical connections between them as a result of clock skew, dispersion, cross talk and unwanted capacitance. But clearly light beam cannot control one another directly and some nonlinear optical material is needed to transmit the information from a control beam to the main output beam. The transmission characteristics of an ideal optical switch is given in Fig.1.10 (b).

Nonlinear optics has led to a variety of optically activated switches. Optical logic gates cover a wide range of switching speed (ps to ms) with reactive devices switching at optical frequencies while absorptive devices are characterized by real transitions involving real time constants (typically ms to ns). They all require switching energy of the order of 10^{-9} to 10^{-6} J. Possibilities, however exist to bring down to picojoules and femtojoules. The working of europium napthalocyanine as an optical inverter used in photonic switching devices is described in this thesis.

1.5.4 Luminescent solar concentrators

All the above discussed applications depend on the nonlinear property of the material. But here the radiative property of rhodamine 6G in the polymer matrix is utilized to efficiently channelling the solar radiation into the photovoltaic sensor. A large amount of solar energy is falling on earth's surface but the high cost of conversion of solar radiation into other convenient types of energy hampers the profitable use of solar energy. One of the ways to make it economical is to use cheap materials and technical devices like luminescent solar concentrators (LSC).

Transparent materials, such as polymers or glass is impregnated with guest luminescent absorbers like organic dye molecules having strong absorption bands in the visible and UV regions of the spectrum and also having an efficient fluorescence quantum

37

yield. Solar photons entering the upper surface of the plate are absorbed and photons are then emitted. Snell's law dictates that a large fraction of these luminescent photons will be trapped by total internal reflection; for example, ≈74% of an isotropic emission will be trapped in a PMMA plate having an index of refraction of 1.49. Successive reflections transport the luminescent photons to the edge of the plate where they can enter an edge-mounted array of solar cells. Fig.1.11 shows the conceptual operation of a LSC.
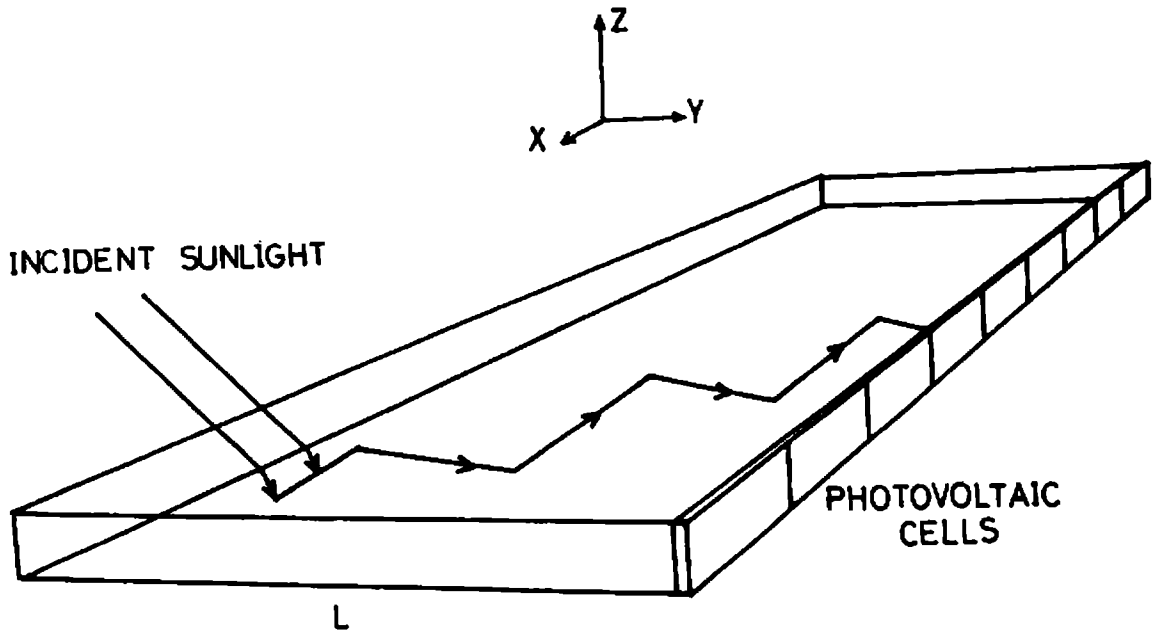
Fig.1.11 The conceptual operation of a planar LSC. Light is trapped in the matrix by total internal reflection and this beam is detected by the photovoltaic cell where it is converted into electricity.

The photon flux at the edge of an idealized LSC is the product of the absorbed flux, the fraction of the resulting luminescence that is trapped and the geometric ratio of the area of the face directly exposed to the sunlight divided by the area of the edge covered by solar cells. But in a practical LSC there will be many parasitic losses. These are inadequate absorption bandwidth, imperfect quantum efficiency, self absorption of the

luminescence, absorption by the matrix material, reflective mismatches, geometrical trapping effects and lifetime of the materials used. The major advantage of LSC's is that a solar tracking system is not needed and they intensify both direct and diffuse solar light where as conventional concentrators and inefficient in collecting scattered radiation. Hence an efficient LSC highly useful to overcome the energy crisis felt now. Rhodamine 6G doped polyacrylamide is studied for its use as LSC and the results obtained are described in Chapter VII.

1.6 Summary

An outline of laser-matter interaction relevant to the present studies as well as an account of the materials studied along with its application in the technological field is given in this Chapter. It has been shown that the field of organic materials is very exciting and promises many fascinating photonic applications. It also demonstrates that a lot of work is needed, however, in order for the potentialities to turn into realities.

References

[1] H M Gibbs, 'Optical Bistability: Controlling Light with Light', Academic Press, NY, (1985).

[2] Lee Goldberg, 'Electronic Design', **45**, 65, (1997).

[3] W E Smith, D Benjamin, Opt. Engg., **34**, 189, (1995).

[4] G I Stegman and A Miller, 'Photonics in Switching', J Midwinter, Ed. Academic Press, Cambridge MA, (1993).

[5] M N Islam, 'Ultrafast Fiber Switching Devices and Systems', Cambridge University Press, UK, (1992).

[6] Y Silberg and P W Smith, 'Nonlinear Photonics', H M Gibbs, G Khitrova, and N Peyghambarian, Eds., Springer-Verlag, Berlin, (1990).

[7] P N Prasad, D J Williams, 'Nonlinear Optical Effects in Molecules and Polymers', Wiley, NY, (1991).

[8] D.L.Mills, 'Nonlinear Optics' Narosa Publishing House, New Delhi, (1993).

[9] E.G.Sauter, 'Nonlinear Optics' Wiley Series in Microwave and Optical Engineering, US, (1996).

[10] George C.Baldwin, 'An Introduction to Nonlinear Optics' Plenum Press, New York, (1969).

[11] Robert W.Boyd, 'Nonlinear Optics' Academic Press, US, (1992).

[12] Richard L. Sutherland, 'Hand Book of Nonlinear Optics' Marcel Dekker, New York, (1996).

[13] Au, C S Wu, S T wu, and U Efron, **34**, 281, (1995).

[14] S S Fukushima, T Kurokawa and M Ohno, Appl. Phys. Lett., **58**, 787, (1991).,

[15] V V Rampal, 'Photonics Elements and Devices', Wheeler Pub., Allahabad, (1991).

[16] a. Fyad, Z Henari, Karl H Cazzini et al., Appl. Phys. Lett., **68**, 619, (1996)., b. K P J Reddy, and P K Barhai, Pramana-J. Phys., **35**, 527, (1990).

[17] G I Stegeman, E M Wright et al., J. Light. Tech., **6**, 953, (1988).

[18] L W Tutt, T F Boggess, Prog. Quant. Electr. **17**, 299, (1993).

[19] G L Wood, A A Said, D J Hagan, M J Soileau, and E W Van Stryland, Proc. SPIE, **1105**, 154, (1989).

[20] R C Powell et al., Proc. SPIE, **1105**, 136, (1989).

[21] G L Wood, W W Clark III and E J Sharp, Proc. SPIE, **1307**, 376, (1990).

[22] M Berggren, A Dodabalapur, and R E Slusher, Appl. Phys. Lett., 2230, (1997).

[23] N Silberberg and I Bar Joseph, Opt. Coomun., **39**, 265, (1981).

[24] Y Yang, H Fei, Z Wei, Q Yang, G Shun, Li Han, Opt. Commun., **123**, 189, (1996).

[25] D D Lo, J F Parris, J L Lawless, Appl. Phys. B, **56**, 385, (1993).

[26] M Faloss, M Canva, et al., Appl. Opt., **36**, 6760, (1997).

[27] A Costela, I Garcia-Moreno, and J M Figuera, Appl. Phy. Lett., **68**, 593, (1996).

[28] D A Gromov, K M Dyumaev, et al., J. Opt. Soc. Am. B, **2**, 1028, (1985).

[29] K M Dyumaev, A A Manenkov, et al., J. Opt. Soc. Am. B, **9**, 143, (1992).

[30] A V Deshpande, E B Namdas, Appl. Phy. B, **64**, 419, (1997).

[31] W H Weber, and J Lanbe, Appl.Opt., **15**, 2299, (1976).

[32] A Goetzberger and W Greubel, Appl. Phys., **14**, 123, (1977).

[33] J S Batchelder, A H Zewail, and T Cole, Appl. Opt. **18**, 3090, (1979).

[34] J S Batchelder, A H Zewail, and T Cole, Appl. Opt. **20**, 3733, (1981).

[35] R Reisfeld, J. Non-cryst. Solids, **121**, 254, (1990).

[36] F Salin et al. Opt. Lett., **14**, 785, (1989).

[37] F.P.Schafer, Topics in Applied Physics, Vol 1, Dye Lasers (1973).

[38] K.H.Drexhage, Vol 1, 'Dye Lasers' F.P.Schafer Ed. (1973).

[39] T.G.Pavlopoulos, IEEE J. Quan. Elec., Vol **QE-9**, 510 (1973).

[40] C.Rulliere and P.Kottis, Chem. Phys. Lett., **75**, 478 (1980).

[41] K H Drexhage, Laser Focus, **9**(3), 35 (1973).

[42] H.Kuhn, 'Progress in the Chemistry of Organic Natural Products', Ed. D.L.Zechmeister, vol.16, Springer, Wein (1958-59).

[43] Y.Miyazol and M.Maeda, J. Opto Elec., **2**, 227, (1970).

[44] Joseph R Lakowicz, 'Principles of Fluorescence Spectroscopy', Plenum press, New York, (1986).

[45] K H Drexhage, Laser Focus, **9**(3), 35 (1973).

[46] N J Turro, 'Molecular Photochemistry', Benjamin, New York (1965).

[47] E L Wehry, 'Structural and Environmental Factors in Fluorescence: Fluorescence, Theory, Instrumentation and Practice', Ed. G.G. Guilbault, Dekker, New York, (1967).

[48] J.B.Birks, 'Photophysics of Aromatic molecules', Wiley Interscience, London, (1970).

[49] Parker C A, 'Photoluminescence of Solutions, Elsiver, Amsterdam (1968).

[50] 'Standards in Fluorescence Spectrometry' Ed. J N Miller, Chapman and Hall, (1981).

[51] P Pringsheim, 'Fluorescence and Phosphorescence' (Interscience, New York (1949).

[52] Forster and Konig, Z Elektrochem., **61**, 344 (1957).

[53] K.K.Rohtagi and A.K. Mukhopadhyay, Photochem. Photobio. **14**, 551 (1971).

[54] Arbeao I L and Ojeeada P R, Chem, Phys. Lett., **87**, 556, (1982).

[55] Kopainsky B and Kaiser W, Chem. Phys. Lett., **88**, 357, (1982).

[56] E Rabinowitch and L F Epstein, J Amer.Chem. Soc., **63**, 69 (1941).

[57] K K Rohtagi and G.S.Singhal, J.Phys. Chem., **70**, 1695 (1966).

[58] R Larsson and B Norden, Acta Chem. Scand., **24**, 2583 (1970).

[59] Roland Wayant and Marwood Ediger, 'Electro-Optics Handbook' McGraw-Hill, Inc, (1993).

[60] P P Sorokin and J R Lankard, IBM J. Res. Dev., **10**, 162, (1966)

[61] H Kogelink and C V Shank, Appl. Phys. Let., **18**, 152, (1971)

[62] I P Kaminov, H P Weber, and E A Chandros, Appl. Phys. Lett., **18**, 497, (1971)

[63] M Kuwata-Gonokami, R H Jordan et al., Opt. Lett., **20**, 2093, (1995).

[64] W Falkenstein, A Penzkofer and W Kaiser, Opt. Commun., **27**, 151, (1978).

[65] J T Verdeyen, 'Laser Electronics', Prentice Hall, India, (1993).

[66] Peter Milloni and Joseph Eberley 'Lasers', John Wiley and Sons.

[67] Yariv A, 'Quantum Electronics' Wiley, NY, (1967).

[68] N. Bloembergen, 'Nonlinear Optics', New York: Benjamin (1965).

[69] Garret C G B, and Robinson F N H, IEEE J Quantum Electron., **QE-2**, 328, (1966).

[70] Su W P, Schrieffer, J R, , Heeger, A, J Phys. Rev. Lett. **42**, 1698, (1979).

[71] Su W P, Schrieffer, J R, , Heeger, A, J Phys. Rev. Lett. **22**, 2099, (1980).

[72] Bredas, J L, Street, G B, Acc. Chem. Res. **18**, 309, (1985).

[73] J P Hermann, J Ducuing, J. Appl. Phys., **45**, 5100, (1974).

[74] H S Nalwa, Appl. Organomet. Chem., **5**, 349, (1991).

[75] J R Helfin, Y M Kai, A F Garito, J. Opt. Soc. Ame. B, **8**, 2132, (1991).

[76] A Persoons, B V Wonterghem, P Trackx, P. Proc. SPIE-Int. Soc. Opt. Eng. **1409**, 220, (1991).

[77] R W Hellwarth, J. Opt. Soc. Am., **67**, 1, (1977).

[78] M Samoc, P N Prasad, J. Chem. Phys., **91**, 6643, (1989).

[79] W E Williams, M J Soileau, E W Van Stryland, Opt. Commun., **50**, 256, (1984).

[80] a M Sheik-Bahae, D J Hagan, E W Van Stryland, Phys. Rev. Lett., **65**, 96, (1990)., b. A D Buckingham, Proc. Phys. Soc. London Sect.B, **69**, 344, (1956).

[81] a G K L Wong, Y R Shen, Phys. Rev. A, **10**, 1277, (1974)., b. S Guha, C S Fraizer, P L Porter, K Kang, S E Finberg, Opt. Lett., **14**, 952, (1989).

[82] a Y R Shen, 'The Principles of Nonlinear Optics', Wiley-Interscience, NY, (1984)., b. J F Reintjes 'Nonlinear Optical Parametric Processes in Liquids and Gases', Academic, NY,(1984).

[83] M Sheik-Bahae, Ali A. Said, Tai-Huei Wei, David J.Hagan, E.W.Stryland, Opt. Lett., **14**, 955, (1989).

[84] M Sheik-Bahae, Ali A. Said, Tai-Huei Wei, David J.Hagan, E.W.Stryland, IEEE J. Quant. Electron., **26**, 760, (1991).

[85] D Wearie, B S Wherrett, D A B Miller, and S D Smith, Opt. Lett., **4**, 331, (1974).

[86] A Hermann, J.Opt.Soc. Amer.B, **1**, 729, (1984).

[87] D S Chemla, J Zyss, Eds. 'Nonlinear Optical Properties of Organic Molecules and Crystals', Academic Press, NY, (1987).

[88] P N Prasad, D R Ulrich, Eds. 'Nonlinear Optical and Electroactive Polymers', Plenum press, NY, (1988).

[89] C M Bowden, M Giftan, H R Robl, 'Optical Bistability' Plenum, NY, (1981).

[90] R Fisher, 'Optical Phase Conjugation', Academic, NY, (1985).

[91] G M Carter, M K Thakur, J Y Chen, J V Hryniewicz, Appl. Phys. Lett. **47**, 457, (1985).

[92] T Hattori, T Kobayashi, Chem. Phys. Lett., 133, 230, (1987).

[93] S R Marder, John E Sohn, and G D Stucky, 'Materials for Nonlinear Optics Chemical Perspectives', ACS Symposium series, 455, Ame. Chem. Soc., Washington D C, (1991).

[94] D J Williams, Angew. Chem., Int. Ed. Engl, 690, (1984).

[95] A J Heeger, J Orenstein, D R Ulrich, Eds. 'Nonlinear Optical Properties of Polymers' Mat. Res. Symp. Proc. Materials Research, Society, Pittsburgh, Vol.109, (1988).

[96] M J Kajzar, D Ulrich, Eds. 'Nonlinear Optical Effects in Polymers' NATO-ARW Series, Kluwer:Dordrecht Vol. E162, (1989).

[97] M J Kajzar, P N Prasad, Eds. 'Organic Molecules for Nonlinear Optics and Photonics' NATO-ARW Series, Kluwer:Dordrecht Vol. E194, (199.).

[98] G Khanarian, Ed. 'Nonlinear Optical Properties of Organic Materials' SPIE-Int. Soc. Opt. Eng. Washington, Vol. 971, (1988).

[99] K D Singer Ed. 'Nonlinear Optical Properties of Organic Materials IV' SPIE-Int. Soc. Opt. Eng. Washington, Vol. 1560, (1991).

[100] J L Brdas R R Chance Eds. 'Conjugated Polymeric Materials: Opportunities in Electronics, Optoelectronics, and Molecular Electronics', NATO-ARW Series, Kluwer:Dordrecht Vol. E182, (1990).

[101] R A Hann, D Bloor Eds. 'Organic Materials for Nonlinear Optics', Royal Society of Chemistry, London, (1989).

[102] P N Prasad, Reinhardt B A, Chem. Mater., 2, 660, (1990).

[103] P.N Prasad, J L Brdas, C Adant, P Tackx, A Persoons, B M Pierce, Chem. Rev., 94, 243, (1994).

[104] M V Bondar, O V Przhonskaya, E A Tikhonov et al., J. Quantum. Electron., 15, 1629, (1985).

[105] A J Vickerst, R M Fredgold, P Hodge et al., Thin solid films, 134, 43, (1985).

[106] W E Moerner, 'Persistent Spectral Hole Burning-Science and Applcations', Springer, Berlin, (1989).

[107] R Reisfeld, J. Non-Cryst. Solids 121, 254, (1990).,

[108] E T Knobbe, B.Dunn, P D Fugu and F Nistrida, Appl. Opt. 29,183, (1990).

[109] F Salin, G LeSaux, P Georges, A Brun, C Bagnall, J.Zarzyck Opt. Lett., 14, 785, (1989).

[110] Donald R Ulrich, J. Non-crystalline Solids, 100, 174, (1988).

[111] S Miyanaga and H Fujiwara, Proceedings of International Conference on Lasers, 795, (1989).

[112] K K Sharma, Divakara Rao, and G Ravindra Kumar, Opt. Quantum. Electron., 26, 1, (1994).

[113] Y Silberg and L Bar Joseph, Opt. Commun., 39, 265, (1981).

[114] H Fujiwara and K Nakagawa, Opt. Commun., 55, 386, (1985).

[115] M A Kramer et al., Phys. Rev. A, **34**, 2026, (1986).

[116] G R Kumar, B P singh and K K Sharma, Opt. Commun., **73**, 81, (1989).

[117] S A Boothyroyd, J Crostowski, and M S Sullivan, Opt. Lett., **14**, 948, (1989).

[118] G R Kumar, B P Singh and K K Sharma, J. Opt. Soc. Ame.B, **8**, 2120, (1991).

[119] M Montechi, M Settembre and M Romangoli, J. Opt. Soc. Ame. B, **5**, 2357, (1988). ,

[120] G R Kumar, B P Singh and K K Sharma, Opt. Lett., **15**, 245, (1990).

[121] Spatial light modulator., Speiser

[122] Kreidl, N J and Rood, J.L., 'Optical Materials, in Applied Optics and Optical Engineering', Vol1, Kingslake, R., Ed., Academic Press, New York, 181, (1965).

[123] K M Dyumaev , V S Nechitailo, et al., Sovt. J. Quant. Electron., **4**, 503, (1983).

[124] O G Peterson and B B Snavely, Appl. Phys. Lett., **12**, 238, (1968).

[125] M J Weber, Ed., 'Organic Dye Lasers', CRC Handbook of Laser Science and Technology Supplement CRC Press, Boca Raton, FL, (1990).

[126] A P Maslyyukov, S Sokolov, M Kaivila, K Nyholm, S Popov, Appl. Opt. 34, 1516, (1995).

[127] M I Ferrer, A U Acuna, F Amat-Guerri, A Costela, J M Figuera, F Florida, and R Sastre, Appl. Opt., **33**, 2266, (1994).

[128] F Amat-Guerri, A Costela, J M Figuera, F Florida, and R Sastre, Chem. Phy. Lett., **209**, 352, (1993).

[129] B D Hames, and D Rickwood 'Gel Electrophoresis: A Practical Approach', IRL press, Oxford (1990).

[130] J M Robertson, J. Chem. Soc., 615, (1935).

[131] a. J M Robertson, J. Chem. Soc., 1195, (1936)., b. R P Linstead, J M Robertson, J. Chem. Soc., 1736, (1936).

[132] J M Robertson, I J Woodward, J. Chem. Soc., 219, (1937).

[133] J Simon , J J Andre, 'Molecular Semiconductors', Springer, Berlin, (1985).

[134] A B P Lever, M R Hempstead, C C Leznoff, W Lin, M Melnik, W A Nevin, P Seymour, Pure Appl. Chem. 1567, (1986).

[135] M Pope C E Swenberg, 'Electronic Process in Organic Crystals', Claderon, Oxford, (1982).

[136] R A Collins, K A Mohammed, J Phys. D, **21**, 154, (1988).

[137] J W Wu, J R Helfin, et al. J.Opt. Soc. Ame. B, **6**, 707, (1989).

[138] K Abe, H Sato, T Kimura, Y Ohkatsu, T Kusano, Makromole Chem., **190**, 2693, (1989).

[139] M K Casstevens, M Samoc, J Pfledger, P N Prasad, J. Chem. Phys., **92**, 2019, (1990).

[140] P N Prasad, M K Casstevens, M Samoc, Proc. SPIE-Int. Soc. Opt. Eng. 1056, 117, (1989).

[141] J Simon, P Bassoul, S Norvez, New J. Chem., **13**, 12, (1989).

[142] D R Coulter, V M Miskowski, J W Perry, T H Wei, E W Van Stryland, D J Hagan, Proc. SPIE-Int. Soc. Opt. Eng. **1105**, 42, (1989).

[143] C Bubeck, D Neher, A Kaltbeitzel, G Duda, et al. in M J Kajzar, D Ulrich, Eds. 'Nonlinear Optical Effects in Polymers' NATO-ARW Series, Kluwer:Dordrecht Vol. E162, p-185, (1989).

[144] D Neher et al., J L Brdas R R Chance Eds. 'Conjugated Polymeric Materials: Opportunities in Electronics, Optoelectronics, and Molecular Electronics', NATO-ARW Series, Kluwer: Dordrecht Vol. E182, p-387, (1990).

48

[145] M Hosada, T Wada, H Sasabe, Jpn. J. Appl. Phys., **31**, 1071, (1992).

[146] M Hosada, T Wada, H Sasabe, Jpn. J. Appl. Phys., **31**, L249, (1992).

[147] a. T Wada, M Hosada, H Sasabe, 'Molecular and Biomolecular Electronics', R R Bringe, Ed. Amer. Chem. Soc. , Washington., b. J W Wu, et al. J. Opt. Soc. Ame. B, **6**, 707, (1989).

[148] J S Shirk, J R Lindle et al., 'Materials for Nonlinear Optics', American Chem. Soc., Washington, p-626, (1991).

[149] J W Perry, et al., Opt. Lett, **19**, 625, (1994).

[150] Gary L Wood, Mary J Miller, and Andrew G Mott, Opt. Lett., **20**, 973, (1995).

[151] Armen Sevian, M Ravikath, G Ravindra kumar, Chem. Phy. Lett., **263**, 241, (1996).

[152] Shekhar Guha, Keith Kang, Pamela Porter, J F Roach, David E R, Franscico J Aranda, D V G L N Rao, Opt. lett., **17**, 264, (1992).

[153] W Krätschmer, L D Lamb, et al. Nature, **347**, 354, (1990).

[154] W Krtschmer, et al. Chem. Phys. Lett., **170**, 167, (1990).

[155] H W Kroto, S C Heath, et al. Nature, **318**, 162, (1985).

[156] J R Heath, R F Curl, R Smalley, J Chem. Phys., **87**, 4286, (1987).

[157] S H Yang, C I Pettiette, et al., Chem. Phys. Lett., 139, 233, (1987).

[158] J S Miller, Adv. Mater., **3**, 262, (1991).

[159] A Kost, L Tutt et al., Opt. Lett., **18**, 334, (1993).

[160] Gong Qihuang et al, J Appl. Phys. **71**, 3025, (1992).

[161] G Neher, G I Stegman et al., Opt. Lett., 17, 1491, (1992).

[162] Riju C Isac, S S Harilal, Geetha K Varier, C V Bindhu, V P N Nampoori, and C P G Vallabhan, Opt. Eng., **36**, 332, (1997).

[163] S Couris, E Koudoumas, A A Ruth, S Leach, Appl. Phys. B, At. Mol. Opt. Phys., **28**, 4537, (1995).

[164] M Cha, N S Saricifti, A J Heeger, J C Hummelen, and F Wudl, Appl. Phys. Lett., **67**, 3850, (1995).

[165] Y Sun, et al., Opt Commun., **102**, 205,(1993).

[166] M J Rosseinsky, A P Ramirez, S H Glarum, D W Murphy, R C Haddon, A F Hebbard, T T M Palstra, A R Kortan, S M Zahurak and A V Makhija, Phys. Rev. Lett., **66**, 2830 (1991).

[167] C H Lee, G G Yu, D Mosses, and A J Heeger, Appl. Phys. Lett., **65**, 664, (1994).

[168] V Blank, M Popov, S Buga, S Davydov, V N Denisov, A N Ivlev, B N Mavrin, V Agatonov, R Ceolin, H Szawarc and A Rassat, Phys. Lett. A, **188**, 281, (1994).

[169] A Hamed, H Rasmusa, and P H Hor, Appl. Phys. Lett., **64**, 526, (1994).

[170] L Zhu, S Wang, Y Li, Z Zhang, H Hou and Q Qin, Appl. Phys. Lett. **65**, 702, (1994).

[171] Lytel et al. Eds. 'Nonlinear Optical and Electroactive Polymers', Plenum, NY, p-415, (1987).

[172] Perry A Miles, Appl. Opt., **33**, 6965, (1994).

CHAPTER II
INSTRUMENTATION

Abstract

In this chapter, a brief description of the main experimental techniques that have been used for the study of radiative and nonlinear processes in photonic materials are described, along with the specifications of the equipment used for it.

51

2.1 Introduction

The accuracy and range of the data gathered in an experiment depends mainly on the experimental technique and the detecting instruments used. The characterization of the sample under study is done by using the data thus obtained. In many situations, proper computer interfacing with necessary software support renders the data acquisition more accurate and less time consuming. In this chapter, the experimental details and the instruments used for nonlinear as well as radiative studies are given. The five major experiments that have been described in this thesis are (1) fluorescence measurements, (2) amplified spontaneous emission (ASE) measurements from dye impregnated polymer matrices, (3) photothermal phase shift spectroscopy, (4) Z-scan measurements and (5) transmission measurements.

2.2 Instrumentation for fluorescence emission studies

There are many ways by which a molecule excited to higher energy state can return to the ground state. One of them is the fluorescence phenomena, in which major part of the absorbed energy is released in the form of radiative emission.
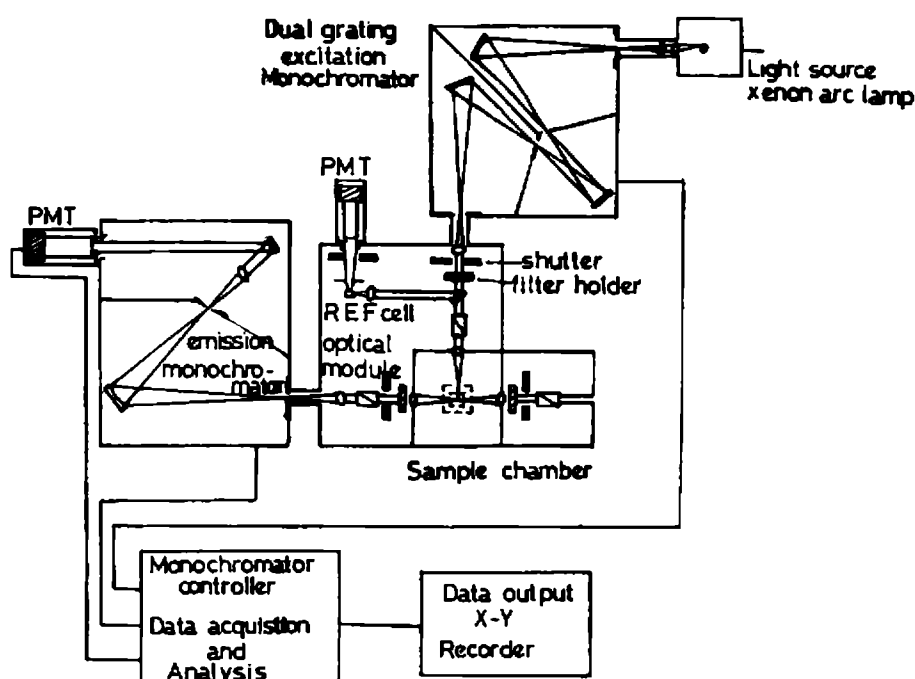

Fig.2.1 Schematic diagram of a fluorometer.

The successful application of fluorescence method requires an understanding of the instrumentation. There are two reasons for this. First, fluorescence is a highly sensitive technique and the gain of the instruments can be increased to obtain observable signals[1]. However these signals may be due to the amplification of background noises and not from the fluorophore of our interest. Secondly, there is no ideal fluorometer which yields true emission spectra, because of the nonuniform spectral output of the light sources and the wavelength-dependent efficiency of the monochromators and photomultiplier tubes. In order to overcome these the entire system is calibrated in wavelength using a Xenon arc lamp with know spectral output. The polarisation of the emitted light can also affect the fluorescence intensities. To obtain reliable spectral data one should be aware of and control these numerous factors. The schematic diagram of a typical fluorometer is given in Fig.2.1. The three principal components of the fluorometer are the source of excitation, the sample holder, and the detector. Fluorescence is initiated by the absorption of a quantum of radiation. Hence an intense steady radiation at a known wavelength is required. Laser has been used as the excitation source in the present studies. The individual components of fluorescence measurement are described below.

2.2.1 Nd:YAG laser

A Q-switched, Nd:YAG laser (Spectra Physics, DCR-11) which has a fundamental infrared beam at 1.06 μm was used[2]. The high peak power of the Q-switched pulses permit second harmonic generation at 532 nm by introducing the KD*P crystal in the beam path. The pulse width (FWHM) is 10 ns and maximum energy per pulse available is 275 mJ at 1.06 μm with a power stability of $\pm 4\%$. The pulse repetition frequency is variable from 1 to 16 Hz. The laser cavity is a diffraction coupled resonator giving a TEM_{01} mode with the beam diffraction limited to a diameter of 6.4 mm. 1.06 μm and 532 nm radiations are linearly polarised in mutually perpendicular directions and the beam divergence is 0.5 mrad. The laser beam has a line width of 1 cm^{-1} with 220 MHz spacing between the longitudinal modes.

Fig.2.2 shows the schematic of the Nd:YAG laser system used in the present studies and Fig.2.3 shows the energy level diagram of neodymium doped Yittrium Aluminium Garnet, the active medium of the laser system. The active medium is optically pumped

by a flash lamp whose output matches with the principal absorption bands in the red and the infrared. Excited electrons quickly drop to the $F_{3/2}$ level where they remain for a relatively long time. The most probable lasing transition is to the $I_{11/2}$ state. emitting a photon at 1.06 μm. Since the electrons in that state quickly relax to the ground state, its population remains low. Hence it is easy to build a population inversion between the upper and lower laser levels. There are other competing laser transitions, but their lower gain and higher threshold than 1.06 μm and wavelength selective optics limit oscillation to 1.06 μm. To increase the peak pulse energy and shorten the pulse duration, Q-switch is used. An electro-optic Q-switch introduces high cavity loss to prevent oscillation. The Q-switch comprises a polarizer. a quarter-wave plate and a Pockels cell. The polarisation characteristic of the Pockels cell is varied by applying a high voltage. With no voltage applied, the Pockels cell doesn't affect the polarisation characteristics of the light passing through it. But when the voltage is applied, it cancels the polarisation retardation of the quarter wave plate and the light suffers less loss.
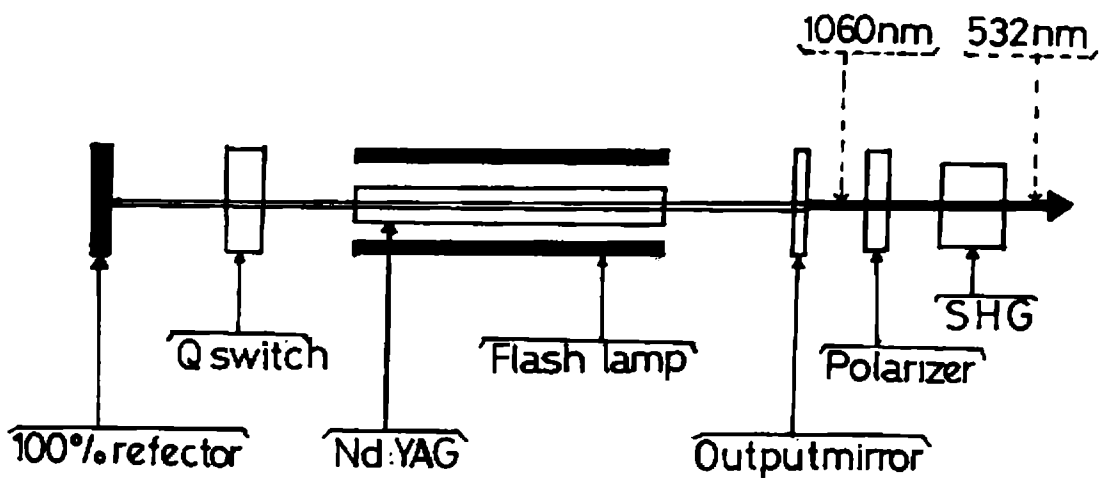

Fig.2.2 The schematic of the Nd:YAG laser

54

The optical cavity resonator of the DCR-11 is an unstable one. In a stable resonator the ray travels close to the optical axis and is reflected toward the optical axis by its cavity mirrors, so it is always contained along the primary axis of the laser and hence can extract energy from only a small volume near the optical axis of the resonator.
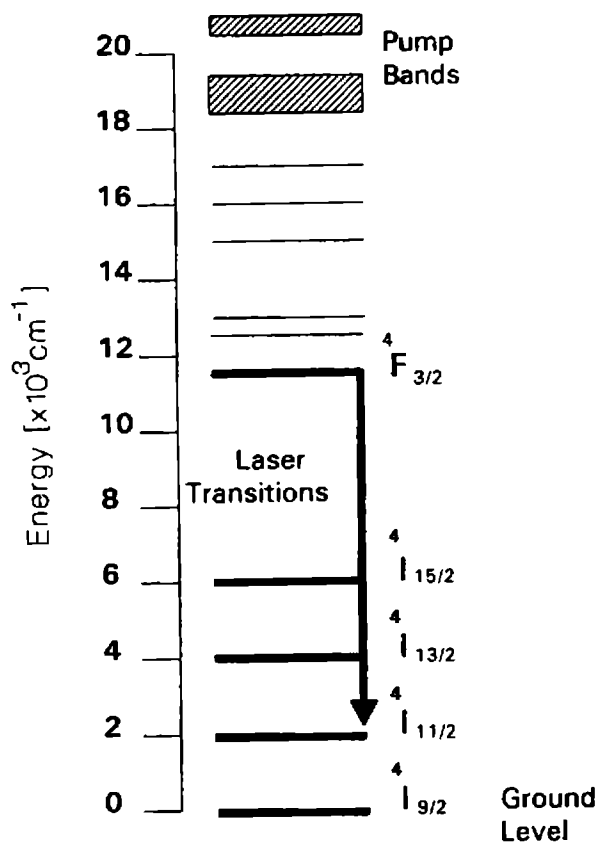
Fig.2.3 The transition scheme and energy level diagram of the neodymium-doped yttrium aluminium garnet (Nd:YAG).

But in an unstable resonator the ray is reflected away from the optical axis by one of the cavity mirrors. The output beam has large diameter and thus they can efficiently extract energy from active media whose cross sectional area is large. The output coupler in an unstable resonator is a small highly reflecting mirror mounted on a clear substrate which lies on the optical axis of the resonator. Energy escapes from the resonator by diffracting around this dot, which gives it the name diffraction coupled resonator (DCR). It delivers a doughnut shaped beam profile with a divergence of 0.5 mrad. This laser provides trigger outputs to synchronize the oscilloscope, boxcar averager etc.

2.2.2 Sample holder

The geometrical arrangement of the exciting beam and the direction of viewing of the fluorescence output light in relation to the specimen is one of the most controversial points in the design of the fluorometer[3]. This is because of the interplay of concentration quenching and inner filter effect, which are geometry dependent phenomena. Fluorescence is collected in the front surface geometry to avoid the reabsorption effects in the sample. But in the case of ASE measurements perpendicular geometry is used beacuse of the directional nature of ASE signal. Because of its freedom from the effects of large amounts of scattered and transmitted excitation, this is the most preferred arrangement[4].

2.2.3 Detector

The detector system of a fluorometer consists of a monochromator-photomultiplier combination interfaced to a PC, using a suitable software. In order to increase the signal to noise ratio a boxcar averager was also used.

2.2.3.1 Monochromator

The basic function of a monochromator is to isolate a narrow band of electromagnetic radiation of required wavelength. The specification of the performance of a monochromator includes the dispersion and the stray light levels. Generally, the dispersion efficiency is given in nm/mm, where the slit width is expressed in mm. Also it must have good light gathering power, minimum ambient light interference and good resolution. The monochromator has input and output slits of variable height and width. The light intensity which passes through a monochromator is proportional to the square of the slit width[1]. Larger slit widths yield increased signal levels, therefore higher signal-to-noise ratios. The finer slit width provides better resolution at the expense of detected power of light. Grating monochromators may have planar or concave gratings. Concave gratings produced by holographic method are preferable in fluorescence studies, since imperfections are rare and stray light and ghost image interferences are absent.

A 1 meter long scanning spectrometer, Spex Model 1704. having a maximum resolution ≈ 0.05 Å was used to conduct fluorescence measurements[5]. The monochromator

56

covers a spectral range 350-950 nm, using a grating with 1200 grooves/mm blazed at 500 nm and spectral band pass 0.1 Å.
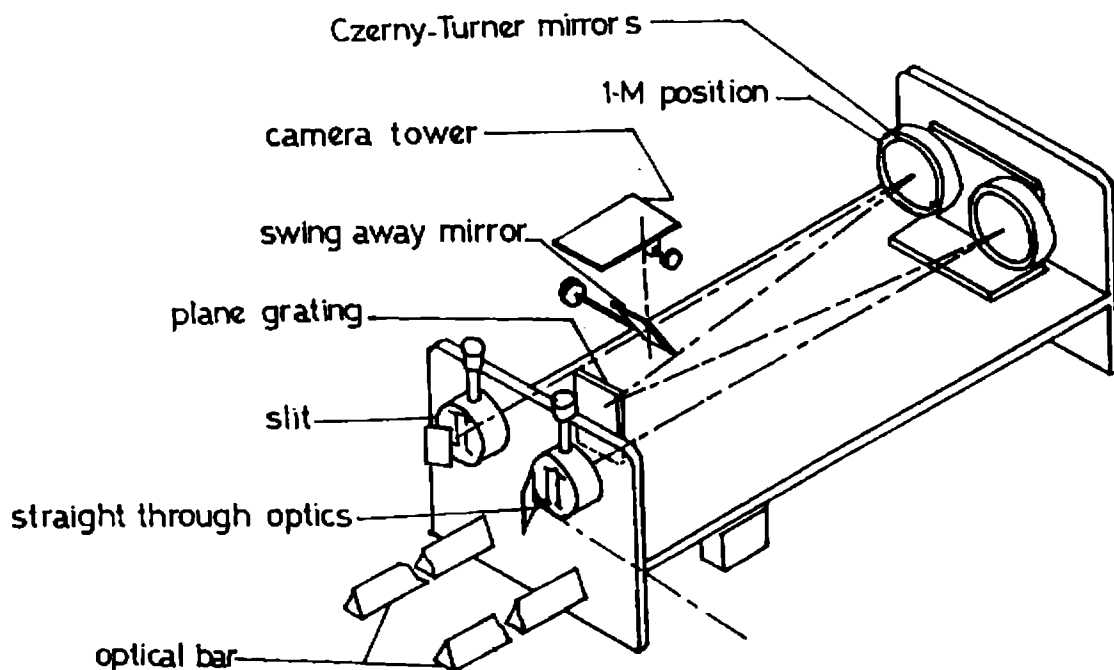

Fig.2.4 Optical layout of the Spex monochromator

The start and end position of the scan and rate of scanning can be programmed using a microprocessor controlled compudrive arrangement. The output of the Spex monochromator is coupled to a thermoelectrically cooled photomultiplier tube (Thorn EMI, model KQB 9863, rise time 2 ns).

2.2.3.2 Photomultiplier tube (PMT)

The photomultiplier combines photocathode emission with multiple cascade stages of electron amplification to achieve a large amplification of primary photocurrent within the envelope of the phototube with the output current of the PMT remaining proportional to the input light intensity[6]. The built-in amplifier system of the PMT containing a series of secondary electrodes (dynodes) may have up to 15 amplification stages, such that one photoelectron can give rise to as many as 10^8 electrons reaching the anode. It is this anode which provides the signal current that is read out. The sensitivity of a

typical PMT can be varied by changing the voltage applied to the cathode and dynodes. The ultimate sensitivity is limited by the dark current which is caused by the ejection of electrons from the cathode by thermal activation or by traces of radioactivity in the surroundings causing luminescence of the envelope.

For a large number of applications, the PMT is the most practical sensitive detector available. The basic reason for the superiority of the PMT over other detectors is the secondary amplification which makes it uniquely sensitive among photosensitive devices currently used. The PMT has a photocathode in either a side-on or a head-on configuration. The side-on type receives incident light through the side of the glass bulb, while the head-on type has a semitransparent photocathode (transmission-mode photocathode) and it provides better uniformity than the side-on type having a reflection-mode photocathode. A schematic representation of a typical photomultiplier tube is given in the Fig.2.5.

The Spex monochromator was coupled to a thermoelectrically cooled (-50°C) Thorn EMI photon counting PMT with S-20 cathode with quantum efficiency of 22%. A high negative voltage bias of 1.7-2.1 kV was usually given to the cathode of the PMT[7]. The spectral response of S-20 cathode is shown in Fig.2.6. To minimize the noise in the signal, the output of the PMT is fed to a boxcar averager.

2.2.3.3 Gated Integrator and Boxcar averager

During pulsed laser experiments, a form of gating and averaging is required so as to have a higher S/N ratio. The gated integrator and boxcar averager is used for analysing the noisy, transient, repetitive signals which are characteristics of experiments with pulsed lasers. We have been using a boxcar averager (Stanford Research Systems) for signal averaging and gating.

The main modules of the system used in the present studies are

(1) Gated integrator and boxcar averager module (SR250)

(2) Gate scanner module (SR200)

(3) System mainframe (SR280)

(4) Display module (SR275)

(5) Computer interface module (SR245)
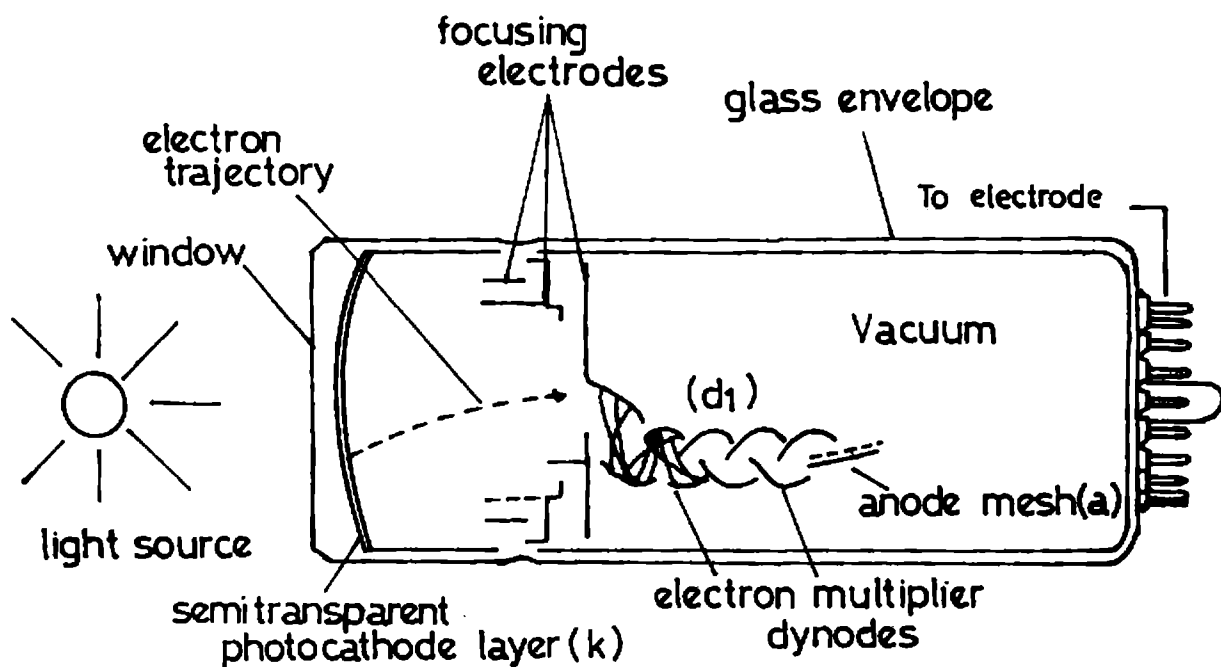
(6) Data acquisition program (SR270)

58

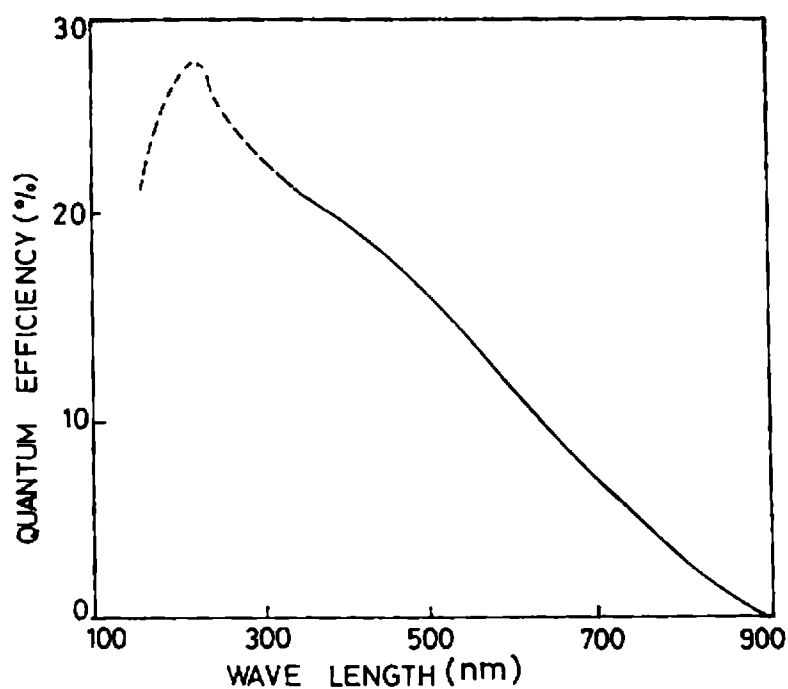Fig.2.5 Schematic representation of a typical photomultiplier tube.

Fig.2.6 Spectral response of S-20 cathode.

The Stanford Research Systems SR250 module consists of a gate generator, a fast gated integrator and exponential averaging circuitry. The gate generator, triggered by the laser pulse, provides an adjustable delay from a few ns to 100 ms, before it generates a continuously adjustable gate the width of which can be varied from 2 ns to 15 ms[8]. The delay may be set by a front panel potentiometer. The signal at the gate is integrated by the fast gated integrator and is normalised by the gate width to provide a voltage which is proportional to the part of the input signal level at the gate. The sensitivity control of the boxcar averager provides further amplification of the signal. By fixing the delay and the gate width, the voltage from the part of the signal pulse alone is measured and improvement in the signal to noise (S/N) ratio of the detection is achieved. A moving exponential average of 1-10,000 samples are available at the averaged output. This traditional averaging technique is useful for pulling out small signals from noisy backgrounds. As one averages many noisy samples of a signal, the average will converge to the mean value of the signal and the noise will average to zero. Usually the signal was averaged for 10 sucessive pulses. Averaging over very large number of pulses increases the S/N ratio, but the time response of the system will suffer.

The SR200 gate scanner provides the signal needed to scan the SR250's delay multiplier (to scan the sample gate through the wave form) and to control the oscilloscope. Single or multiple scans may be done in the forward or reverse direction over any portion of the waveform. The X-axis output always ramps between 0 and 10 Vdc, regardless of the dial settings, providing a convenient interface to chart recorder.

The SR280 and SR275 provides the power necessary to the SRS modules and has three displays for monitoring the outputs. The SR245 computer interface is a versatile module capable of providing a variety of scanning, counting and communication functions. The SR270 is a software designed to acquire, display and manipulate data taken from the SR250 Boxcar integrator with the SR245 computer interface module. The system is connected to the personal computer through the serial port.

2.2.4. Experimental setup for fluorescence studies

The 532 nm beam from the pulsed Nd:YAG laser was used as the excitation source. For the measurement of the degree of polarisation, a polariser was kept in the emission

60

beam path. The samples were of size (13x10x1.5) mm^3 and were mounted in such a way that fluorescence emission was collected from the front surface to avoid reabsorption of the emitted light. Using collimating optics, the emission was made to fall onto the entrance slit of the Spex monochromator to which a PMT is connected head-on. Proper filters were used to avoid the entry of the scattered laser radiation into the monochromator. The emission was wavelength scanned in the desired region and the optical intensity was detected by the Thorn EMI photomultiplier tube. The signal from the PMT is gated and averaged using the gated integrator and boxcar averager and its output is interfaced to the computer to obtain the fluorescence spectrum.

2.3 Instrumentation for gain spectroscopy

Interest in investigating stimulated emission from organic dyes has made it necessary to develop a system that will measure gain of the medium. The spontaneously emitted photons travelling along the path of the exciting pulse in dyes are amplified by stimulated emission. Using ASE, gain and other related properties of the laser active medium can be found. Gain spectroscopy can provide information which are not available from ordinary absorption and emission spectroscopy[9]. The experimental setup and the principal hardware components of the gain spectroscopy are similar to that of fluorescence studies, with the exception that the excitation beam is focused onto the sample using a cylindrical lens, so that larger area of the medium is excited. Also the emission is observed with a transverse geometry in which the detection system is kept in a direction perpendicular to the excitation beam.

The experimental setup consists of a source of excitation, the sample holder, and the detector. The discussion of these components are given in sections 2.2.1 - 2.2.3. The gain studies were done by varying the excitation intensity as well as the dye concentration in the sample. For measuring the laser energy during the experiment, a laser power energy meter was used. For temporal studies, a computer interfaced digital storage oscilloscope was used to monitor the PMT output.

2.3.1 Laser power energy meter

In order to measure the power output at 532 nm a laser power meter (Scientech model 362) was used. The detector is a disc calorimeter that employs a calibrated thermopile

61

which generates a voltage proportional to the heat that is liberated from the absorption of the input laser flux. Many thermoelectric junctions are arranged in series and sandwiched between the absorption surface which produces heat due to laser absorption. The heat flow is proportional to the power output of the laser beam and substantially independent of the laser beam spatial distribution. The thermopile output is a linear low impedance, dc signal of approximately 0.09 volts/Watts[10]. It has flat spectral response in the region of 400 nm to 1200 nm, and can be used with CW and pulsed lasers for measuring from 0 to 10 Watts.

2.3.2 Digital storage oscilloscope

A digital storage oscilloscope from Tektronix, 100 MHz, (TDS 220) was used to monitor the signal from the PMT. It has a 1 GS/s sampling capability with storage and averaging facilities. The oscilloscope was synchronised with the laser pulse. RS232 communication port was used for transfering data to the personal computer for futher processing[11].

2.3.3 Experimental setup for gain spectroscopy
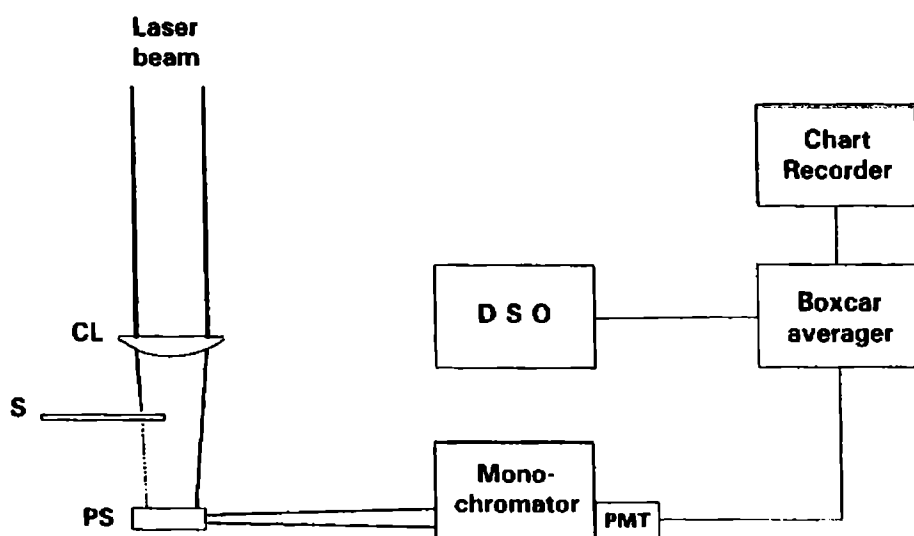
CL-Cylindrical lens, S-Shutter, PS-Polyacrylamide sample, PMT-Photomultiplier tube. DSO-Digital storage oscilloscope.

Fig.2.7 Schematic experimental setup for gain spectroscopy

The schematic of the experimental setup is shown in Fig.2.7. The 532 nm, 10 ns pulses from an Nd:YAG laser (Quanta-Ray DCR-11) is used as the pump laser source. A cylindrical lens is used to focus the beam to a line onto the sample, thereby defining the gain region. By using an optical shutter the length of the pumped region can be varied from L to L/2 where L is the length of the sample. The ASE output was taken from the transverse direction and was allowed to fall onto the slit of a one meter Spex monochromator (1200 grooves/mm, 100 mm by 100 mm grating blazed at 500 nm). The output from the monochromator was passed through a thermoelectrically cooled Thorn EMI photomultiplier tube (PMT, model KQB 9863) which was coupled to a boxcar averager/gated integrator (Stanford Research Systems, SR250) and interfaced to a computer using SR270 data acquisition program. For temporal studies a computer interfaced Tektronix 100 MHz storage oscilloscope was used.

2.4 Photothermal phase shift spectroscopy

For the application of polymers as host-matrix, the resistance to laser damage is of vital importance. Photothermal phase shift spectroscopy (PTPS) was used to study the damage threshold of these matrices[12]. The idea of PTPS is simple: a laser beam (pump beam) passing through the medium causes heating of the medium of interest. The heating modifies the refractive index of the laser irradiated region. The change in the refractive index of the medium is detected by a low power laser beam (probe beam).

The principal part of PTPS consists of a Michelson Interferometer (MI). For the construction of the MI, a 5 mW He-Ne laser was used as the light source along with two highly reflecting end mirrors equidistant from the beam splitter so that interference fringes are obtained. On one of its arm, close to the beam path, the sample whose damage threshold is to be measured is kept. A focused high power Nd:YAG beam is allowed to fall on the sample, which produces plasma when the laser intensity is above damage threshold. The presence of the plasma causes a refractive index variation in the path length of the probe beam, which can be detected as fringe shift in the MI. The shift in the interference fringe produced can be measured as intensity variation over an optical detector which is position sensitive. An optical fiber was used for this purpose. One end of the fiber acts as an aperture to sample the variation of

probe beam intensity. The other end of it is introduced into the monochromator-PMT assembly whose output is connected to a digital storage oscilloscope and the fringe shift is measured as a voltage variation. The use of optical fiber introduces a certain amount of geometrical flexibility in the experimental setup.

The description of most of the instruments were given in the above sections. He-Ne laser which is used as a probe beam in PTPS and power meter to measure the 1.06 μm radiation incident on the sample while studying the damage threshold are described in the following sections.

2.4.1 He-Ne laser

As the probe beam in PTPS we have used 632.8 nm emission from a He-Ne laser (Model 105-1, Spectra Physics). It has TEM_{00} mode, with a power of > 5 mW. The beam divergence is 1 mrad[13].

2.4.2 Power meter

In order to measure the energy of 1.06 μm radiation, pulsed laser energy monitor (Delta Developments) was used. This is an on-line energy meter and uses a polarisation compensated beam splitter to sample the beam, 85% of which is transmitted[14]. The sampled beam strikes a retroreflecting diffuser and reaches the photo-diode via a 'range plate' which attenuates the light appropriately for the range of energies being measured. The geometry of the energy meter is such that all positions on the diffuser give equal signals. Different range plates can be used for different energies and wavelengths being measured. The wavelength response of the energy meter can be varied from 200 nm to 1100 nm. Each range plate gives a factor of 30 in the energy giving full scale deflection. It has a usable range of 100:1. A switch allows readings to be referred to either the energy entering or leaving the instrument. BNC sockets provide pulse shape, pulse energy, trigger input, trigger output etc. The energy meter can be triggered externally with laser pulses or internally.

2.4.3 Experimental setup for phase shift spectroscopy

The basic element of PTPS is a Michelson Interferometer, with a 5 mW He-Ne laser beam as the light source (probe beam), as shown in Fig.2.8. The optical setup is aligned so as to get a well defined fringe pattern. The beam in one of the arms of MI

passes parallel and very close to the target surface. High power laser radiation from a pulsed Nd:YAG laser (pump beam) at wavelengths 1.06 μm and 532 nm were focussed on to the target in order to produce plasma.
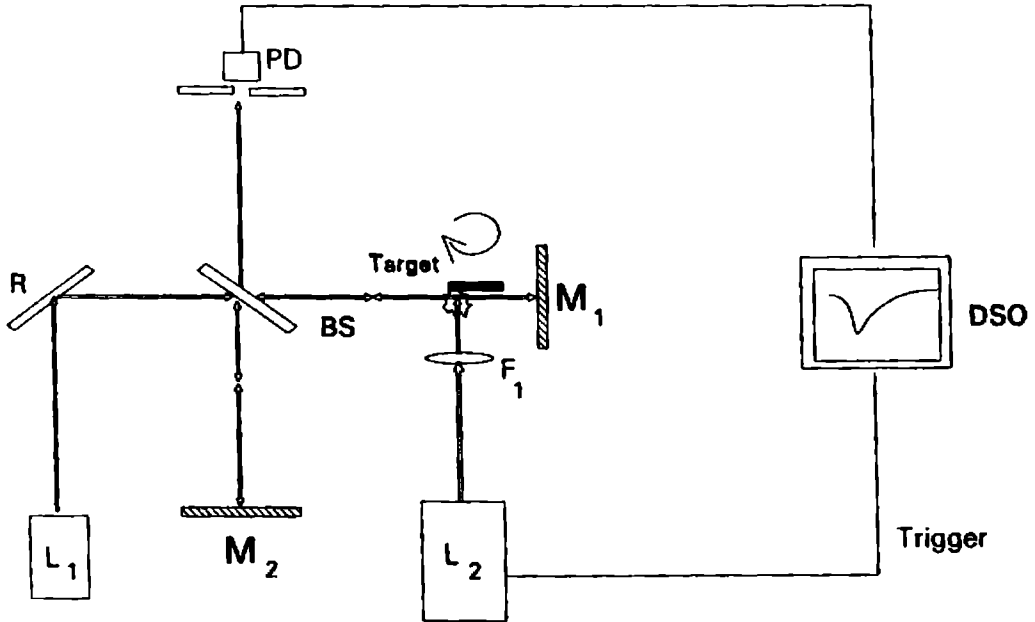
L_1-He-Ne laser, L_2-Nd:YAG laser, M_1, M_2-Mirrors, BS-Beam splitter, F_1-Focussing lens, PD-photodiode, DSO-Digital storage oscilloscope

Fig.2.8 Experimental setup for phase shift spectroscopy

The samples used were discs of PMMA and dye doped polyacrylamide. The point of irradiation was shifted by mechanically rotating the target after each measurements so that fresh location is available for each pulse. The probe beam passes grazing the sample surface so that the length of the plasma near the target is taken as equal to the pump laser spot size. The shift in fringe pattern is measured as a voltage change using a PIN photodiode and displayed on the digital storage oscilloscope. The whole setup was properly vibration isolated by using a vibration isolation table. The schematic of the experimental setup for the PTPS is as shown in Fig.2.8.

2.5 Instrumentation for Z-scan technique

Using Z-scan technique which is a simple single beam method, the refractive and absorptive nonlinearity of certain nonlinear materials were studied[15]. The Kerr as well

65

as the thermal nonlinearity can be studied using this method. This technique is based on the principle of spatial beam distortion and has a very high sensitivity.

In Z-scan technique a Gaussian laser beam is used, whose transmittance through a nonlinear medium as a function of sample position Z with respect to the focal plane is measured in the far field with an aperture (closed Z-scan) and without an aperture (open Z-scan) to measure refractive and absorptive nonlinearities respectively. The medium acts as a lens whose effective focal length varies with the incident intensity. When the medium is moved through the focal plane the varying intensity causes changes in the transmission of the beam. This change will be reflected in the intensity distribution at the aperture in the far field. The amount of energy transmitted by the aperture will depend on the sample location on the z-axis and on the sign of the nonlinearity. A Gaussian laser beam is used to induce the nonlinearity, a translator stage moves the sample through an intensity gradient obtained by a focussing lens and a detector to measure the transmittance of the sample are the different parts of the experimental setup. A general account of the equipment necessary for this technique is given below. As the exciting source Ar^+ laser was mainly used. In the case of CW lasers for increasing the ratio of signal to noise Lock-in detection was made use of. Chopper, photodiode and power meter form other parts of the measuring system.

2.5.1 Ar^+ laser

CW Ar^+ laser was also used for Z-scan and emission studies. The Spectra Physics Model 171 CW Ar^+ laser system gives high CW laser output power[18]. It consists of a laser head, power supply and a separate power meter to monitor the output power. The laser head houses the beryllium oxide plasma tube and optical resonator structure. The power meter continuously monitors the output power and the output laser power varies only within $\pm 5\%$ over periods of days. The major wavelengths of the laser output are 514.5, 496.5, 488, 476.5 and 457.9 nm. The laser has a water cooling system that cools the plasma tube.

2.5.2 Translator and sample holder

A motorised translator was used to move the sample along with the holder through the focal plane. It is graduated and the focusing lens is adjusted so that the focal point

comes at the middle of the translator. The height of the sample holder with cuvette mounted on it can be adjusted.

2.5.3 Detector

For the measurement of absorptive nonlinearity the total transmitted power through the sample was measured. For this Scientech power meter with large aperture was used. The details of the power meter was described in section 2.3.1. In order to measure the refractive nonlinearity in the far field the transmittance of the sample with an aperture was done. A silicon photodiode was used for the measurements.

2.5.3.1 Silicon photodiode

HP-4207 silicon planar PIN photodiodes are ultra-fast light detectors for visible and near infrared radiation[17]. The speed of response of these detectors is less than one nanosecond. Laser pulses shorter than 0.1 ns may be observed. The frequency response extends from dc to 1 GHz. It has a sensitivity of NEP < -108 dBm.

2.5.4 Mechanical chopper

Mechanical choppers are designed to be used with a Lock-in amplifier for the purpose of synchronous detection. The optical chopper Model SR 540 C from Stanford Research systems was used in the present experiments[18]. It is used to square wave modulate the intensity of optical signals. The chopping frequency can be varied from 4 Hz to 400 kHz with a frequency stability of 250 ppm. It also provides the reference signal to the Lock-in amplifier.

2.5.5 Lock-in amplifier

Lock-in amplifiers are used to detect and measure very small ac signals. Accurate measurements may be made even when the small signal is obscured by noise sources even thousand times larger. They use phase sensitive detection to single out the component of the signal at a specific reference frequency and phase. Lock in measurements require a frequency reference. Typically an experiment is conducted at an optimized frequency from an optical chopper. The lock-in detects the response from the experiment at the reference frequency. The Lock-in amplifier used was SR 850 DSP from Stanford Research Systems[19]. It has a full scale sensitivity of 2 nV to 1 V with a CMRR of 90 dB.

67

The spectral data can be stored in a 3.5 in diskette or the instrument can be diretly interfaced to a personal computer.

2.5.6 Experimental setup for Z-scan

The experimental setup, along with theoretical details for Z-scan is given in Chapter I. A cuvette of thickness 0.49 cm was moved along the intensity gradient produced by a focusing lens of focal length 18 cm. The absorptive nonlinearity was measured by monitoring the input and output laser powers using a power meter. Using Ar^+ laser thermal nonlinearity produced has been measured. For detecting the absorptive nonlinearity, a powermeter was used, but for the refractive nonlinearity in the far field (with aperture) a silicon pin diode connected to a Lock-in amplifier for detection was used. Triggering of the lock-in amplifier was done using the output from a mechanical chopper. For studying the Kerr nonlinearity high power Nd:YAG laser was used.

2.6 Conclusions

The various aspects of the instrumentation used for the nonlinear and radiative studies are described in this chapter. Some variation in the instrumentation was necessary for further studies in nonlinearity which are described in the relevant sections.

References

[1] Joseph R Lakowicz, 'Principles of Fluorescence Spectroscopy', Plenum press, New York, (1986) .

[2] Instruction manual, Nd:YAG laser, Quanta Ray DCR 11.

[3] Parker C A, 'Photoluminescence of Solutions', Elsiver, Amsterdam (1968).

[4] 'Standards in Fluorescence Spectrometry' Ed. J N Miller, Chapman and Hall, (1981).

[5] Instruction manual, Monochromator, Spex 1704 Spectrometer Spex USA, Instruction manual, Spex CD 2A Compudrive, Spex USA.

[6] David L Andrews and Andrey A Demidov, 'An Introduction to Laser Spectroscopy', Plenum press, NewYork, (1995).

[7] Instruction manual, Photomultiplier tubes, EMI.

[8] Instruction manual, SRS Boxcar Averager and Gated Integrators, Stanford Research Systems.

[9] C V Shank, A Dienes and W T Silfvast, Appl. Phy. Lett., 17, 307, (1970).

[10] Instruction manual Scientech 362 power energy meter.

[11] Instruction manual, Digital Storage Oscilloscope, Tektronix Co.

[12] B Monson, Reeta Vyas, and R Gupta Appl. Optics, 28, 2554, (1989).

[13] Instruction manual, Scientific Helium-Neon laser, Spectra Physics.

[14] Instruction manual, Laser Energy Meter, Delta Developments.

[15] M. Sheik-Bahae, Ali A. Said, Tai-Huei Wei, David J. Hagan, E.W.Van Stryland, IEEE J. of Quant Electron. 26, 760, (1991).

[16] Instruction manual, 171 Argon Ion laser, Spectra Physics.

[17] 'Optoelectronics Design Catalogue' Hewlett Packard.

[18] Instruction manual, Optical chopper, SR540, Stanford Research Systems.

[19] Instruction manual, SR850 Lock-in amplifier, Stanford Research Systems.

CHAPTER III

STUDIES ON DYE DOPED POLYMERS

Abstract

The fluorescence and amplified spontaneous emission characteristics of rhodamine 6G impregnated in polyacrylamide is reported in this chapter. Using amplified spontaneous emission gain radiative and related properties of this dye doped matrix was measured. It was found that photostability of rhodamine 6G is unusually high in this matrix compared to other polymer hosts like polymethylmethacrylate.

3.1 Introduction

Transparent polymeric materials have found one of their most promising applications in lasers, in which they can be used as active elements with lasing dyes, antireflective filters for Q-modulation, laser optics etc.[1-4]. The solid matrix-dye lasers make possible the combination of the advantages of solid state lasers with the possibility of tuning the radiation over a broad spectral range, which overlaps almost completely the visible region. Polymers like polymethylmethacrylate (PMMA), polyurethane, sol gels and silica gels etc. can be employed as matrices for impregnating laser dyes[5-10]. The basic requirement of the polymeric matrix being the transparency in the region from UV to 1.3 μm as well as resistance to optical damage at the pumping wavelength.

3.2 Dye doped polymers

The most attractive and distinguishing feature of the organic dye lasers is their tunability over the visible region of the spectrum. This is because of the broad absorption as well as emission band in the visible region. In most conventional dye laser systems, the active medium is contained in a flowing dye solution, which eliminates the need for cooling and reduces the bleaching effect. But the disadvantage is that they are subject to stagnation and evaporation, thereby requiring periodic replacement of the solution or addition of solvents. Such systems are elaborate, i.e., neither lightweight nor compact. These drawbacks can be eliminated by replacing the dye liquid with an inexpensive, lightweight, disposable dye doped solid polymer-host. The first polymer-host dye laser was reported in 1967[11].

By now almost the entire visible range has been covered by different polymer-host devices. The photochemical processes that take place in these systems are discussed in the next section. The relatively low usage of polymers in high power laser systems is their comparatively low optical strength (i.e., low laser damage threshold). Chapter IV reviews the causes of this low laser damage threshold and measure the value of the damage threshold using the technique of photothermal phase shift spectroscopy.

3.2.1 Photochemical properties of doped polymer

The number of dyes available, as active dopants for lasers, has notably increased the

72

number of light transmitting polymers. The spectral luminescence and lasing properties of the active elements are determined both by the properties of the luminophors and the polymeric matrix into which they are incorporated and also by their interaction in the process of operation. The polymeric base affects the location of the absorption and luminescence maxima of the luminophor[12]. It should be noted that the photochemical resistance of most of the dyes depend on the nature of the polymeric medium.

Photobleaching is the light-induced fragmentation of the active laser dye molecules into components that no longer absorb at the pump wavelength. It is an irreversible process, which is delirious to laser action in doped polymer hosts. Photobleaching and its severity in dye lasers were first studied by Ippen et al[13]. From their studies it was shown that the bleached dye molecular fragments did not absorb in the visible portion of the spectrum. The first report of the observation of photobleaching in polymer-host dye lasers were made by Kaminov et al[14]and also Ulrich and Weber[15]. The Benzrodnyi et al.[8] have studied the photobleaching of dyes doped into polymeric matrices, which enabled them to identify the main causes of photodecomposition.

3.2.1.1 Interaction of dye molecules with free radicals

After polymerisation, the solid matrix always contains unreacted molecules of the initiator which form free radicals during subsequent illumination within the absorption region (for example during operation of the laser element). These free radicals attack and destroy the closely packed molecules of the dye. An effective method for eliminating this channel of photodecomposition is neutralisation of unreacted molecules of initiator.

The reviews of Bezrodnyi et al.[16] and Gromov et al.[17] have discussed in detail the effect of impurities, particularly free radicals. Bezrodnyi et al. have reported that laser dyes with extended π electron system are very sensitive to the action of free radicals and hence prone to photobleaching. He has shown that polyurethane doped with the dye PK-890, bleaches faster than rhodamine 6G which has much shorter π electron chain, in the same matrix. It is the residual initiator molecules which doesnot participate in the polymerization process, that generate free radicals later during device operation and cause photobleaching.

Gromov et al[17] have suggested that instead of polymerisation initiator being the

73

source of destructive free radicals, radicals are produced from polymer molecules when the dye and polymer molecules interact during vibrational relaxation of the excited electronic states of the dye. Photobleaching occurs when the radical product induces the excited dye molecule to lose an electron, thereby producing a reduced and inactive form of dye. To reduce photobleaching, they suggested the use of additives in the polymer matrix that would retard the generation and branching of free radical chains by inducing cross relaxation between the vibrational levels of the polymer molecules and those of the additives and also found that with the addition of carbonic acid ether, the conversion efficiency decreases only slowly.

Stringent requirements are placed for the manufacture of polymers like careful purification of luminophor, repeated distillation of the monomer, temperature control to ensure optical uniformity, degassing the initial solution to avoid slow polymerisation in the presence of gaseous inhibitors etc. to mention a few. Kaminov et al.[18], from the studies of bleaching of dyes in epoxy and PMMA concluded that impurities play a greater role than matrix rigidity in photobleaching.

3.2.1.2 Interaction with atmospheric oxygen dissolved in the matrix

On exposure of organic dye molecules to light with a maximum corresponding to long wavelength absorption band (500 to 1000 nm), photoaddition of molecular oxygen takes place. The quantum efficiency of photo-oxidation depends on the molecular structure of the organic dyes. Thus for polymethene dyes with similar terminal heterocycles but differing in the length of polymethene chain, elongation of the conjugated chain leads to an increased fraction of decomposed molecules[8]. Study of this process revealed the formation of a variety of intermediate products and subsequent formation of colourless dyes. These results show that the photoresistance of organic dyes can be improved appreciably by the removal of atmospheric oxygen from the matrix and neutralisation of the initiator molecules.

3.2.1.3 Effect of temperature

Basic studies to understand and reduce photobleaching were done by Fork and Kaplan[19], Kaminov et al.[18] and Reich and Neumann[20]. Fork and Kaplan have found that, if rhodamine 6G doped PMMA samples were cooled to 193 K, only 22% of the dye

74

was bleached. The cooling either reduces the mobility of the impurities that catalyse the dye photodegradation process or increases the microscopic rigidity of the polymer macromolecules surrounding the dye molecules. This rigid macromolecules would act as a protective polymer cage that becomes more rigid with lower temperatures.

Photobleaching studies of the samples after heat treatment was done by Higuchi and Muto[21]. Rhodamine 6G doped copolymer [MMA and methylacrylate] showed an improved resistance to photobleaching when heat treated at 353 K for 4 days. But if the heat treatment temperature is close to the glass transition temperature of the material, significant thermal bleaching of the dye occurred. Gromov et al.[22] have predicted the existence of two different mechanisms of photodestruction of xanthene dyes in polymeric matrices, radical and anionic. These are given in detail in Chapter IV. Inspite of the disadvantages described above, doped polymers are useful in a variety of applications, some of which are described in the next section.

3.3 Applications of dye doped polymers

Fluorescent polymers and polymer formulations are extensively used in various fields of science and technology. There are different fields like nuclear power engineering, the exploration of outer space, the application of radioactive isotopes in chemistry, biology, medicine etc., which require reliable methods of ionising radiation detection. In scintillation method, the ionising radiation energy is transformed into light energy in the detector, with the subsequent recording of the light energy by a photomultiplier tube. Plastic scintillators which are polymer scintillation formulations or compounds are also of much use in some of the applications noted above.

Recently, there has been a growing interest in making use of dye doped polymers to harness solar energy. At present, photoelectric generators are, uncompetitive with regard to the cost of 1 kWh of electric power and the efficiency of photoelectric converters is low. To improve the efficiency, luminescent polymer solar concentrators (LSC) can be used[23]. Thin film dye laser oscillators and related devices, utilizing the waveguiding properties hold great promise as active elements in integrated optical networks on which future communication systems may be based, though a rather serious difficulty may be the photobleaching of the organic dye molecules which limits the life of such active thin-film waveguides.

The advent of lasers has initiated immense advances in the field of optoelectronics, especially in the development of light modulators, frequency mixers, and other non-linear devices which are useful in the field of optical communications[24,25]. Thin-film dye laser amplifiers and oscillators are important elements which can be incorporated in integrated optical systems since they can eliminate the use of discrete elements, such as prism or grating couplers, to couple light from the outside into waveguiding films. Moreover, nonlinear saturation behavior may enable them to take over some of the tasks of other nonlinear devices like spatial light modulators. With so many applications to its credit it is worth exploring other polymeric matrices, which may have higher photostability as well as damage threshold. In the following sections the characteristics of a novel porous polymer, polyacrylamide is described.

3.4 Polyacrylamide

Polyacrylamide is a synthetic polymer of acrylamide monomer and is prepared from highly purified reagents. The basic components for the polymerisation reaction are commercially available at reasonable cost and high purity. In addition, polyacrylamide gel is chemically inert, stable over a wide range of pH, temperature and ionic environments and is highly transparent.

3.4.1 Chemical structure

Polyacrylamide gel results from the polymerisation of the acrylamide monomer into long chains and the cross linking of these by bifunctional compounds such as N,N'-methylene bisacrylamide (usually abbreviated as bisacrylamide) reacting with free functional groups at chain termini. Other crosslinking reagents have also been used to impart particular solubilization characteristics to the gel for special purposes. The structure of the monomers and the final gel structure are shown in Fig 3.1.

3.4.2 Preparation and properties of polyacrylamide gel

3.4.2.1 Reagents required for the gel preparation

Acrylamide and bisacrylamide (30:0.8): Both acrylamide and bis acrylamide monomers are highly toxic if absorbed by skin or inhaled as monomer powders. Once polymerisation has occurred, the resulting polyacrylamide gel is non-toxic. The purity of most commercially available monomers is adequate to get good quality polymer. The

76

stock solution is prepared by dissolving 30 gm of acrylamide and 0.8 gm of bisacrylamide in a total volume of 100 ml of double distilled water. The solution is filtered through Whatman No.1 filter paper. The acrylamide-bisacrylamide solution should not be kept for long periods since hydrolysis of acrylamide monomer occurs to yield acrylic acid and ammonia.

Ammonium persulphate (1.5%): 0.15 g of ammonium persulphate is dissolved in 10 ml of water. This solution is unstable and should be made fresh just before use.

N,N,N'N'-Tetramethylethylenediamine (TEMED): The TEMED used is a colourless liquid. It must be kept in a dark bottle and undiluted form at $4^\circ C$ to remain stable.
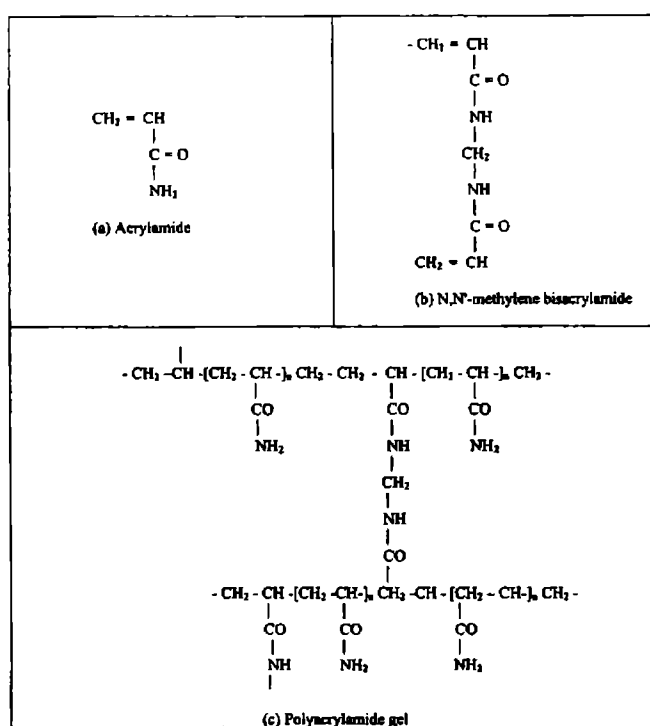

Fig.3.1 Chemical structure of acrylamide, N,N'-methylene bisacrylamide, polyacrylamide gel

3.4.2.2 Polymerisation catalysts

Polymerization of acrylamide is initiated by the addition of ammonium persulphate. In addition N,N,N'N'-Tetramethylethylenediamine (TEMED) is added as accelerators of

the polymerization process. In the ammonium persulphate-TEMED system, TEMED catalyses the formation of free radicals from persulphate and these in turn initiate polymerization. Since the free base of TEMED is required, polymerization may be delayed or even prevented at low pH. Increase in either TEMED or ammonium persulphate concentration increases the rate of polymerisation.

3.4.2.3 Preparation of slab gels

The slab gel plates are to be perfectly cleaned to obtain good gel adhesion to glass. Clean the glass plates by soaking them in chromic acid overnight, rinse them in water, and then with ethanol. Put the plates on a clean tissue paper, with the side which is to be in contact with the gel uppermost and swab it with acetone-soaked tissue held in a gloved hand. After a final rinse with ethanol, allow the plates to air-dry. The glass plates are held in the correct distance apart by thin plastic spacers which are of uniform thickness. Usually three spacers are used, one for each vertical side and one for the base of the glass-plate assembly. These are sealed by dripping molten agarose around the edges of the assembly. The plate assembly is clamped together with strong metal clips just over the spacer position. While pouring the gel the plate assembly is held vertical. 10 ml of acrylamide-bisacrylamide (30:0.8), 1.5 ml of 1.5% ammonium persulphate and 18.5 ml of water was taken in a small thick-walled flask. After degassing this mixture for 1 min TEMED was also added and transferred without delay to the glass mold. After about 30 minutes the gel polymerize to form polyacrylamide.

3.4.2.4 Effective pore size

Polyacrylamide is widely used in electrophoresis, for the separation of proteins. The effective pore size of the polyacrylamide gels is greatly influenced by the total acrylamide concentration in the polymerisation mixture, effective pore size decreasing as the acrylamide concentration increases. Gels with concentrations of acrylamide about 30% can trap molecules with relatively low molecular mass hence is useful in the case of laser dyes like rhodamine 6G. The porous nature of polyacrylamide helps the stability of dye in the matrix.

3.5 Studies on rhodamine 6G doped polyacrylamide

3.5.1 Introduction

The first important step in exploring the feasibility of a doped polymer is the demonstration of optically pumped luminescence and stimulated emission, gain and lasing from the prospective active medium. The spontaneously emitted photons travelling along the path of the exciting pulse in dyes are amplified by stimulated emission. In order to study the gain of the medium, this amplified spontaneous emission (ASE) characteristics is helpful.

Dye doped medium, even if excited, by moderate pump energies can have very high optical gain. In such case the spontaneous emission is amplified as it propagates along the line shaped excited volume and forms a low divergence beam which is called amplified spontaneous emission. It, at times, act as a background noise in the case of strong pumping intensities. But it has also been developed by some workers as a new light source. In this chapter, details of the work done on the fluorescence as well as the ASE characteristics of rhodamine 6G doped polyacrylamide are presented.

3.5.2 Experimental details

The host matrix viz. polyacrylamide is prepared from the monomer, acrylamide along with bisacrylamide taken in the ratio 30:0.8 gm per 100 ml of distilled water. 1.5 ml of ammonium persulphate (1.5%) is added to 10 ml of the above solution along with 18.5 ml double distilled water. 0.15 ml of N,N,N'N' Tetramethyl ethylenediamine is added as a polymerizing agent. The whole solution is transferred to a mold made of two glass plates with a separation of 1.5 mm and kept until the polymerization is complete. The details of the preparation is given in section 3.4. The polymer samples were immersed in rhodamine 6G-methanol solution with known concentration and taken out after about 36 hours when it was well stained with dye molecules. The adsorption and desorption dynamics of the laser dyes on porous silicate sol-gel glasses were described in detail by Penzkofer et al. in a recent article[27]. The samples were dried at room temperature and then used for further studies. The concentration of the dye molecules in the samples were estimated from the transmission measurements of the remaining solution using a spectrophotometer. The samples were found to be

highly fluoresceing under lase excitation. The experimental details of the fluorescence and gain measurements employed in the present work is described in Chapter II.

3.5.3 Intensity dependent studies on Rh 6G doped polyacrylamide

The sample used for intensity study has a dye concentration of 4×10^{-4} m/l. All the measurements made here is for this concentration unless specified otherwise. Fluorescence measurements were done under low pump laser intensity with front surface emission configuration to avoid reabsorption whereas for ASE transverse measurements are preferred. For the measurement of the degree of polarisation, a sheet polarizer (Melles Griot) was inserted before the monochromator with polarisation direction parallel or perpendicular to the polarisation of the excitation beam. The fluorescing laser dye rhodamine 6G has been found to be uniformly adsorbed in the solid matrix polyacrylamide.
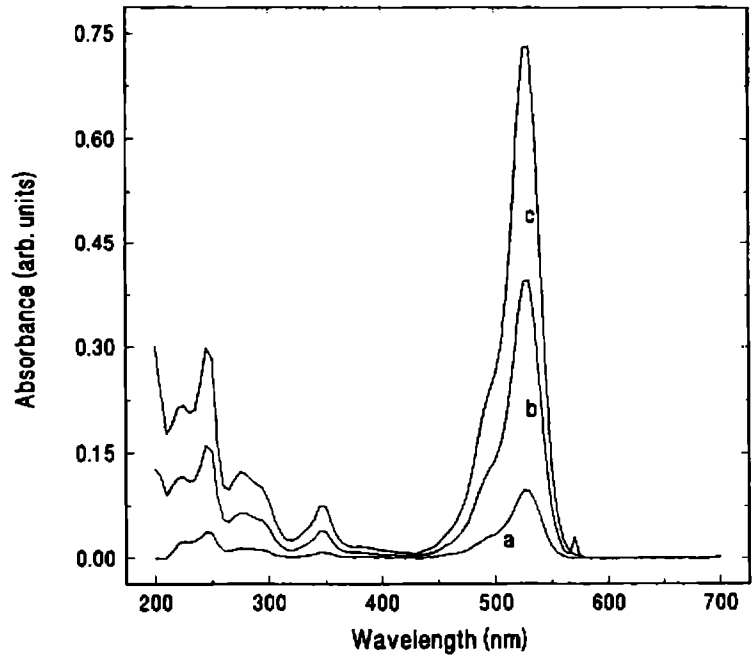

Fig.3.2 Absorption spectrum of the dye doped polyacrylamide at different concentrations. (a) 1.9×10^{-4} m/l, (b) 4.6×10^{-4} m/l, (c) 1.3×10^{-4} m/l. The absorption spectrum is similar to that of dye solution

80

Fig.3.2 shows the absorption spectrum of the polymer sample doped with rhodamine 6G obtained with a Perkin-Elmer Lambda spectrophotometer. There is a strong absorption band around 514 nm similar to that of rhodamine 6G in solution. The input laser light from the frequency doubled Nd:YAG laser was line focused onto the sample using a cylindrical lens. The length of the irradiated region was about 1 cm. The dye molecules absorb the green laser light. The optical absorption cross section of the dye molecules depends on their orientation relative to the pump beam polarisation[28].

The excited molecules emit light polarised in the plane formed by the transition moment and the propagation direction. The emission cross section depends on the angle ψ between the transition vector and the propagation direction by the relation[29]

$$\sigma_{em} = \sigma_{em}(0)\sin^2\psi \tag{1}$$

This emission cross section is maximum along the direction given by $\psi = \pi/2$ since the input laser light is linearly polarised. The molecular reorientation during the laser pulse does not take place effectively due to the rigid solid matrix. Thus during amplification of spontaneous radiation, the emission is highly anisotropic and it is mostly concentrated perpendicular to the pump beam propagation direction. But at low laser intensities, the fluorescence emission is isotropic which does not show any directional effects.

The transverse excitation geometry for ASE measurements has some advantages over longitudinal excitation, such as the uniform distribution of pump laser energy in the travelling direction, easy synchronisation between pump and ASE pulses and least restriction on concentration of dye that could be used etc.[30]. Moreover high gains in dye medium can be achieved since a long region of small width was excited by focusing the pump laser beam with a cylindrical lens.

The ASE intensity corresponding to full length pumping of the sample I_L at wavelength λ in the monochromator slit kept at a distance p (p $\gg$ L) is[31]

$$I_L = \frac{C}{\alpha_\lambda}p^2[\exp(\alpha_\lambda L) - 1] \tag{2}$$

where α_λ is the gain coefficient at the wavelength λ and is a constant. Writing a similar equation for half length sample pumping ($I_{L/2}$) and combining we get

81

$$\alpha_\lambda = \frac{2}{L} \ln \left[\frac{I_L}{I_{L/2}} - 1\right] \tag{3}$$

Thus by exposing the full and half lengths of the sample and by measuring the corresponding ASE intensities the single pass gain of the medium can be deduced.
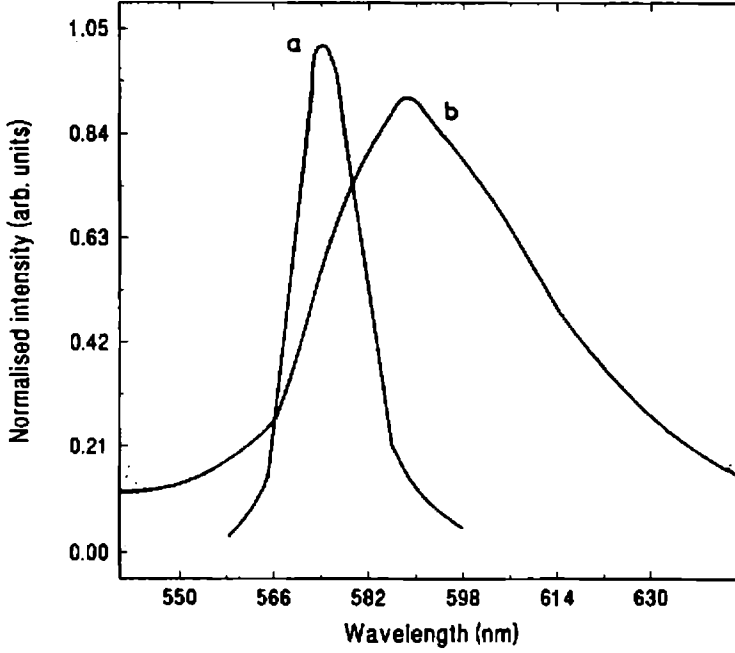

Fig.3.3 (a) Transverse amplified spontaneous emission, (b) fluorescence emission spectra from the polymer sample pumped with a laser intensity of 2.2 GWcm^{-2} and slit width of the monochromator is 6 μm and 100 μm respectively

Fig.3.3 shows the fluorescence spectrum as well as the ASE spectrum from the dye impregnated polymer sample. The two spectra were recorded with different monochromator slit widths since the intensity of ASE is very high compared to the fluorescence intensity. The amplified emission is concentrated along the direction perpendicular to the pump laser beam with an angular distribution of about 0.2 radians. There exists a threshold pump intensity for ASE at around 0.1 GWcm^{-2} for 532 nm radiation. The typical full width at half maximum (FWHM) of the fluorescence spectrum is 100 nm whereas for the ASE spectrum it is around 8 nm. Decrease in emission bandwidth is

one of the characteristics of ASE and it is the frequency dependence of the fluorescence emission cross-section σ_{es} which results in spectral narrowing[28,32]. The frequency components with the largest emission cross sections are most effectively amplified. At high laser intensities this spectral narrowing is given by[33]

$$\Delta\nu_F(I_L) = k^{-1/2}\Delta\nu_F(0) \tag{4}$$

where $k = (\sigma_{em,max} - \sigma_{ex})N_1(I_L)L$, σ_{em} is the emission cross section, σ_{ex} is the excited state absorption cross section, N_1 the population of the emitting level and L is the length of the sample. Also N_1 $(I_L$)$\rightarrow$N at higher laser peak intensities.
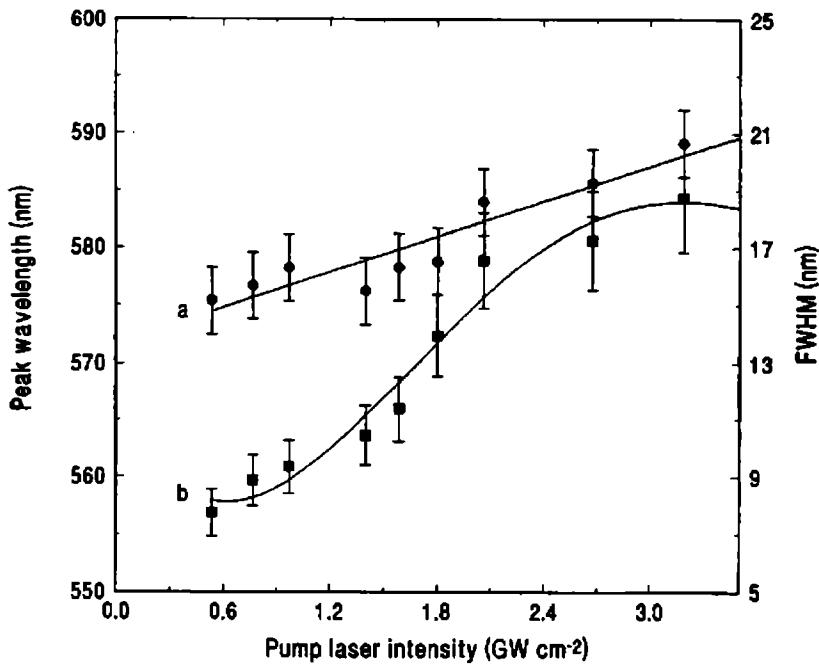

Fig.3.4 Variation of (a) ASE peak wavelength and (b)spectral width as a function of pump laser intensity

At a typical laser intensity of 2.2 $GWcm^{-2}$ the fluorescence peak is obtained at a wavelength of 593 nm whereas the ASE peak wavelength is at 577 nm. There is an appreciable blue shift in the peak wavelength of the ASE from the fluorescence spectrum and this is due to the difference in ASE gain at the two wavelengths. The

ASE peak wavelength shows a redshift and the spectral width increases with the pump laser intensity as shown in Fig.3.4. The peak shifts from 575 nm to 590 nm in the range of intensity considered. The spectra became significantly broader, increasing from 8 to 18 nm. That is, the amplification occurs for much wider wavelength range which is a favorable situation for dye laser operation. The increase in the spectral width of ASE can be attributed to the reduction in the reabsorption of the fluorescence light at higher intensities because, at higher laser intensities the ground state population is small due to absorption saturation. As intense pump pulses bleach the ground state, the reabsorption is reduced and the frequency of maximum ASE shifts towards the frequency of optimum σ_{em}.
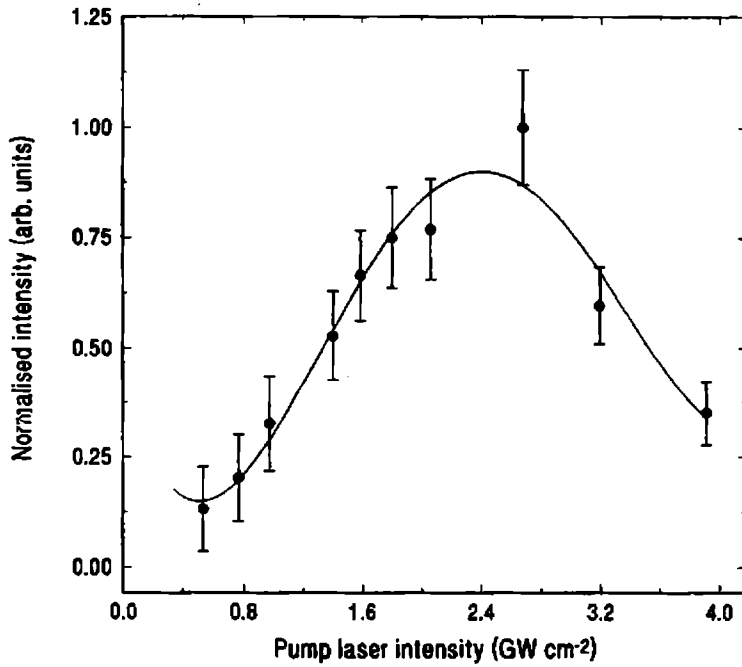

Fig.3.5 Wavelength integrated ASE intensity as a function of pump laser intensity. The decrease in emission intensity beyond 2.7 GWcm^{-2} is due to nonlinear phenomena like excited state absorption, and two photon absorption

The degree of polarization of the emitted light was estimated for both the fluorescence and ASE by the relation

$$P = \frac{\int S_{I\parallel}(\lambda)d\lambda - \int S_{I\perp}(\lambda)d\lambda}{\int S_{I\parallel}(\lambda)d\lambda + \int S_{I\perp}(\lambda)d\lambda} \tag{5}$$

84

where $S_{I\parallel}$, $S_{I\perp}$ are the transmitted intensities when the polarisation direction of the polarizer parallel and perpendicular to the exciting light polarisation direction. Even though the pump wavelength was linearly polarised, the fluorescence emission was found to be unpolarised. But the degree of polarization of the amplified emission was more than 95 %. For amplified emission, intense laser pulses are necessary and under such conditions nearly all molecules in the ground state with orientations parallel to the pump polarisation were excited and the corresponding emission became more or less completely polarised. Thus the amplified emission maintained the pump beam polarisation direction.
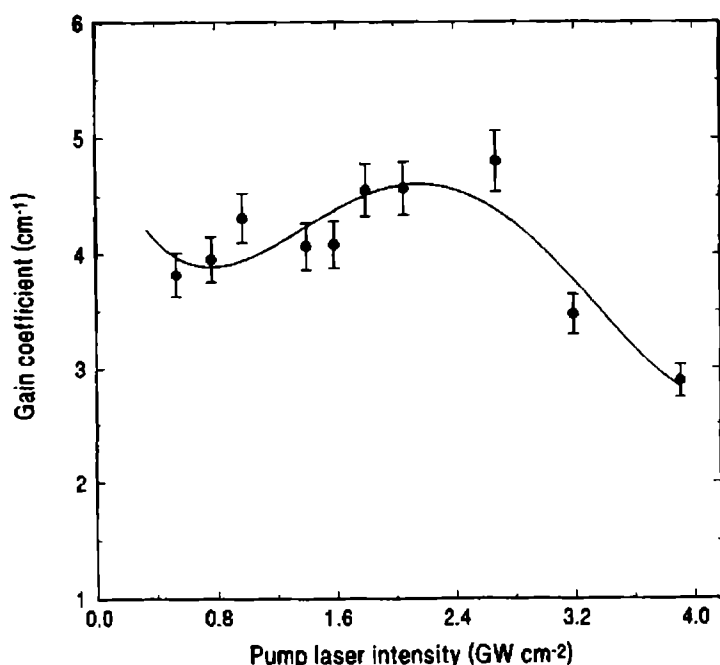

Fig.3.6 Variation of wavelength-integrated gain coefficient with pump intensity. The gain shows a decrease after 2.7 $GWcm^{-2}$ due to nonlinear interactions

Fig.3.5 shows the dependence of the wavelength-integrated ASE intensity on the pump laser intensity. During low laser intensities, there is a linear increase in the emission and it attains a maximum value. But after 2.7 $GWcm^{-2}$ the emission intensity decreases. This is not due to the damage of the matrix, since upon reduction of the

85

laser power, the curve can be traced back. Such reduction in intensity of the amplified emission can be due to different nonlinear phenomena like excited state absorption and multiphoton absorption[34]. The dependence of the wavelength integrated gain coefficient with pump intensity is shown in Fig.3.6.
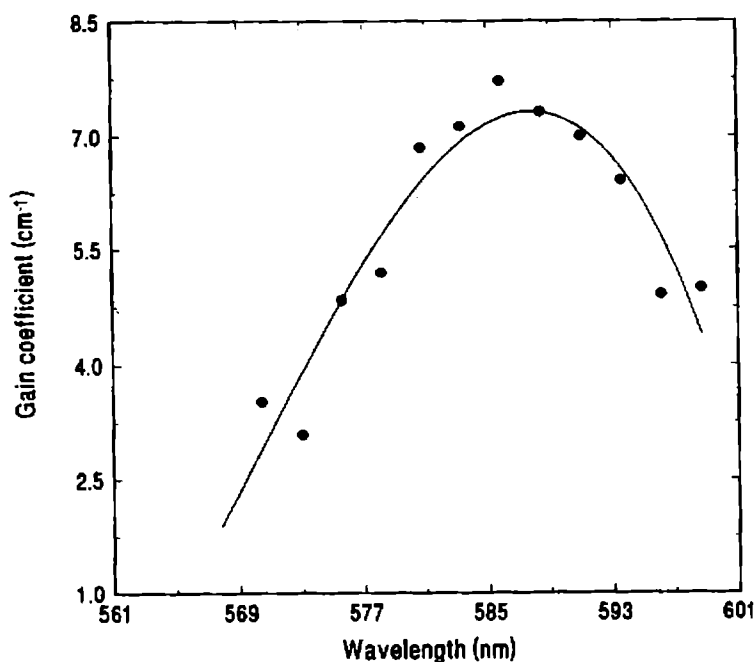

Fig.3.7 Single pass optical gain as a function of wavelength for a pump laser intensity of 2 GWcm^{-2} . Gain is maximum around 585 nm

For the intensity range considered in the present work, there was an increase in gain coefficient as a function of pump laser intensity. In this case also there is a decrease in the gain coefficient after 2.7 GWcm^{-2} due to various nonlinear phenomena. The single pass optical gain depends on the emission wavelength also. Fig.3.7 shows the optical gain as a function of wavelength. It is seen that the optical gain is maximum at a particular wavelength depending on the pump laser intensity. The quantity that can be used as a sensitive indicator of the performance of a dye laser is the conversion efficiency which is defined as I_{ASE} (max)/I_P , where I_{ASE} (max) is the ASE intensity under the full length exposure and I_P is the pump intensity of the laser beam. Both the

pump laser intensity and ASE pulse energy were measured using laser energy meter (Coherent, Model LMP10). The plot of conversion efficiency with pump intensity is shown in Fig.3.8 from where it can be seen that the conversion efficiency is reduced as the laser intensity is increased. The decrease in conversion efficiency at higher pump laser intensity is due to photo-quenching resulting from various phenomena like excited state absorption, multiphoton absorption etc.
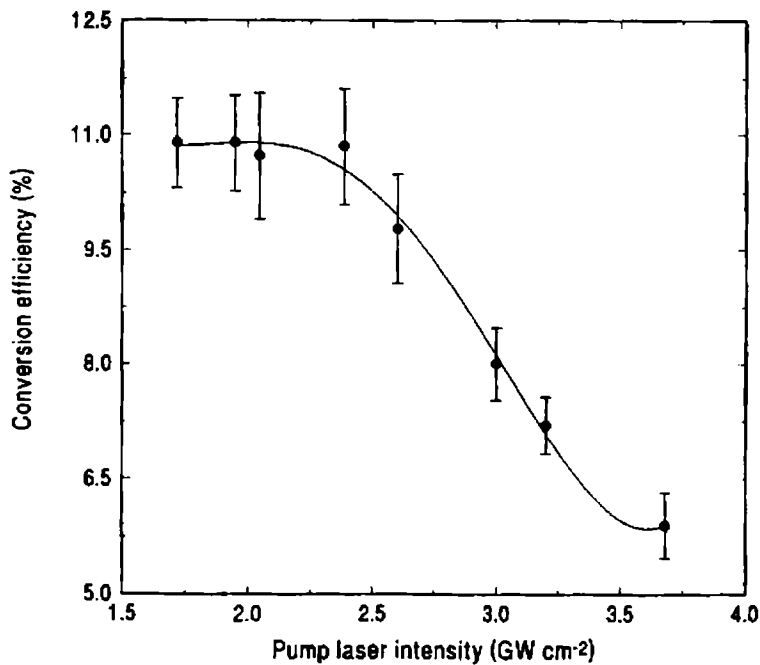

Fig.3.8 Plot of conversion efficiency as a function of laser intensity. Maximum single pass conversion efficiency is 11%

The temporal width of the ASE pulse, was measured with varying pump laser intensity. A typical temporal profile of ASE at a pump laser intensity 0.17 GWcm^{-2} was shown in Fig.3.9. The FWHM is about 6 ns which is considerably less than the pump laser pulse width. Fig.3.10 shows the variation of the ASE pulse width as a function of the pump laser intensity. During low intensities the pulse width has a large value of 7.5 ns and as the laser intensity is increased the pulse width decreases from 7.5 to 5 ns and for still higher intensities it attains a constant value.
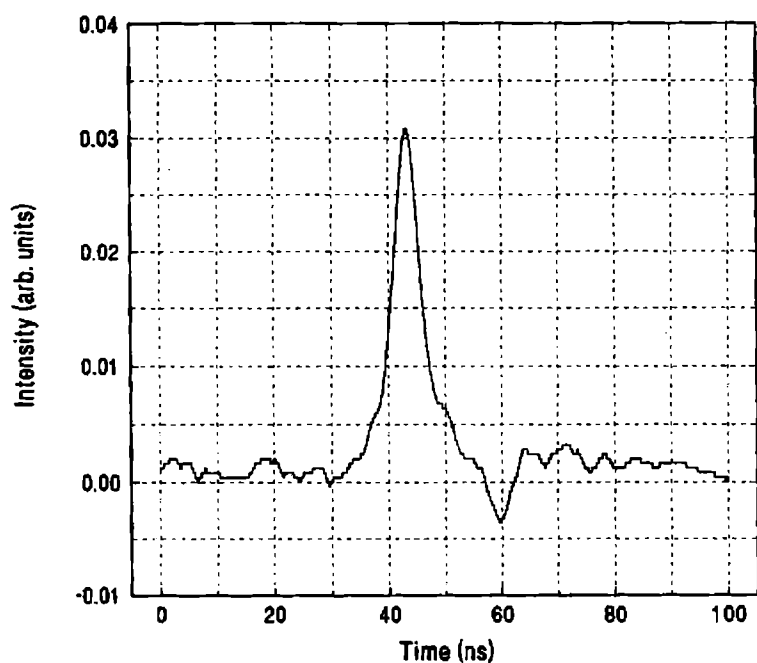
Fig.3.9 The temporal profile of the ASE pulse at a laser intensity of 0.2 GWcm^{-2} . The pulsewidth is approximately 6 ns
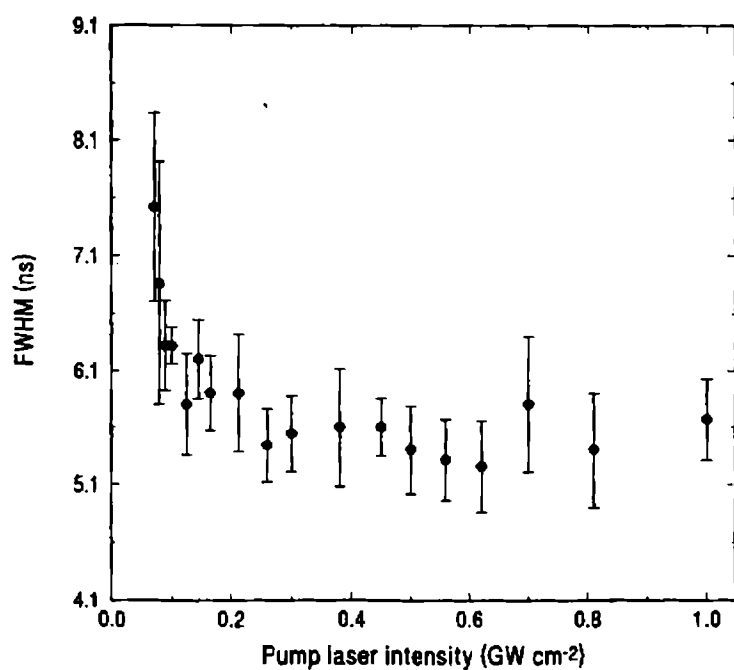

Fig.3.10 FWHM of the ASE temporal profile as a function of laser intensity. The FWHM decreases with increasing pump laser intensities

The various factors influencing the pulse shortening in dye solutions were described in detail by Penzkofer and Falkenstein[33]. At low pump intensities the ground state population is large and the fluorescence light is reabsorbed. It is an established fact that the reabsorption enhances the fluorescence decay time[35] i.e., the reabsorbed fluorescence light is remitted at a later time. With increasing pump intensity, the amplification of the spontaneous emission is so high that it depletes the population of the emitting level faster and causes a decrease of amplification together with a shortening of the fluorescence pulse width.

The pulse shortening can be studied by analysing the depopulation rate of the emitting level. The ASE intensity depends exponentially on the emitting level population, N_e

$$N_e(t) = N_e(0)\exp\left\{-\left(\frac{1}{\tau_E} + \frac{\sigma_{em}I_E}{h\nu_E}\right)\right\} \qquad (6)$$

I_E is the emission intensity, ν_E the frequency of the ASE emission, τ_E is the fluorescence life time and σ_{em} the emission cross section.

The depopulation time constant τ of the emitting level depends on the level population density N_e through the relation[33] .

$$\tau = \frac{\tau_E}{1 + q_E\left(\frac{\Delta\Omega}{4\pi}\right)\{\exp\left[(\sigma_{em} - \sigma_{ex})N_e(z)\right] - 1\}\{\sigma_{em}/(\sigma_{em} - \sigma_{ex})\}} \qquad (7)$$

q_E the fluorescence quantum yield, $\Delta\Omega$ the emission solid angle, σ_{em} the emission cross section and σ_{ex} the excited state cross section. The shortest output pulse is obtained when the emitting level population is equal to the sample concentration. That is all molecules are excited to the higher levels by the pump pulse. The shortest output pulse is obtained when the emitting level population is equal to the sample concentration. That is, when all molecules are excited to the higher levels by the pump pulse.

3.5.4 Concentration dependent studies on Rh 6G doped polyacrylamide

The gain studies were done with samples of varying concentrations. In Fig.3.2 the absorption spectrum of the samples with different concentration is given. As the concentration increases the absorbance also increases. The ASE spectrum is obtained using the same experimental setup described in the beginning of this section with samples

89

of varying concentration but the laser intensity was maintained at 2.4 $GWcm^{-2}$. The linewidth narrowing which is the characteristic of ASE is also observed.

Waveguiding is critical to gain narrowing. The optical path of the emitted light does not exceed the gain length without the aid from the waveguide. In such waveguides, there is light amplification by stimulated emission of radiation (laser) action, but there is no resonant feed-back mechanism for imposing a well-defined optical mode with the corresponding properties of coherence and directionality, as is typically implied in the modern usage of laser[36].

The variation of the FWHM and peak wavelength of the ASE is give in Fig.3.12. With increasing concentration the FWHM value decreases. The peak wavelength shows a red shift with increasing concentration. This behavior can be explained on the basis of fluorescence lifetime. At higher concentrations lifetime decreases and the peak wavelength get shifted to higher wavelength side[37].

The plot of gain vs wavelength for different concentration is shown in Fig.3.13. The region under the gain curve changes with concentration. i.e., the wavelength with maximum gain changes with concentration. The peak gain value increases with concentration upto a range of 8.3×10^{-4} m/l. This is due to the increase in fluorescence life time due to radiation trapping. While the tendency to decrease at higher concentrations is due to photoquenching or concentration quenching[34]. It is observed that the output initially increases with concentration and reaches a maximum value and then decreases. This is attributed to concentration quenching effect and aggregation of the dye molecules[38,39].

Fig.3.16 gives the decay curve which indicates that the emission intensity decreases to 50% after about 3000 pulses when the exciting laser intensity is 5 $GWcm^{-2}$ (10 ns, 10 Hz) which is comparatively better than many polymer matrices reported recently[40]. Also the dye in the matrix remains unbleached even after storage for about six months at room temperature. This seems to be the major advantage of the polyacrylamide matrix over other matrices like PMMA in which dye molecules degrade due to aging.

Even though the results reported here were obtained with flat slab samples, polyacrylamide is suitable for casting as rod-shaped samples, with good optical quality. The sample can be placed in a translator stage in such a way that,
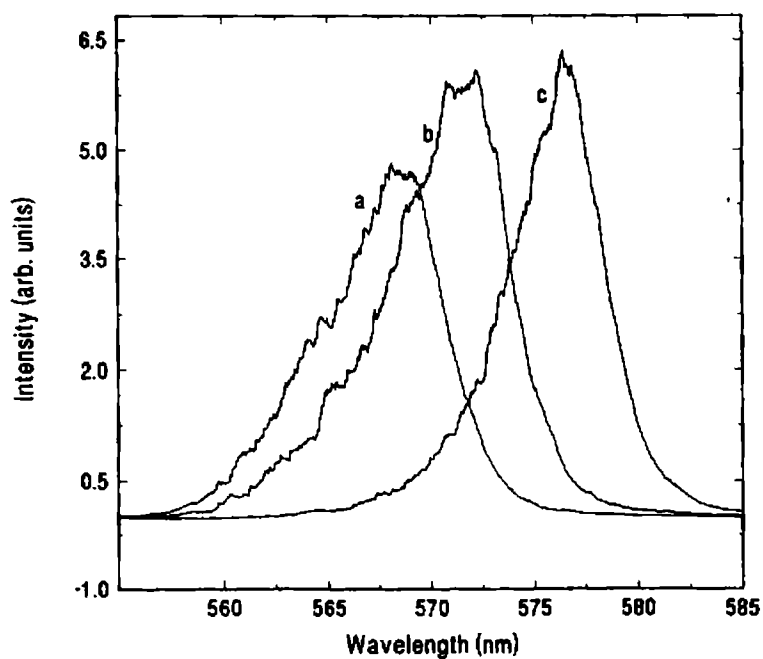
Fig.3.11 The line narrowed amplified spontaneous emission spectrum at three different concentrations (a) 1.9×10^{-4} m/l, (b) 4.6×10^{-4} m/l, (c) 1.3×10^{-4} m/l
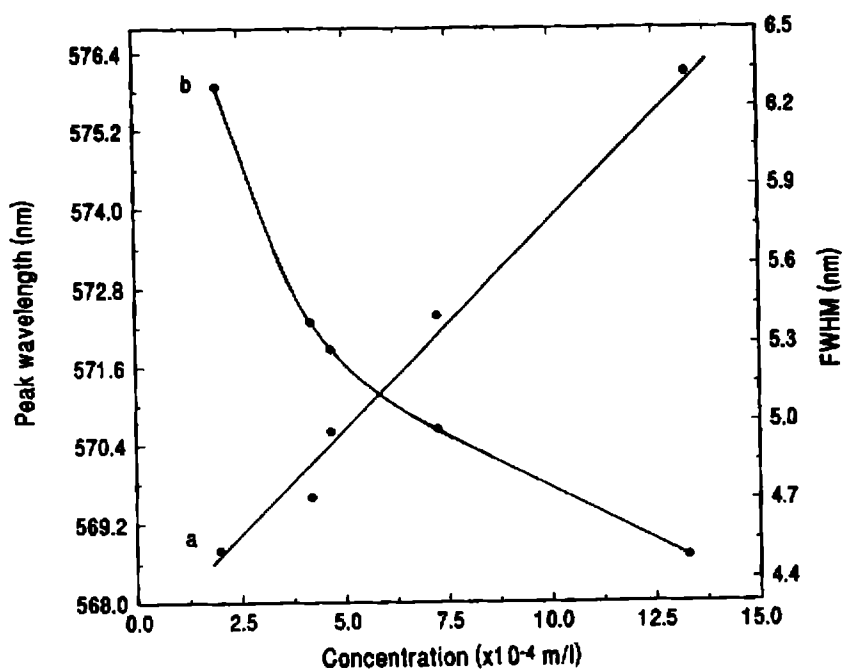

Fig.3.12 Variation of ASE peak wavelength (a) and spectral width (b) as a function of the concentration of dye
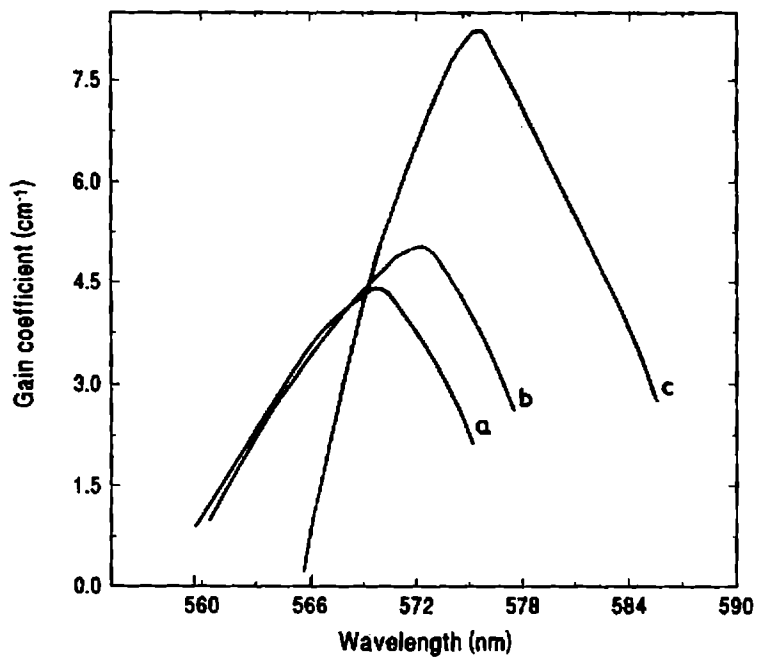
Fig.3.13. The plot of gain vs wavelength for different concentration (a) 1.9×10^{-4} m/l
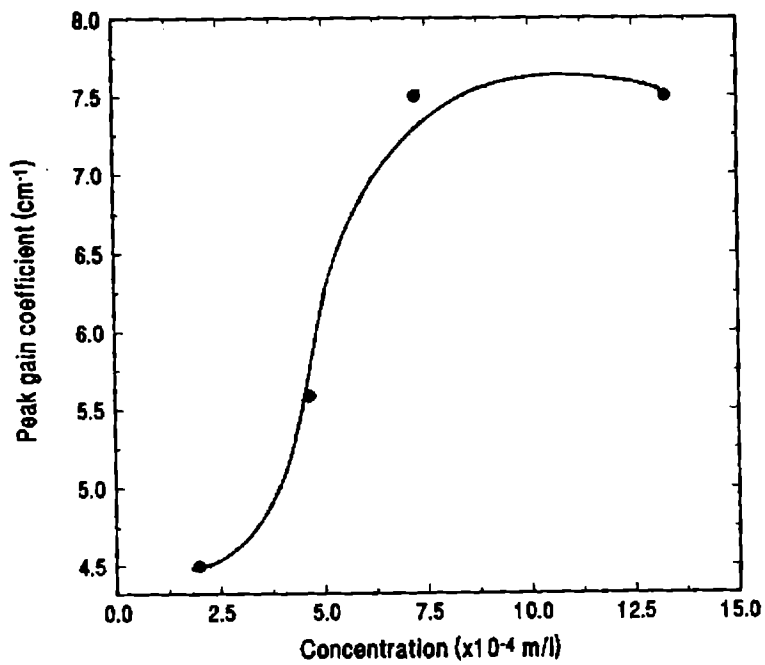(b) 4.6×10^{-4} m/l (c) 1.4×10^{-3} m/l

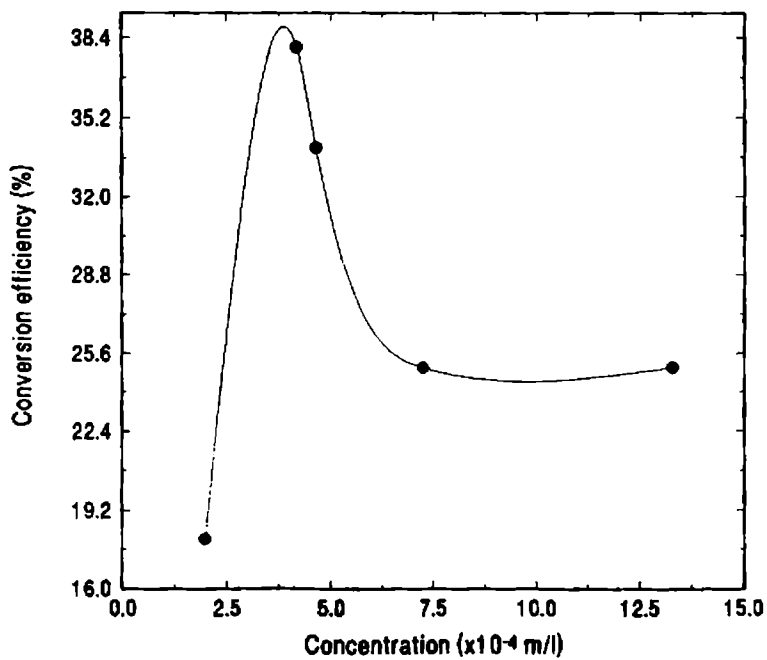Fig.3.14 The peak gain vs concentration

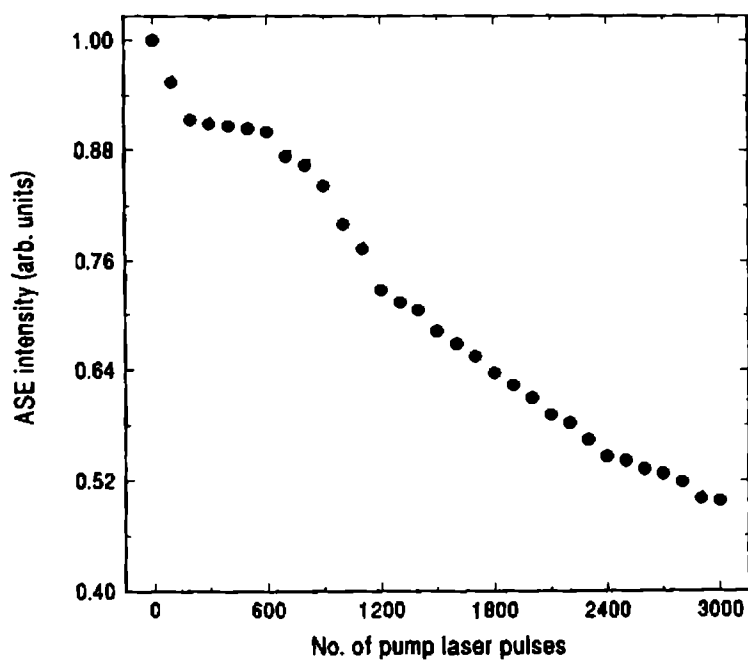Fig.3.15 The plot of conversion efficiency with concentration

Fig.3.16 Response of ASE intensity to number of laser pulses. The ASE intensity decreases to 50% of the original value after $\approx$3000 pulses

after using a spot on the sample for a few thousand shots, the sample can be moved to expose a fresh surface[41,42]. Since the sample can be made very large, this procedure would enable the use of the same sample for thousands of shots before exhausting its full capacity. Using a proper laser cavity, including the incorporation of a dielectric mirror for output coupling, the efficiency of rhodamine 6G doped polyacrylamide can easily be increased. The increased photostability of the rhodamine 6G doped polyacrylamide films can be explained as due to the porous nature during the gel state, the dye molecules are trapped in the pores, without actually forming bonds with the matrix molecules. In the dried samples the diffusion of the oxygen molecules at the surface is hindered by the rigid matrix. The absorption and emission characteristics show that the properties are similar to that of dye molecules in solutions.

Table 1 gives the list of different matrices for rhodamine 6G, the pumping source and parameters for the pumping source and the number of pumping pulses giving 50% reduction in the intensity of the material.

3.6 Conclusions

The amplified spontaneous emission properties of the dye molecules embedded in a porous polymer matrix, polyacrylamide has been studied. It seems that the intrinsic properties of the dye molecules were less affected by the presence of the solid matrices. The fluorescence and ASE properties are similar to that in liquid solutions. The problem of solvent evaporation found in solutions is absent in solid matrix. In host materials like PMMA or its derivatives the problem of aging of dye molecules is severe but in polyacrylamide, the dye molecules are embedded in the pores and not firmly linked to the matrix molecules hence the host-dye interactions are less and dye degradation reduced. Also the properties are more or less similar to that obtained in solutions.

The particular choice of polymeric material is determined by the operating conditions of the laser medium. The present studies show that by properly controlling the pump laser intensity and concentration of the dye molecules, polyacrylamide-rhodamine 6G system can be used as the active medium for solid state lasers.

No	Matrix	Pump source and parameters	Pulses for 50% reduction	Reference
1	Modified PMMA	530nm (Nd:glass, SHG), 0.5-1.4 J/cm^2, (50 ns)	200	[17]
2	Poly(2hydroxy ethyl methacrylate)	337nm, 1.8mJ (5ns), 0.14Hz	300	[09]
3	Copolymer of HEMA and MMA	337nm, 1.2mJ, (5ns), 2Hz	3000	[43]
4	Alumina film	337nm, 500μJ, (5ns), 1Hz	600	[44]
5	Aluminosilicate xerogel	511nm, (dye laser), 2mJ, 1Hz	1500	[45]
6	ORMOSIL	539nm, (dye laser), (15ns), 1Hz	2700	[01]
7	Rh B/ Polyacrylic acid	337nm, 1-2mJ, (7ns), 2 Hz	2600	[40]
8	Rh 6G/Polyacryl amide	532nm, 2.5mJ, 910ns), 10Hz	3000	This work

Table 1: Table of lasing efficiency

References

[1] E T Knobbe, B Dunn, P D Fugu and F Nistrida, Appl. Opt., **29**, 183, (1990).

[2] F Salin, G LeSaux, P Georges, A Brun, C Bagnall, J.Zarzyck, Opt. Lett, **14**, 785, (1989).

[3] Donald R Ulrich, J. Non-crystalline Solids, **100**, 174, (1988).

[4] K M Dyumaev, A A Manenkov, A P Maslyyukov, G A Matyushin, et al. Sovt. J. Quant. Electron., **4**, 503, (1983).

[5] S Miyanaga and H Fujiwara, 'Proceedings of International Conference on Lasers', 795, (1989).

[6] K M Dyumaev, A A Manenkov, A P Maslyyukov, G A Matyushin, V S Nechitailo, A M Prokhorov, J. Opt. Soc. Am. B, **9**, 143, (1992).

[7] A P Maslyyukov, S Sokolov, M Kaivila, K Nyholm, S Popov, Appl. Opt., **34**, 1516, (1995).

[8] M L Ferrer, A U Acuna, F Amat-Guerri, A Costela, J M Figuera, F Florida, and R Sastre, Appl. Opt., **33**, 2266, (1994).

[9] F Amat-Guerri, A Costela, J M Figuera, F Florida, and R Sastre, Chem. Phy. Lett., **209**, 352, (1993).

[10] D Lo, J E Parris and J L Lawles, Appl. Phys. B, **56**, 385, (1993).

[11] B H Soffer, and B B McFarland, Appl. Phys. Lett., **10**, 266, (1967).

[12] Y V Naboikin, L A Ogurtsova, V P Podgorny et al., Opt. Spectro., **28**, 528, (1970).

[13] E P Ippen, C V Shank, and A Dienes, IEEE J. Quant. Electron., **QE-7**, 178, (1971).

[14] I P Kaminov, H P Weber, and E A Chandross, Appl. Phys. Lett., **18**, 497, (1971).

[15] R Ulrich, and H P Weber, Appl. Opt., **11**, 428, (1972).

[16] V I Bezrodnyi, O V Przhonokaya, E A Tikhonov, Sov. J Quantum Electronics, **12**, 1602, (1982).

[17] D A Gromov, K M Dyunaev, A A Manenkov, et al. J Opt. Soc. Am B, **2**, 1028, (1985).

[18] I P Kaminow, L W Stultz, E A Chandross and C A Pryde, Appl.Opt., **11**, 1563, (1972).

[19] R L Fork, and Z Kaplan, Appl. Phys. Lett., **20**, 472, (1972).

[20] S Reich, and G Neumann, Appl. Phys, Lett., **25**, 119, (1975).

[21] F Higuchi, and J Muto Phy. Lett. **81A**, 95, (1981).

[22] D A Gromov, K M Dyunaev, A A Manenkov et al. An USSR Phys. Series, **7**, 1394, (1984).

[23] J S Batchelder, A H Zewail, and T Cole, Appl. Opt., **29**, 3733, (1981).

[24] C Hu and S Kim, Appl. Phys. Lett., **29**, 582, (1976).

[25] P Burlamacchi, R Pratesi, U Vanni, Appl. Opt, **15**, 2684, (1976).

[26] B D Hames, and D Rickwood 'Gel Electrophoresis: A Practical Approach', IRL Press, Oxford (1990).

[27] A Penzkofer, H Gratz and P Weider J. Non-crystalline Solids, **189**, 55, (1995).

[28] L W Casperson and A Yariv, IEEE J. Quant. Elect., **QE-8**, 80, (1972).

[29] Landau and Lifshitz 'Classical Field Theory', Springer Verlag.

[30] Zs.Bor, S Szatmari and Alexander Muller, Appl. Phys. B, **32**,101, (1983) .

[31] C V Shank, Reviews of Modern Phys., **47**, 649, (1975).

[32] A. Yariv, 'Quantum Electronics' Wiley, Newyork, (1975).

[33] A Penzkofer, W Falkenstein, Opt. & Quant. Electron., **10**, 399, (1978) .

[34] Arun Gaur, L Taneja, A K Sharma, D Mohan and R D Singh, Opt. Commun., **83**, 235, (1991).

[35] John Briks, 'Organic Molecular Photophysics', John Wiley & Sons, (1973).

[36] Fumitomo Hide, Maria A, Diaz-Garcia, and Alan J Heeger, Laser Focus World, **33**, 151, (1997).

[37] M Terade and J Muto, Opt. Commun., **59**, 199, (1986).

[38] L J Cotnoir, Appl. Opt., **20**, 2331, (1981).

[39] A H Sasaki, Y Kobayashi, S Muto, Y Kurokawa, J A. Ceram. Soc., **73**, 453, (1990).

[40] A V Deshpande and, E B Namdas, Appl. Phy. B, **64**, 419, (1997).

[41] A Costela, Appl. Phy. Lett., **68**, 593, (1996).

[42] A Costela, J. Appl. Phys., **80**, 3167, (1996).

[43] A Costela, Garcia-Morenco, and J M Figuera, F Amat-Guerri, and R Sastre, Appl. Phys. Lett., **68**, 593, (1996).

[44] Y. Kobayashi, Y. Kurokawa, Y lman, S Muto, J Non-Crys. Solids, **105**, 198, (1988).

[45] J M McKiernan, S A Yamanaka, B Dunn, J I Zink, J. Phys. Chem., **94**, 5652, (1990).

CHAPTER IV

EVALUATION OF LASER DAMAGE THRESHOLD IN POLYMER SAMPLES

Abstract

The characterization of the laser interaction with polymers like polymethyl methacrylate and polyacrylamide was done using photothermal phase shift spectroscopy. The optical damage threshold of samples were measured using this technique.

4.1 Introduction

The interaction of intense laser pulses with solid materials is currently of considerable interest in view of the development of new techniques and devices involving nonlinear effects. For example, laser ablation of polymeric materials is being used in photolithography and in the fabrication of micro electronic systems[1,2]. Some of the transparent polymers are being used as optical components as well as non-linear optical materials[3,4]. Very good optical transparency of polymethyl methacrylate (PMMA) in the visible range of the electromagnetic spectrum helps them to be useful in optics. PMMA is also suitable for the fabrication of optical fibre core as well as cladding.

When pulsed laser radiation falls on the surface of an organic material, the surface layer is spontaneously etched away and the resultant molecular fragments get rapidly ablated from the target surface and the photochemistry is more or less simplified as explosive thermal decomposition. Materials used in high power applications should have high damage threshold under laser irradiation. Polyacrylamide is being used as polymeric hosts for dye molecules which can be used in tunable solid state dye lasers[5-10]. The use of dye doped polymer matrices in high power dye lasers demands the accurate knowledge of its laser damage threshold at different doping concentrations.

When a low power laser beam is passed through a material, no irreversible effects are observed, but at sufficiently high power or energy density, transient or permanent effects like refractive index changes, removal of material from the surface, production of internal voids, melting, vaporization and even ablation occur. There is a threshold value for the power density of laser beam so as to produce such irreversible damage effects and this value is called Laser Damage Threshold (LDT) for the particular material. The mechanism of LDT is not yet fully understood and moreover, since there are numerous parameters that determine the LDT of a material, a technique that can be used to determine this quantity accurately for different kinds of samples is highly useful.

The effect of high power lasers on transparent polymeric materials is different from that of transparent dielectrics. The polymer has a lower laser damage threshold as compared to the dielectric crystals, a strong dependence of the optical strength on the micro-elastic properties and temperature, a wide range of radiation intensities below

100

damage threshold in which cumulative effects are observed, the occurrence of micro damage of dimensions 10 μm, not accompanied by bright spark and the absence of formation of soot during damage process[6-10]. Another feature of the polymer materials is their higher surface optical strength as compared to their bulk optical strength[6,11]. The actual measurement of LDT involves three steps, viz.,

(1) to irradiate the samples at several laser energy densities,

(2) to measure the absolute characteristics of the laser pulse and

(3) to determine which of the laser pulses caused the damage to the target.

Though the steps described are quite simple, the process of an absolute measurement of this quantity is beset with various problems. Some of these problems faced are discussed below[12].

Since the laser pulse energy varies with the pulse width and the beam profile, these parameters must also be measured accurately. Sophisticated instruments like the streak camera, recticon[13]or pyroelectric or photodiode arrays are often required for these measurements. In such cases, the serious problem is that regardless of how the image is recorded, there is a background noise level which greatly complicates the interpretation of the low-intensity wings of the profile. This can be eliminated to an extend by placing an aperture, the diameter of which is approximately equal to the spot size of the profile. For such a setup with laser pulse width of about 1 ns, the uncertainties in LDT measurements due to the laser energy, flux and intensity are ±3, ±5-7 and ±10-15% respectively. The absolute accuracy in the energy density measurements, however depends on the accuracy of the calorimeter used to determine the pulse energy, which, using commercial energy meters, can be measured with good precision within an error margin of 1%. Since it is the measurement of beam profile that involves serious problems, often, only the results of LDT measurements without shot-to shot determination of the beam profile are reported. Obviously, the margin of the experimental error is enlarged in these cases. Even the ability to determine the laser flux within a 5% error does not imply that the laser damage threshold can be measured with the same degree of accuracy since uncertainties can be introduced by the large step-sizes in flux during the sequence of shots used for irradiation or due to the indecision as to which particular shot has caused the damage. The laser spot size

101

must be big so as to ensure that the worst-case defects have been encountered.

The test area must be illuminated uniformly to within the desired precision of the LDT measurement. Since damage is a cumulative effect, multiple shots at the same site will lower the LDT. It is better to expose a new site to each shot so that the surface morphology is uniform within the measurement error. For testing of laser optics, it is needed to know as to how many shots the surface can endure before damage sets in. For such studies multiple exposure is ideal, so long as the pulse-to-pulse stability of the shots are ensured. The work in this chapter has followed the method of single shot laser damage threshold measurements. Moreover, there is no a-priori guarantee that different sites will respond alike to the same flux level.

The total energy Q in terms of energy density E(r) at the focal plane can be expressed as[14]

$$Q = E(r) \int_0^\infty 2\pi r dr \tag{1}$$

and $E_0 = 2Q/\pi r_0^2$ where E_0 is the peak on-axis energy and r_0 the radius at which the intensity has fallen to $1/e^2$ of its original value. In terms of the peak on-axis intensity, the damage threshold, I is given by

$$I = \frac{2Q}{\pi \, r_0^2 \tau_L} \tag{2}$$

The r.m.s electric field associated with this intensity is,

$$E = 19.41 \left[\frac{I}{\eta} \right]^{1/2} \tag{3}$$

where τ_L is the laser pulse width and η is the refractive index of the material. The total energy Q is related to the incident energy on the focusing lens (Q_{in}) as,

$$Q = Q_{in} T_L T_S \tag{4}$$

T_L and T_S are the transmittance of the focussing lens and the sample respectively.

The sample surface must be polished carefully cleaned with organic solvents since dust or other minute inclusions at the focal sites reduce the LDT at those sites. Scratches and residue on the surface as a result of cleaning can also cause lower LDT.

102

Even then there is no guarantee that each point on the sample surface can give an absolute average value of the damage threshold.

Even though many methods have been reported for the detection of LDT, none of them can be acclaimed as accurate and fool proof for all kinds of samples. It is seen that LDT measurements are influenced by many parameters relating to the experimental conditions like pulse width, repetition rate, beam diameter, beam focussing, temperature, laser frequency, optical pumping conditions etc. And the different techniques used are (a) Emission of spark/ light, (b) Change in scattering/reflection, (c) Particulate plume, (d) Microscopy (e) Breath-fogging etc. to mention a few. This chapter describes how the photothermal phase shift spectroscopy[15,16] (PTPS) can be used for the measurement of the laser damage threshold of PMMA and dye doped polyacrylamide when irradiated with a pulsed high power Nd:YAG laser beam.

4.2 Photothermal phase shift spectroscopy

Photothermal spectroscopy is an active area of research at recent times[17-19]. A wide range of applications of this technique has been developed. The basic idea underlying this technique is well known. A laser beam (pump beam) passes through the medium of interest. The laser is tuned to an absorption line of the medium and the optical energy is absorbed by the medium. If the collisional quenching rate in the medium is much higher that the radiative rate, most of this energy appears in the rotational-transitional modes (heating) of the molecules. The heating of the medium modifies the refractive index of the laser irradiated region. The change in refractive index of the medium is detected by a second laser beam (probe beam). There are three different methods of measuring this refractive index change, viz., namely photothermal phase shift spectroscopy, photothermal deflection spectroscopy and photothermal lensing spectroscopy. In photothermal phase shift spectroscopy, the refractive index change is measured directly by placing the sample in one of the arms of the Michelson interferometer or inside a Fabry-Perot cavity. The refractive index change produces a change in the optical path length which is detected as a fringe-shift.

In photothermal deflection spectroscopy (PTDS) the pump beam has a spatial profile (generally assumed to be Gaussian) and hence, the refractive index of the pump beam irradiated region also acquires a similar spatial profile. This non-uniform re-

103

fractive index causes a deflection of the probe beam, which can easily be detected by a position sensitive optical detector. The signal is proportional to the gradient of refractive index.

In photothermal lensing spectroscopy (PTLS) the non-uniform refractive index also produces a lensing effect in the medium. A probe beam passing through the medium changes shape, resulting in a change in the intensity of the probe beam passing through a pin-hole. In this technique the signal is proportional to the second derivative of refractive index. These techniques were discovered and developed separately by various workers. PTPS was developed by Stone and by Davis[20,21] and has found applications in analytical chemistry. PTDS was developed by Amer, Boccara, Fourier and collaborators[22-25] and is used as a diagnostic tool. PTLS is the used in the measurement of the collisional relaxation rates of molecules as well as in analytical chemistry[26-28].

Among the above mentioned three different methods in photothermal spectroscopy we have used PTPS as the diagnostic tool for the present measurements. A detailed theoretical treatment of PTPS in fluid medium is considered. The temperature distribution created by the absorption of the pump beam is given by the solution of the differential equation[16]

$$\frac{\partial T(r,t)}{\partial t} = D\nabla^2 T(r,t) - v_x \frac{\partial T(r,t)}{\partial x} + \frac{1}{\rho C_p} Q(r,t) \tag{5}$$

where $T(r,t)$ is the temperature above the ambient, D is the thermal diffusivity, ρ is the density, and C_p is the specific heat at constant pressure of the medium. v_x is the flow velocity of the medium which is assumed to be in the x-direction, and $Q(r,t)$ is the source term. The first, second and third terms on the right in hand side of eq.5 represent, respectively the effects of the thermal diffusion, flow and heating due to the pump beam absorption. If a pulsed laser is used, the heat produced per second per unit volume by the absorption of laser energy $Q(r,t)$ is given by

$$Q(r,t) = \alpha I(r,t) = (2\alpha E_0/\pi a^2 t_0)\exp(-2r^2/a^2) \text{ for } 0 \leq t \leq t_0$$
$$= 0 \text{ for } t > t_0 \tag{6}$$

Here α is the absorption coefficient of the medium and the medium is assumed to be optically thin (weakly absorbing). $I(r,t)$ is the intensity of the beam and the total

104

energy per pulse is E_0.

We assume that the pump beam propagates in the z-direction. If there are no inhomogeneity in the medium along the pump beam, eq.5 may be solved in two dimension (x and y). The boundary conditions given by

$$T(x,y,t)|_{t=0} = 0; \quad T'(x,y,t)|_{t=0} = 0$$

$$T(x,y,t)|_{x=\pm\infty} = 0; \quad T(x,y,t)|_{y=\pm\infty} = 0 \tag{7}$$

where the laser is turned on at t = 0 and T' represents the gradient of the temperature. With the boundary condition one may obtain the to the desired temperature distributions due to the pulsed laser irradiation as

$$T(x,y,t) = (2\alpha E_0/\pi t_0 \rho C_p) \int_0^{t_0} 1/\{[8D(t\text{-}\tau)] + a^2\} \exp\{-2\{[x - v_x(t - \tau)]^2 + y^2\}$$

$$/ [8D(t - \tau) + a^2]d\tau \text{ for } t > t_0 \tag{8}$$

In order to measure the laser damage threshold of polymeric samples, the variation of the fringe shift is measured as a function of laser power density. At a point where the damage occurs to the polymer matrix electrons, atoms and ions will be ejected out of the target and the measurement of electron density as a function of laser power density near the ablated surface will directly give the damage threshold. We have used eq.11 to derive the expression for the refractive index variation and hence the electron density of plasma generated in one of the arms of the Michelson interferometer. The intensity distribution of the fringe pattern of a Michelson Interferometer is given by,

$$I(t) = A^2 + B^2 + 2AB\cos[(\phi_A - \phi_B) - \gamma(t)] \tag{9}$$

where A and B are the amplitudes, and ϕ_A and ϕ_B the phases of the two interfering beams respectively and $\gamma(t)$ is the phase difference introduced due to the presence of the plasma. This derivation is made in accordance with the arguments given in Monson et al.[15,17].

The shift in the fringe pattern resulting from this time dependent phase factor can be measured as voltage change in the output of the photodiode. For the intensity

to be very sensitive to small changes in $\gamma(t)$, the operating point is chosen such that $(\phi_A - \phi_B) = (m + \frac{1}{2})\pi$. Then the change in the output voltage of the photodetector $\delta V(t)$ is,

$$\delta V(t) \propto 2AB \sin\left[\frac{4\pi}{\lambda}\right] \int_0^l \Delta\mu(t)dl \qquad (10)$$

where λ is the wavelength of the probe laser beam, l the lateral extension of the plasma and $\Delta\mu(t)$ is the change in refractive index due to the presence of the plasma. When the phase difference $(\phi_A - \phi_B)$ is taken through a phase change of π, i.e., the operating point is moved from the bright to the dark fringe center the corresponding difference in intensities $(I_{max} - I_{min})$ will be proportional to $4AB$ in the absence of plasma. With a linear response for the photodetector, the corresponding voltage difference $V_{max} - V_{min}$ denoted by V is proportional to $4AB$. Therefore from eq. 13,

$$\gamma(t) = \sin^{-1}\left[\frac{2\delta V}{V}\right] \qquad (11)$$

Assuming negligible absorption and light scattering at the probe wavelength, the index of refraction μ of the plasma is given by[29]; $\mu^2 \cong n_e/n_c$ where n_e is the plasma electron density and n_c the critical plasma electron density given by $n_c = (\omega^2 m \varepsilon_0)/e^2$ where ε_0 is the permittivity of free space, m the electron mass, e the electron charge and ω the angular frequency of the pump laser radiation. n_c has a typical value 9.92 x 10^{20} cm^{-3} when the Nd:YAG laser of wavelength 1.06 μm is used as the pump beam. When the critical density $n_e/n_c \ll 1$, we get

$$\gamma(t) \cong \frac{e^2}{mc\omega\varepsilon_0} \int_0^l n_e dl \qquad (12)$$

for a path length l in the plasma. One can write the line averaged electron density from eq.15 as,

$$n_e \cong \frac{k\gamma(t)}{\lambda l} \qquad (13)$$

where k = 1.778 x 10^{12} cm^{-1} . The phase factor $\gamma(t)$ in eq.16 is experimentally found out using eq.14.

4.3 Characterization of polymeric samples

With the advent of the use of the so called 'organic glasses' i.e., transparent polymeric materials for laser optics, laser damage threshold measurements in various bulk and thin films of polymeric materials such as those in the methacrylate series like polymethyl methacrylate (PMMA) and their co-polymers as well as polymers containing additives in the form of various plastics like dimethylphthalate have gained great importance. Many of these materials are now being used as laser optical elements and thus the need exists to study the laser induced damage process in these polymeric materials[30].

The laser induced damage in polymeric materials has been attributed to various mechanisms depending on the kind of results obtained. Multiphoton photo-destruction of the polymer chains is one of the major causes leading to damage in these materials[31]. Another possibility for damage to occur in polymers is due to the mechanisms involving the formation of highly absorbing products and inclusions resulting from chemical changes at high temperatures produced following irradiation by laser beam[9,32,33].

Irradiation of a polymethyl methacrylate target using a pulsed Nd:YAG laser causes plasma formation in the vicinity of the target. The refractive index gradient due to the presence of the plasma is probed using phaseshift detection technique. The phaseshift technique is a simple but sensitive technique for the determination of laser ablation threshold of solids. The number density of laser generated plasma above the ablation threshold from polymethyl methacrylate is calculated as a function of laser fluence. The number density varies from $2 \times 10^{16} cm^{-3}$ to 2×10^{17} cm^{-3} in the fluence interval 2.8 - 13 J cm^{-2} .

4.3.1 Experimental setup

The experimental setup is as shown in Fig.2.8. The basic element in PTPS technique is a Michelson interferometer. Laser radiation from an intensity stabilized 5 mW He-Ne laser source (Spectra Physics) is used to construct the Michelson interferometer (MI). Optical setup is aligned so as to get well defined straight fringe pattern. The beam in one of the arms of MI passes parallel and very close to the target surface. High power laser radiation from a pulsed Nd:YAG (Quanta ray DCR 11) laser at wavelength 1.06 μm with pulse duration 10 ns is focused on to the target in order to produce plasma. The sample chosen for our study is a disc of PMMA having diameter 15 mm and

107

thickness 4 mm. The point of irradiation is shifted by mechanically rotating the target after each measurements so that fresh location is available on the target surface for each pulse. The probe beam passes gracing to the sample surface so that the length of the plasma near the target is taken as equal to the pump laser spot size. The shift in fringe pattern is measured as a voltage change using a PIN photo diode (HP - 4207) and it is displayed on a digital storage oscilloscope (Iwatsu, 200 MHz). The whole setup has been properly vibration isolated by using an indigenously built vibration isolated table. Measurements were taken for different laser pulse repetition frequencies.

The presence of the plasma on one of the arms of the interferometer changes the effective path length on that arm and the corresponding phase change $\gamma(x,t)$ will shift the fringe pattern which is proportional to the change in refractive index. This shift in fringe pattern can be measured as a voltage change $\delta V(x,t)$ in the output of a photodiode from which γ can be calculated using eq.15 And the line averaged electron density can then be obtained by using the eq.16. The electron density was calculated for varying laser fluence using this equation.

4.3.2 Results and discussion

The oscilloscope trace of the signal obtained corresponding to the interference fringe shift is shown in Fig.4.1. Variation of electron density with laser intensity is given in Fig.4.2 which shows that electron density varies nonlinearly with respect to laser fluence. The graph exhibits regions of different slopes corresponding to different mechanisms for laser beam interaction with the target surface. At the point A, there is an abrupt change in the electron density of the plasma. It can be explained in terms of surface damage. For the values of the energy densities near the point A, the surface temperature is very high so as to produce intense ionization, thereby causing rapid ionic and electronic emission from the surface. This rapid ionization causes an abrupt change in the electron density which marks the surface damage threshold of PMMA at the laser fluence of ≈ 3.5 Jcm^{-2}. Above the damage threshold there is a marked increase in the plasma electron density for a fluence upto about ≈ 7.5 Jcm^{-2}. Above this fluence the slow increase in electron density can be attributed partly to the increased electron-ion recombination forming a quasi-stable state and partly to the absorption of the incident laser radiation by the plasma plume[34].
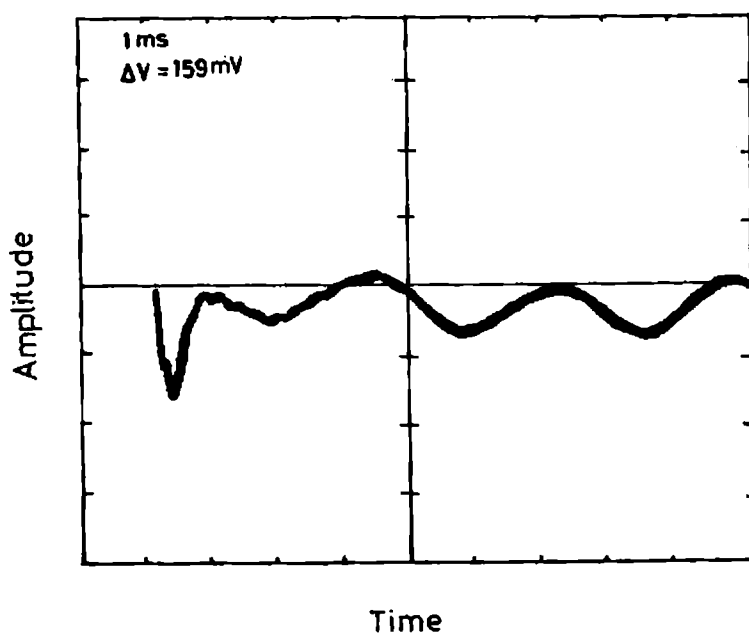
108

Fig.4.1. Signal observed in the oscilloscope, fringe shift was detected as voltage varia-
tion.

Fig.4.3 shows the dependence of the damage threshold on the pulse repetition fre-
quency. At 16 Hz repetition frequency the ablation threshold comes down to 2.8 Jcm^{-2}
compared to 3.5 Jcm^{-2} at 2.5 Hz. That is, the damage threshold decreases linearly
with increasing laser pulse repetition frequency. At higher laser pulse repetition rate,
damage threshold is low due to the influence of the thermal energy contribution from
the previous pulse. This indicates that the process of ablation is thermal in nature.
Similar studies were done on dye doped polyacrylamide, undoped polyacrylamide is
transparent in the visible region. The studies on dye doped polyacrylamide were done
at were done at 532 nm instead of 1.06 μm since it is the pumping wavelength for the
dye emission. The measurement of damage threshold in this wavelength is important in
understanding the utility of the polymer as a solid matrix for dyes. The samples used
were of size (20x10x1) mm^3, with varying rhodamine 6G concentrations. (The prepa-
ration and impregnation method of rhodamine 6G doped polyacrylamide is described
in Chapter III). The experimental details are same as that for PMMA.
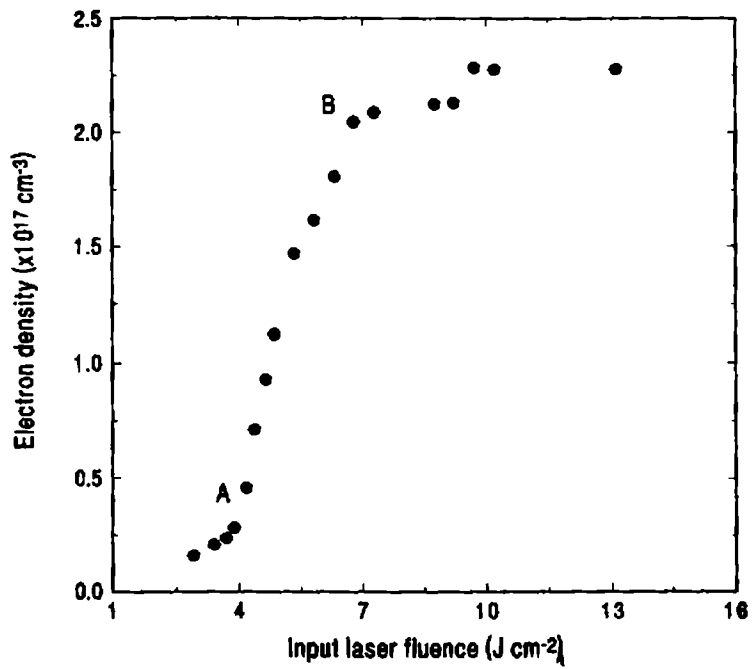
109

Fig.4.2 Electron density of laser produced plasma as a function of laser fluence at a pulse repetition rate of 2.5 Hz
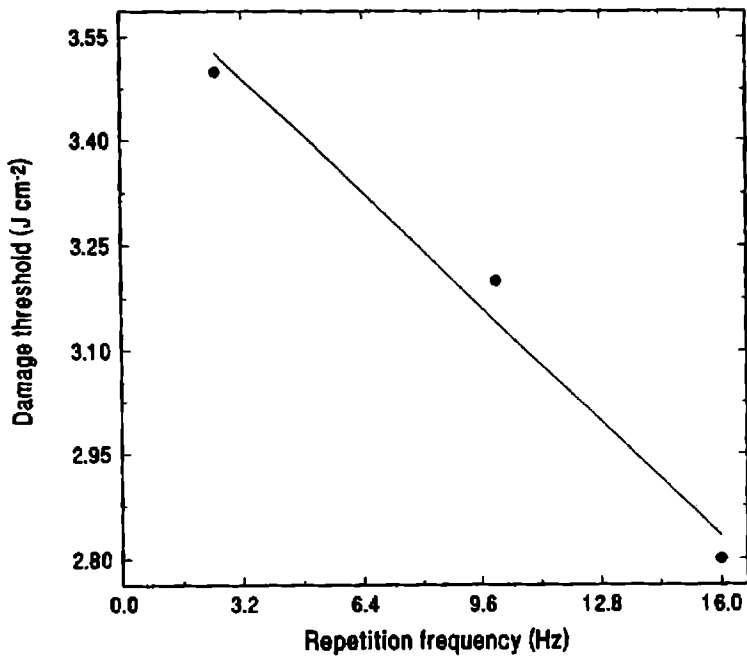

Fig.4.3 Variation of damage threshold with laser pulse repetition frequency. The solid line gives a linear fit to the observed data

110

Fig.4.4 shows the variation of damage threshold with the concentration of dye molecules. As the dye concentration is increased, the damage threshold intensity decreases. This is because of the higher absorption of the laser radiation by the highly concentrated samples. But the damage threshold is fairly high when compared to other materials.

The determination of LDT is a purely destructive testing process and permanent damage to the sample studied occurs. It would be appropriate to divide the damage occurring in polymers under laser radiation as that occurring in ideally pure media and that caused by impurities. The mechanisms causing damage are different. In pure media, it is optical rupture, which is qualitatively similar to gas rupture: in media containing impurities, it is damage caused by the superheating of impurities[35,36].
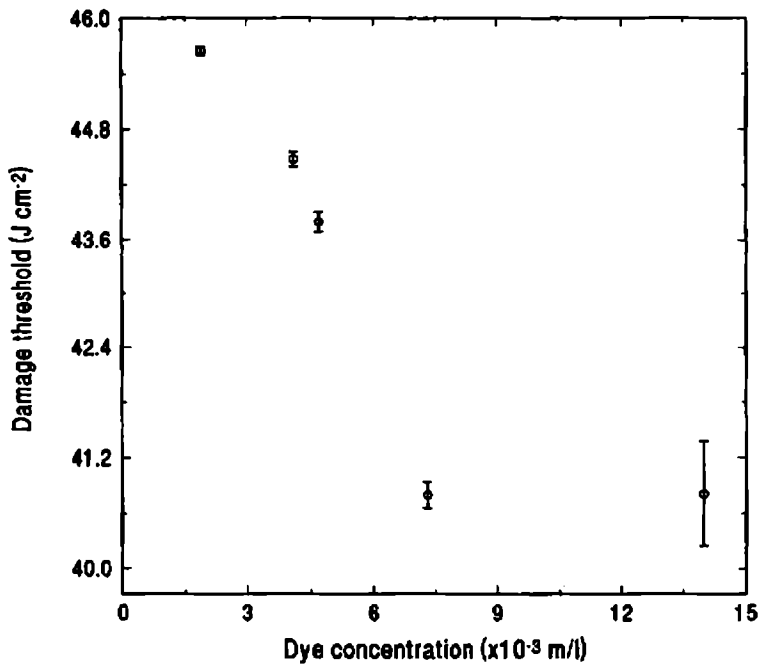

Fig.4.4 The variation of laser damage threshold with dye concentration

In dye doped polymers photo-destruction of dyes take place at higher laser fluences. Detailed studies are needed to understand the role played by this decomposed dyes on photoablation of the samples. They may act as absorbing inclusions in the matrix. The

anomalous micro-elastic properties of polymers can lead to damage in these materials even when the heating of absorbing inclusions is negligible[8]. A mechanism of non-linear absorption of the incident laser radiation associated with triboprocesses in the matrix surrounding the inclusion accompanied by the formation of micro cracks in the matrix has been proposed by Danileiko et al.[37]. This mechanism could explain the visible damage of dimensions >1 μm initiated by small inclusions (0.1 μm). This essentially involves surface electronic states being formed during micro crack formation process, and these are capable of absorbing the incident energy to cause damage. The existence of such states have been shown by the sub-threshold luminescence in the Vis-near-UV regions due to radiative de-excitations[38] . In this analysis, the damage mechanism for a spherically symmetric absorbing defect comprising of a small region of dimension (smaller than the wavelength) and having an absorption coefficient appreciably larger than the surroundings, under irradiation for a short pulse is considered. This induced thermo-elastic stresses increase with time in the matrix. At the damage threshold, these stresses reach micro-breaking magnitudes leading to micro cracks. A further increase in the laser energy causes the increased density of these micro cracks and thus the concentration of electronic states capable of further absorption of the laser energy increases. Assuming the thermo-elastic stress near an inclusion to be proportional to its temperature, the process of non-linear heating in the matrix can be described in terms of a heat conductive equation which describes the absorption of laser energy by the inclusion and possibly by the electronic states formed at the damage sites., the solution of which gives the expression for the temperature at the centre of the defect. The LDT can be estimated from the conditions of loss of stability of the steady state solution of the equation for the temperature with respect to time. This mechanism accounts for damage mechanisms like micro-cracks and micro-damages.

4.4 Methods for improving laser resistance in polymeric media

An increase in the ambient temperature to the level at which the matrix passes from the glassy into the highly elastic state leads to a significant increase in the damage threshold[39]. This effect is dependent on the intensity as well as the wavelength of the radiation.

It has been found that introduction of plasticizers increases the damage threshold.

112

Low molecular dopants improve the optical transparency[42] and reduces the mechochemical reactions and hence responsible for the suppression of the accumulation effect. The influence of plasticizers on the rate of destruction of polymeric samples is associated with the transfer of energy by hot radicals to the dopant[43]. For example a significant improvement in the laser resistance of PMMA was observed by the addition of the plasticizier viz. ethanol.

Another method of enhancing the laser resistance of polymeric matrices used in active laser media, along with the technological uniformity (absence of dust particles, bubbles etc.) and the introduction of plasticizers, is a significant improvement of the structural uniformity of the polymeric systems and a more uniform distribution of the dye in the matrix.

4.5 Conclusions

The various aspects of laser induced damage process have been discussed in detail. Photothermal phase shift technique was used to characterize the laser polymer interaction. The photothermal phase shift effect has been applied to the estimation of the laser damage threshold in PMMA and polyacrylamide. There exists abrupt change in the PTPS signal in the region of laser damage threshold. Also the method of determination of electron density in experimental plasma studies using interferometric technique has some advantages compared to other methods like spectroscopic methods and electronic probing[44,45]. Spectroscopic determination of electron density requires absolute calibration of the detector in the entire spectral range of interest and in electronic probing, the flow pattern of the plasma is perturbed due to probe insertion. PTPS technique that we have described offers a simple, sensitive technique for determining the laser plasma densities and avoids the use of complex detection systems and painstaking calibration procedures.

113

References

[1] P E Dyer and J J Sidhu, Appl. Phys., **57**, 1420, (1985).

[2] Srinivasan R and Bodil Braren, Chem. Rev., **89**, 1303, (1989).

[3] G F Lipscomb, A F Grito and P S Narang, J. Chem. Phys., **75**, 1509, (1981).

[4] D Milan, Appl. Opt., **16**, 1204, (1977).

[5] A Costela, F Flondo, I Garina-Moreno, R Duchowicz, F AmatGuerri, Figuera and R Sastre, Appl. Phys. B., **60**, 383, (1995).

[6] A A Manenkov, V S Nechitailo, A S Tsaprilov, Sov. J. Quantum. Electron., **11**, 502, (1981).

[7] B M Ashkindaze et al., Sov. Phys., JETP, **23**, 788, (1966).

[8] M I Aldoshin, et al. Sov. J. Quantum. Electron., **9**, 1102, (1979).

[9] A S Bebchuck et al., Sov. J. Quantum. Electron, **6**, 986, (1976).

[10] A V Butenin, and B Y Kogan, Sov. J. Quantum. Electron., **6**, 611, (1976).

[11] A A Manenkov and V S Nechitailo, Sov. J. Quantum. Electron., **10**, 347, (1980).

[12] D Milam, SPIE proceedings, Vol.140, 'Optical Coatings-Applications & Utilization-II', 52, (1978).

[13] B E Newnam and D H Gill 'Laser Induced Damage in Optical Materials' NBS special publication No.462, p-292 (1976).

[14] M J Soileau et al., 'Laser Induced Damage in Optical Materials' NBS special publication, No. 541, 309, (1978).

[15] B Monson , Reeta Vyas and Gupta R, Appl. Opt., **28**, 2554, (1989).

[16] J A Sell 'Photothermal Investigations of Solids and Fluids', Academic, New York, (1988).

[17] R.Gupta, in 'Proceedings of the International Conference on Lasers'86', R.W.McMillan, Editor (STS press, McLean, VA, 1987).

[18] A C Tam, Rev. Mod. Phys., **58**, 381 (1986).

[19] S E Bialkowski, Spectroscopy, **1**, 26 (1986).

[20] J Stone, J. Opt. Soc. Am., **62**, 327 (1972)., Appl. Opt., **12**, 1828, (1973).

[21] C.C.Davis, Appl. Phys. Lett., **36**, 515, (1980).

[22] A C Boccara, D Fournier, W B Jackson, and N M Amer, Opt. Lett., **5**, 377 (1980).

[23] A C Boccara, D Fournier, J Badoz, Appl. Phys. Lett., **36**, 130, (1980).

[24] D Fournier, A C Boccara, N M Amer, and R Gerlach, Appl. Phys. Lett., **37**, 519 (1980).

[25] W B Jackson, N M Amer, A C Boccara, D Fournier, Appl. Opt., **20**,1333 (1981).

[26] J P Gordon, R C C Leite, R S Moore, S P S Poto, and J R Whinnery, J. Appl. Phys., **36**, 3 (1965).

[27] H L Fang and R L Swoford, 'Ultrasensitive Laser Spectroscopy', D S Kliger, Ed. (Academic, Newyork, 1983).

[28] R Vyas and R Gupta, Appl. Opt., **27**, 4701 (1988).

[29] L Spitzer, 'Physics of Fully Ionized Gases', Interscience, NewYork, (1956).

[30] K M Dyumaev et al., Sov. J. Quantum. Electron., **13**, 503, (1983).

[31] M B Agranat et al. Sov. Phys. JETP, **33**, 944, (1971).

[32] M A Liberman and M I Tribelskll, Sov. Phys. JETP, **47**, 99, (1978).

[33] A A Kovalev et al., Sov. Tech. Phys. Lett., **6**, 142, (1980).

[34] K Singh Rajive and J Narayan, Phys. Rev. B, **41**, 8843. (1990).

[35] N B Delone, 'Interaction of Laser Radiation with Matter', Moscow, Nauka. p 280. (1989).

[36] H Kusakawa, K Takahashi, K Ito, Appl. Phys., **10**, 3954, (1969).

[37] Danileiko et al., 'Proceedings of the 4th All Union Conference on Non-linear Interaction of Optical Radiation'.

[38] A A Manenkov et al., Izv. Akad. Nauk. SSSR, **44**, 1770, (1980).

[39] V E Mnuskin, B F Trinchuk et al., Soild-Dye Lasers, Electr. Technika, Series II, p-3, (1987).

[40] T A Speranskaya, L I Tarutina, 'Optical Properties of Polymers', p-136, Leningrad, Khimiya (1976).

[41] K M Dyumanev, A A Manenkov, et al., An SSSR Phys. Series, **8**, 1387, (1987).

[42] H R Griem, 'Plasma Spectroscopy', McGraw Hill, New York, (1964).

[43] R F G Menlen Broeks, M F Q Steewbakkers, Z Qing, M C M Van de Sanden and D C Schram, Phys. Rev. E, **49**, 2272, (1994).

CHAPTER V

NONLINEAR OPTICAL PROPERTIES OF EUROPIUM PHTHALOCYANINE AND EUROPIUM NAPHTHALOCYANINE

Abstract

The role of nonlinear optical materials in applications such as optical switching, amplification, limiting etc. has resulted in a search for newer and efficient photonic materials. Phthalocyanine is one such material whose optical nonlinearity has not yet been studied completely. The versatility of phthalocyanine allows the tailoring of novel materials with enhanced optical nonlinearities. The nonlinear refractive index can be varied substantially by altering the π-electron system as well as by substitution of the central metal atom. With this objective in mind, studies were conducted on the nonlinear optical properties of europium phthalocyanine as well as europium naphthalocyanine. In the present chapter optical limiting characteristics of europium naphthalocyanine under continuous wave laser irradiation were studied using different wavelengths of Ar^+ laser.

5.1 Introduction

When an electromagnetic wave propagates through a medium, it induces a polarization (electric dipole moment per unit volume) and magnetization (magnetic dipole moment per unit volume) in the medium as a result of the motion of the electrons and nuclei in response to the fields of the incident waves. These induced polarizations and magnetizations oscillate at frequencies determined by a combination of the properties of the material and the frequencies contained in the incident light waves. The interference of the fields radiated by the induced polarization or magnetization of the incident fields defines the optical properties of the medium as well as the characteristics of the radiation that is transmitted through it. Various linear optical interactions include absorption, refraction, elastic and inelastic scattering etc.

At sufficiently high intensities, the nonlinear optical interactions arises from

(i) The larger motion of the electrons and ions in response to the stronger optical fields. Examples of the processes that occur in this manner is harmonic generation and parametric frequency mixing.

(ii) In the second type of nonlinear response called self action effects in which some properties of the medium is changed, which in turn affects the propagation characteristics of the light wave, including both absorption and focussing properties. They can also change the spatial, temporal, and spectral distributions of the incident wave, as well as its state of polarization. An example of such type of response is a change in refractive index of the medium induced by the optical wave. Such changes can occur because of the orientation of anisotropic molecules along the incident fields, because of the changes in density of the medium as a result of electrostriction or as a result of temperature variations in the medium following absorption of incident wave. Schematic representation of wavefront distortions in a nonlinear medium resulting in self focussing and defocussing is given in Fig.5.1.

The nonlinear index of refraction is an important parameter in the applications of nonlinear optics[1-5]. It leads to a variety of phenomena which can in turn be used to measure the nonlinear refractive index of the material. To characterize the third-order optical nonlinear properties of the materials several techniques exists like degenerate

118

four-wave mixing, third harmonic generation, optical Kerr gate, self focusing methods, surface plasmon studies, Z-scan etc., which is the subject of several articles[5-12].
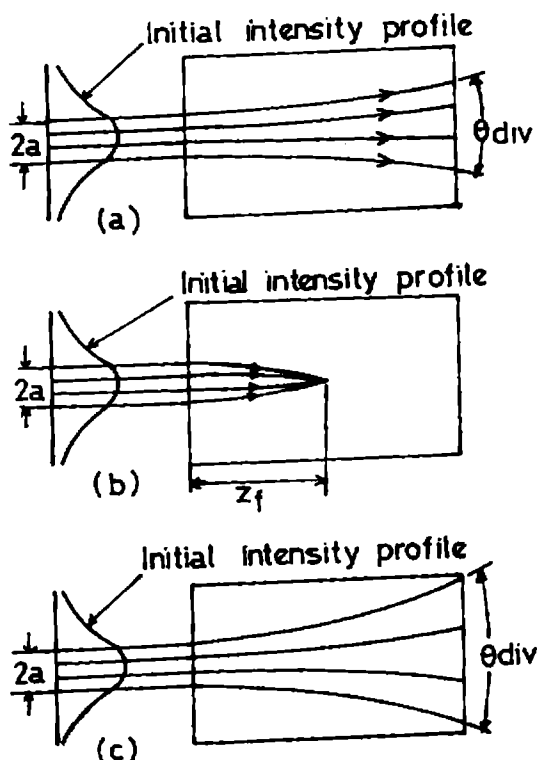

Fig.5.1 Schematic representation of wavefront distortions in (a) linear, nonlinear medium with (b) self focussing and (c) defocussing.

In 1989, Sheik-Bahae et al. developed a sensitive measuring technique called Z-scan in which the intensity-dependent transmission of the laser beam through the sample is measured with and without an aperture in front of the detector[11,12]. An open aperture scan gives information on purely absorptive nonlinearity whereas the closed aperture Z-scan gives out information on dispersive nonlinearities. The ratio of the normalized closed and open aperture scans generate a curve due to purely dispersive nonlinearity. The detailed description of the Z-scan technique is given in section 1.3.5.

5.1.1 Nonlinear optical materials

Phthalocyanines (Pc) are stable, robust organometallic materials that have recently been shown to be attractive candidates for nonlinear optical (NLO) applications[13-19].

119

Similar to organic materials organo-metallic compounds also offer the advantages of architectural flexibility, ease of fabrication and tailoring. An important aspect of utilizing organo-metallic structure for applications in nonlinear optics is their unique charge transfer capability associated with transitions either from metal to ligand or ligand to metal. The metal to ligand bonding in organo-metallics gives rise to large molecular hyperpolarisabilities due to the transfer of electron density between the metal atom and the conjugated ligand atoms. In addition, the diversity of central metal atom, oxidation states, their size and the nature of ligand helps in tailoring materials with optimized optical interactions[20]. Phthalocyanine macrocycle is a two-dimensional π-conjugated system which allows incorporation of as many as 60-70 different metal atoms. A number of modifications can also be made by substituting side groups at the peripheral sites of the ring. This architectural flexibility facilitates in tailoring chemical and physical properties of metallo-phthalocyanines (MPc) over a broad range and as a result MPcs have proven to be useful materials for solid-state technology and biomedical engineering. Recently metallo-naphthalocyanines (MNcs) also have attracted attention in the field of electronics, as near infrared dyes, organic semiconductors, photoconductors, lasers and optical disk materials[21-23]. The extensively delocalized π-electron system of phthalocyanine holds considerable promise for the development of nonlinear optical devices. Also the third order nonlinear susceptibilities of MPcs vary dramatically depending on the metal atom and peripheral substitution[24,25]. For example in tetrakis(cumylphenoxy)phthalocyanines, the hyperpolarisability varies by 1-2 orders of magnitude depending on the central metal atom that has been substituted[25].

Phthalocyanines and naphthalocyanines are structural analogs of porphyrines. The structural diversity of phthalocyanines and naphthalocyanines is the main factor responsible for their importance in various physico-chemical and biological studies. This structural diversity opens up unlimited possibilities for studying the effect of functional substituents and central atoms on the properties of the compounds. Such studies will enable us to provide an answer to the question why nature was choosy to evolve the porphyrins, which is the basic element of chlorophyll and blood.

5.1.2 Structure of Phthalocyanine and Naphthalocyanine

The inner ring system of Pcs and Ncs is made up of pyrrole rings joined together by

aza (-N=) groups. A benzene ring is attached to the β position of each of the pyrrole groups to form a phthalocyanine molecule and a naphthalocyanine ring attached to the β position forms a naphthalene molecule.

In MPcs as well as in MNcs, the central atom displaces two hydrogen ions from the isoindole group and practically finds itself in a symmetrical electrostatic field of four nitrogen atoms with which it may form four equivalent or almost equivalent coordinate donor-acceptor bonds as shown in Fig.5.2 and forms diphthalo and dinaphthalo cyanines which has a large number of conjugated π-electron systems.

In this chapter, the details of synthesis, characterization and the nonlinearities of Europium phthalocyanine [Eu(Pc)₂] and Europium naphthalocyanine [Eu(Nc)₂] are given.

5.1.3 Synthesis and characterization of Eu(Pc)₂ and Eu(Nc)₂

5.1.3.1 Europium phthalocyanine

The phthalocyanine complexes of various rare earth elements were synthesized according to the method of Kirin et al.[26]. Anhydrous europium acetate and phthalonitrile were mixed in the stoichiometric ratio 1:8 and heated to 280⁰C in a nitrogen atmosphere for two hours.
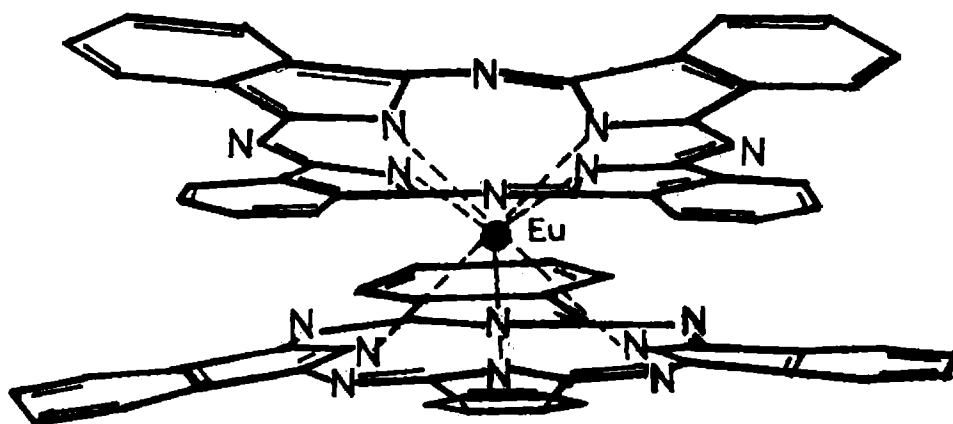

Fig.5.2 Structure of Europium phthalocyanine.

121

The product was column chromatographed over neutral alumina using di-methyl formamide (DMF) as solvent. These are sandwich compounds with two phthalocyanine rings coordinated to a single trivalent atom[27].

5.1.3.2 Europium naphthalocyanine

A mixture of 0.14 g of anhydrous europium acetate and 0.68 g of 2,3-DCN were heated to 250^{0}C for two hours in a nitrogen flushed evacuated glass tube. Eu(Nc)$_2$ thus synthesized was dissolved in DMF and column chromatographed over neutral alumina using DMF as eluent. DMF was evaporated off and Eu(Nc)$_2$ was dried at 130^{0}C *in vacuo* for four hours.

5.2 Studies on optical nonlinearities of Eu(Pc)$_2$

The nonlinear characteristics of Europium phthalocyanine dissolved in DMF was studied using Z-scan technique. Eu(Pc)$_2$ is sparingly soluble in most of the organic solvents but fairly soluble in DMF. The percentage transmittance of the solution in the linear regime at a wavelength of 514.5 nm was 60%.

Z-scan technique was employed for studying the optical nonlinearities with an intensity stabilized CW Ar$^+$ laser as the excitation source. Theoretical aspects as well as the schematic experimental setup for Z-scan studies is given in 1.3.5. Europium phthalocyanine solution was taken in a cuvette of thickness 0.49 cm and the laser beam was focussed using a lens of focal length 18.5 cm so that the thickness of the sample is smaller than the diffraction length (z_0) of the focussed beam where $z_0 = kw_0^2/2$, and $k = 2\pi/\lambda$ is the light wavenumber and w_0 is the minimal Gaussian beam waist radius. The sample was scanned in the focal region using a motorized translation stage. In the open aperture Z-scan the detector used to measure the transmittance through the medium was a power meter so that the entire beam is falling on the detector head, and for closed aperture it was a PIN photodiode. A lock-in amplifier interfaced with a personal computer is used to analyze the photodiode output. A mechanical chopper at a frequency of 25 Hz was used to enable lock-in detection. The open and closed aperture Z-scans were done at 476.5 and 514.5 nm wavelengths.

The absorption spectrum of Eu(Pc)$_2$ is given in the Fig.5.3 which shows two prominent ground-state absorption bands: the Q-band in the 600-800 nm (visible) range

and the Soret band or B band in the 300-400 nm (near UV) range. The Q band is strongly dependent on the ligand (Pc ring)and the central metal atom causes only a small change. In the 400-600 nm, the ground-state absorption of MPc's is very weak. It has been reported by Chufei Li et al.[28] that different metal phthalocyanine have the excited-state absorption maxima located in the wavelength range around 500 nm, which is the location of minimum ground-state absorption. Hence metal phthalocyanines shows reverse saturable absorption in this wavelength region.
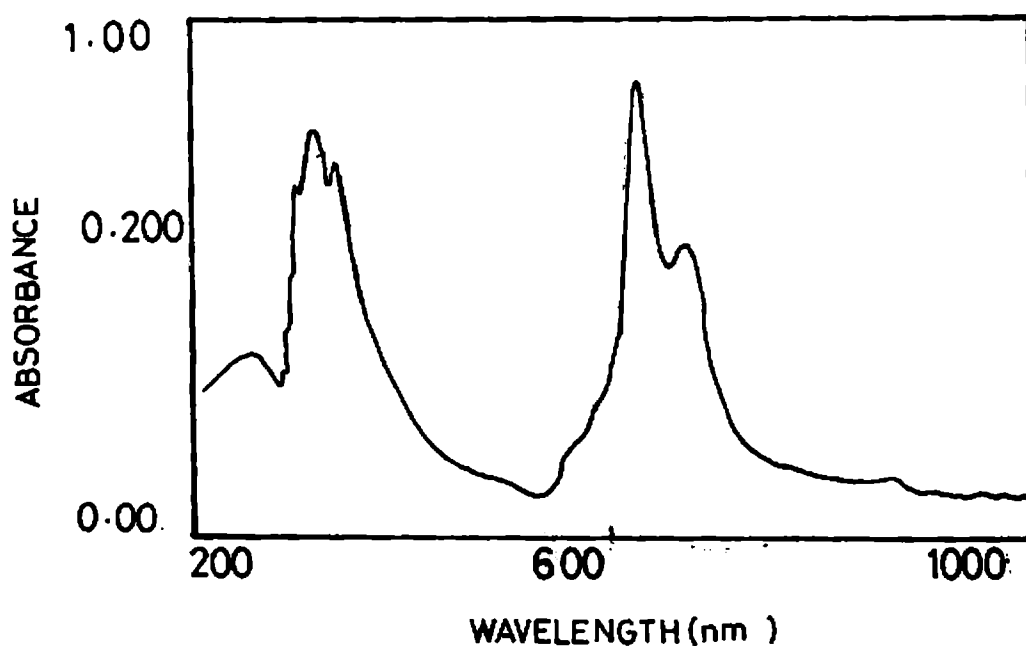

Fig.5.3 Absorption spectrum of Europium phthalocyanine solution in dimethyl formamide.

Fig.5.4 shows the intensity-dependent transmission of the sample measured without an aperture, i.e., the open aperture Z-scan at 476.5 nm. For the open aperture scan the sample solution is taken in a cuvette of thickness 0.49 cm, so that the Rayleigh range (z_0) 0.83 cm is greater than the sample thickness, which is an essential criteria for Z-scan measurements. The intensity of the input beam at the focus is 458 Wcm^{-2}. In this case the normalized power transmittance decreases at the focus by 0.93 times that of the low power transmittance.

The value of the nonlinear coefficient β was obtained by fitting the experimentally observed plot using the equation.

$$T(z) = \sum_{m=0}^{\infty} \frac{[-q_0(z,0)]^m}{(m+1)^{3/2}}, \text{where } q_0 = \beta I_0(t) \, L_{eff}/ \, (1 + z^2/z_0^2)$$

where $T(z)$ = Transmittance of the sample, L_{eff} = the effective length of the sample, z = the sample position, z_0 = the Rayleigh range and I_0 = the input laser intensity. [The detailed derivation is given in Chapter I]. The value obtained was 125.1 cm/W. Similar plot was obtained using 514.5 nm beam and is shown in Fig.5.5 The intensity of incident beam at the focus is 604 Wcm^{-2}. The normalized power transmittance decreases at the focal point by 0.87 times that of the low power transmittance. In this case the value of β obtained is 187.03 cm/W.
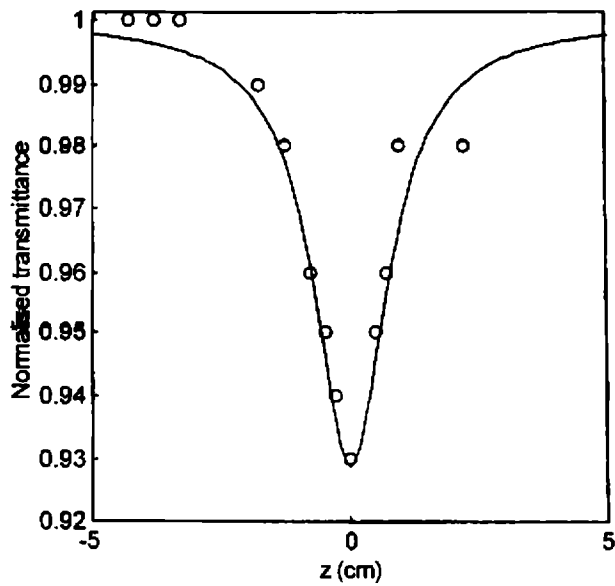

Fig.5.4 Open aperture Z-scan curve of Eu(Pc)$_2$ at 476.5 nm. The solid line shows the theoretical fit with the value of β equal to 125.1 cm/W.

Here Eu(Pc)$_2$ shows considerable amount of nonlinear characteristics even at moderate laser intensities from continuous wave lasers. This is a highly promising result since not many materials exhibit optical nonlinearity at such low light levels.

124

For studying the refractive nonlinearities, a closed aperture Z-scan was performed in which the far field transmittance with an aperture in front of the detector was measured as a function of the distance on either side of the focal point.
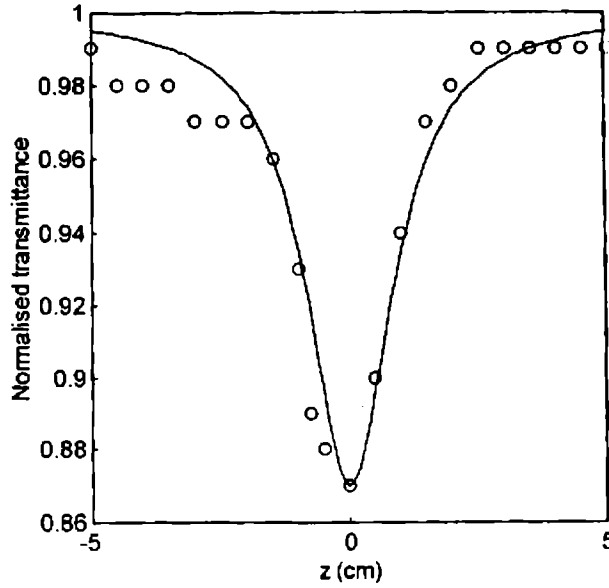

Fig.5.5 Open aperture Z-scan curve for Eu(Pc)$_2$ at 514.5 nm. The solid line shows the theoretical fit, from which the value of β was found to be 187.03 cm/W.

The detector was kept at a distance of 2 m from the focal point. The aperture radius was 0.5 mm so that the value of S = 0.0012. The closed aperture Z-scan at 476.5 nm, and 514.5 nm is shown in Figs 5.6 and 5.7 respectively. From the peak-valley separation ($\Delta T_{p\text{-}v}$) of the closed Z-scan the nonlinear refractive index change of Eu(Pc)$_2$ can be obtained using the equation

$$\Delta n(t) = \frac{\Delta T_{p\text{-}v}}{0.406\ (1\text{-}S)^{0.25}\ k\ L_{eff}}$$

where $\Delta n(t)$ = the nonlinear refractive index, S = aperture linear transmittance (= 1-exp(-2r^2/w^2), with w denoting the beam radius and r the aperture radius), k (= 2π/λ) is the wave number and L$_{eff}$ = the effective length of the sample. At 476.5 nm the value obtained is 4.5 x 10^{-4} whereas that for 514.5 nm the value is 6.8 x10^{-4}.
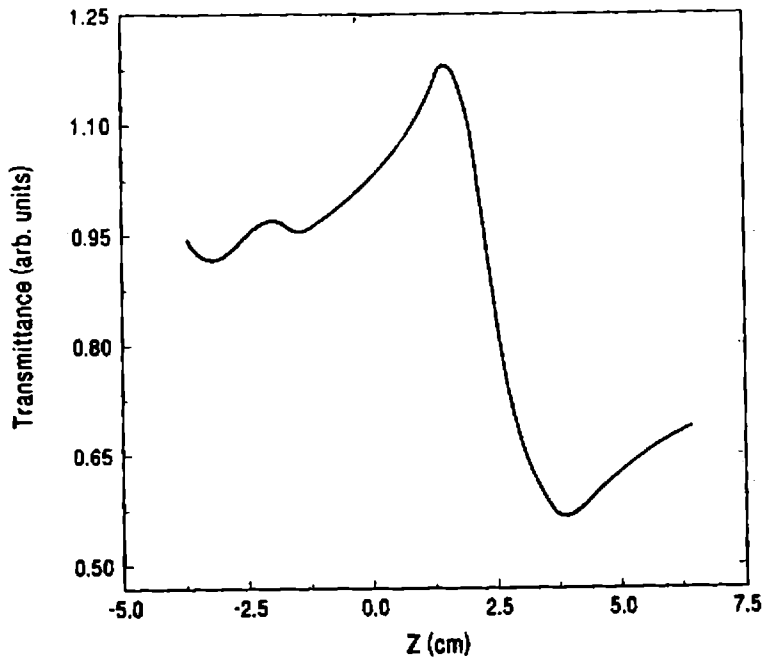
125

Fig.5.6 Closed aperture Z-scan trace at 476.5 nm. From ΔT_{p-v} the value of nonlinear refractive index was calculated as 6.8 X 10^{-4} .
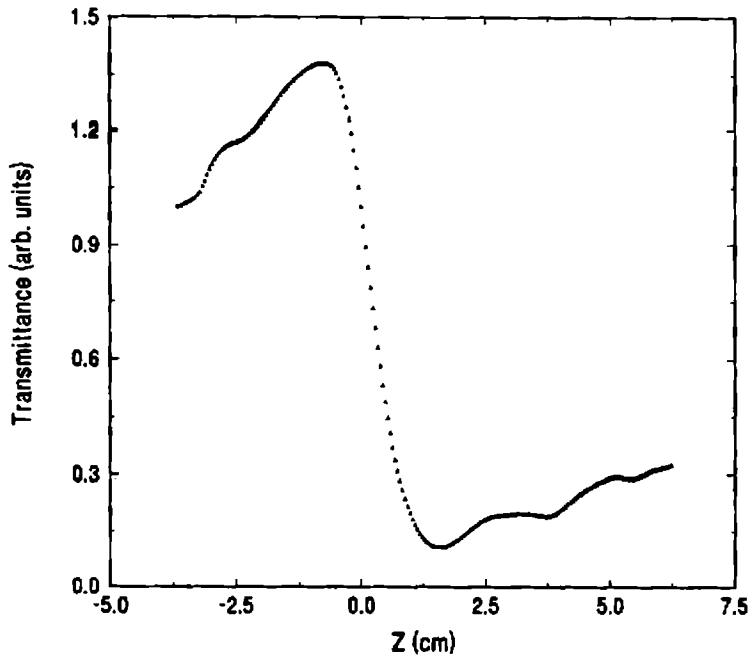

Fig.5.7 Closed aperture Z-scan trace at a pump wavelength of 514.5 nm. The nonlinear refractive index was measured as 4.5 x 10^{-4} .

5.3 Studies on optical nonlinearities of Eu(Nc)$_2$

Naphthalocyanines have an additional benzene attached to each of the free end of the pyrrole ring. Thus napthalocyanines offer additional π-electron conjugation. The heavy metal ion of Europium incorporated in the naphthalocyanine ring increases the nonlinearity compared with metal free compound.

The absorption spectrum of Eu(Nc)$_2$ is given in the Fig. 5.8. It can be seen that the Q-band shows a red shift compared to that of Europium phthalocyanine. This is due to the influence of the increased number of conjugated molecules in the ring structure.

The open aperture Z-scan curve at 476.5 nm is shown in Fig.5.9. The intensity of incident beam at the focus is 428 Wcm^{-2}. The normalized power transmittance decreases at the focal point by 0.80 times that of the low power transmittance. In this case the value of β obtained is 901.03 cm/W. Here Eu(Nc)$_2$ more nonlinear than Eu(Pc)$_2$ described in the previous section.
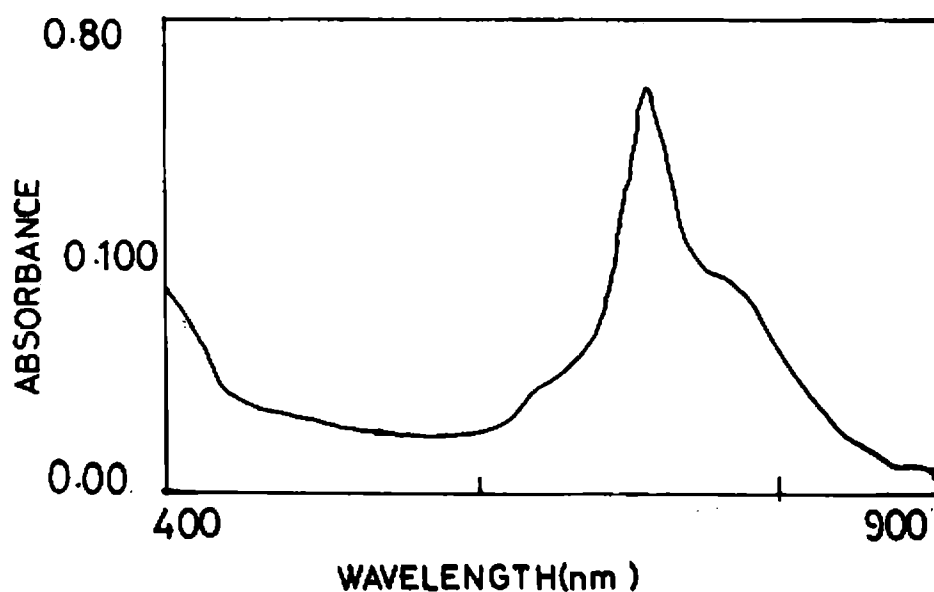

Fig.5.8 Absorption spectrum of Europium naphthalocyanine in dimethyl formamide.

Similar plot was obtained using 514.5 nm beam and is shown in Fig.5.10. The intensity of incident beam at the focus is 358 Wcm^{-2}. The normalized power transmit-

tance decreases at the focal point by 0.82 times that of the low power transmittance. In this case the value of β obtained is 787 cm/W.

For refractive nonlinearity studies a closed aperture Z-scan was performed on $Eu(Nc)_2$ solution. The setup used was the same as that for $Eu(Pc)_2$. The transmittance measured using closed aperture Z-scan at 476.5 nm and 514.5 nm is shown in Figs.5.11 and 5.12. The curve shows an asymmetry in shape before and after the focal point. From the peak-valley separation of the closed Z-scan the nonlinear refractive index change of $Eu(Nc)_2$ was obtained. At 476.5 nm, the value obtained is 3.48 x 10^{-4} whereas that for 514.5 nm the value is 1.1x10^{-4}. The values obtained for nonlinear refractive index Δn, of $Eu(Pc)_2$ and $Eu(Nc)_2$ is of the same order of magnitude to that porphyrin derivative measured by Kandaswamy et al.[29].

Different processes can contribute to the high value of nonlinearity. It can be seen that the nonlinear refractive index of these materials are high. It can bee seen from the studies on $Lu(Pc)_2$ that the phthalocyanines are intervalence compounds.
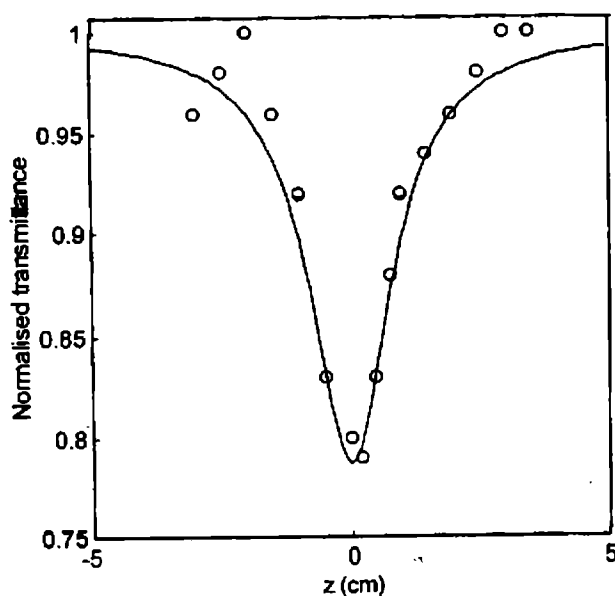
Fig.5.9 Open aperture trace of $Eu(Nc)_2$ at 476.5 nm. The solid line shows the theoretical fit, from which the value of β was found to be 901.03 cm/W.

128
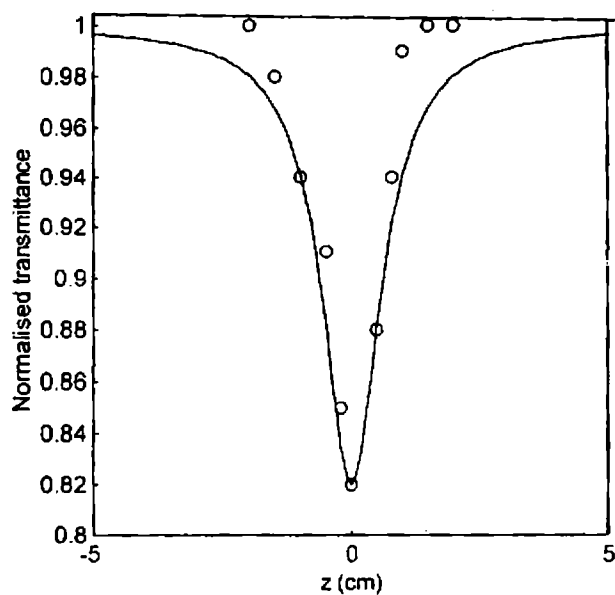
Fig.5.10 Open aperture trace of $Eu(Nc)_2$ at 514.5 nm. From the theoretical fit, the value of β was found to be 787 cm/W.
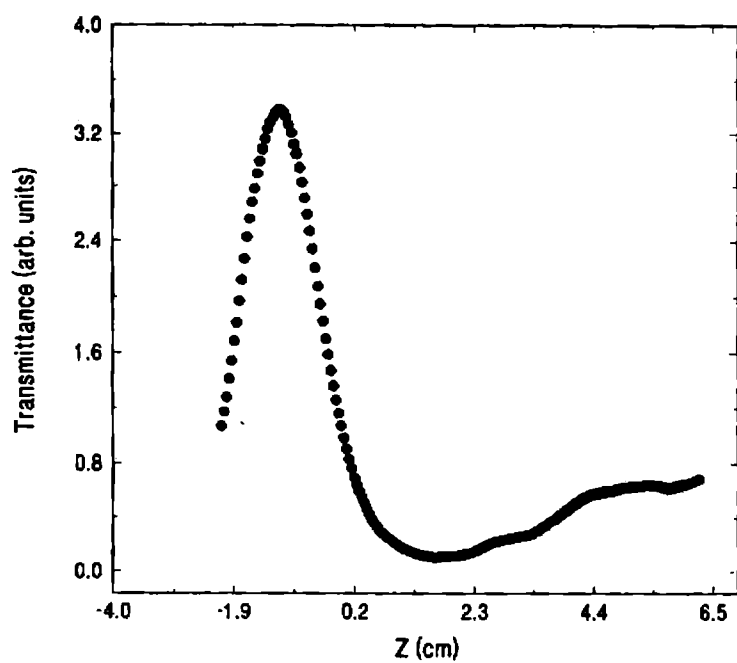

Fig.5.11 Closed aperture Z-scan trace at 476.5 nm. From ΔT_{p-v} the value of nonlinear refractive index was measured as 3.48×10^{-4}
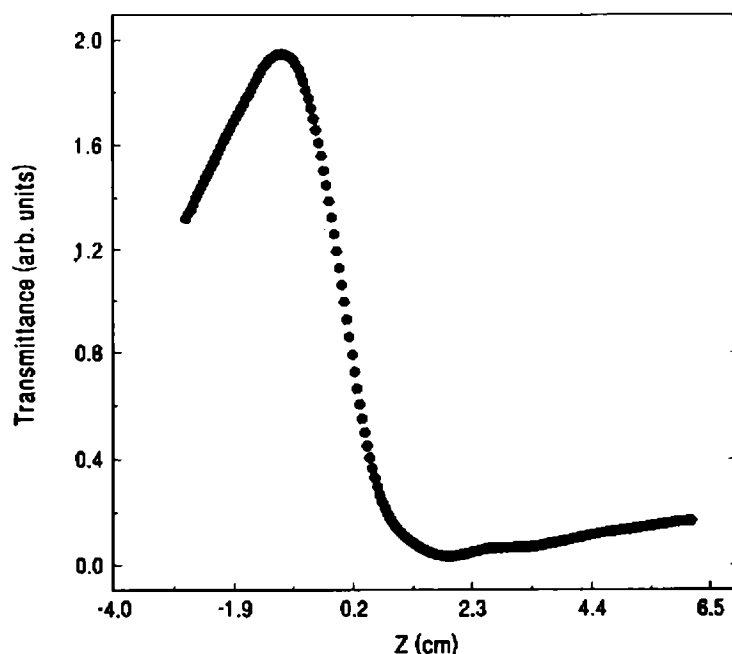
Fig.5.12 Closed aperture Z-scan trace at 514.5 nm. The nonlinear refractive index was measured as 1.1 X 10⁻⁴

These molecules have an odd number of electrons and the unpaired electron resides on the phthalocyanine rings[30]. The intervalence compounds have a characteristic electronic transition that involves considerable charge transfer[31–33]. In addition to having delocalized-electronic structures, the intervalence transition may provide a new degree of freedom for charge redistribution under the influence of the optical field[34]. This redistribution can contribute to the nonlinear refractive index. Since $Eu(Pc)_2$ and $Eu(Nc)_2$ belongs to the same family of molecules, charge redistribution can play a vital role in high value of optical nonlinearity.

In the closed aperture Z-scan the valley is broad and a very definite peak is found. Castillo et al.[35] have attributed it as characteristic of the thermal contribution of nonlinearity. Also even at larger distance from the focus the intensity never reaches the initial value. So thermal contribution play the lead role in the high value of nonlinearity.

Another contribution arises from the reverse saturable absorption in the wavelengths studied. Reverse saturable absorption can occur when states with an absorption cross section higher than that of ground state are produced. When nanosecond and picosecond pulses are used the excited levels mostly involved are singlet levels since

130

the triplet population achievable during this time domain are limited by the small intersystem crossing rate, k_{isc} for these molecules[36,37]. When the atomic number of the central metal atom is increased, k_{isc} for the central metal atom is increased[37]. From the time resolved spectroscopic studies of MPc complexes it is seen that T-T absorption is actually larger by a factor of 2 than the S-S excited state absorption[38]. Hence by using phthalocyanines with heavy metal atom reverse saturable absorption can be enhanced and hence its applicability in optical limiting performance.

5.4 Optical limiting using CW radiation

An optical limiter is a device used to protect optical devices from high intense beams. Its output is proportional to the input when the input is low. When the input intensity has reached a certain threshold, the output becomes either saturated or decreases, safeguarding the sensor. Optical intensity limiters based on nonlinear refraction has been widely investigated for a variety of optical magnitudes and wavelengths[39,40]. The practical application is as intensity protector for various kinds of sensors or detectors. Their high value of nonlinear refractive index, of the order of 10^{-4} makes $Eu(Pc)_2$ and $Eu(Nc)_2$ potential optical limiter material. Limiting action is usually studied using pulses of short duration. But here, studies conducted using CW radiation shows that it can be used as an optical limiter even in this domain. Fig.5.13and Fig.5.14 shows optical limiting characteristics of $Eu(Nc)_2$ using 476.5 nm and 514.5 nm radiations. The cause of optical limiting is reverse saturable absorption. With larger time scale the more prominent triplet-triplet absorption comes into play. Hence it was possible to obtain optical limiting even under low laser intensities intensities[41]. An additional thermal contribution arises from heating of the solvent which arises from absorption by $Eu(Nc)_2$ molecules. It has been shown that this heating increases the excited state absorption which enhances the optical limiting behavior[42]. The optical limiting behavior observed is more prominent with 514.5 nm. The same behavior has been observed while studying optical limiting of KNSBN.Ce crystal using Ar^+ laser[43].

5.5 Conclusion

In conclusion the nonlinearity produced by $Eu(Pc)_2$ and $Eu(Nc)_2$ were studied using Z-scan technique. The order of this nonlinear refractive index was 10^{-4},
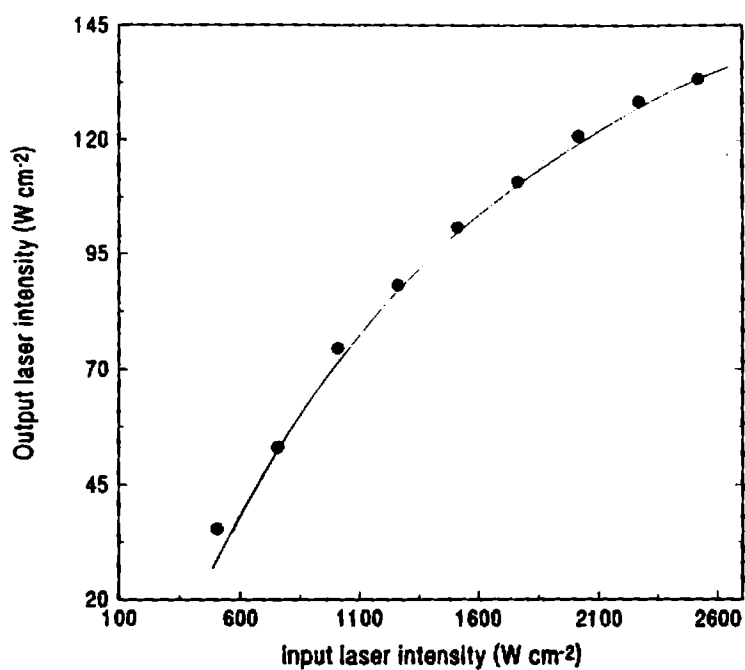
Fig.5.13 Optical limiting characteristics obtained from Eu(Nc)$_2$ using 476.5 nm

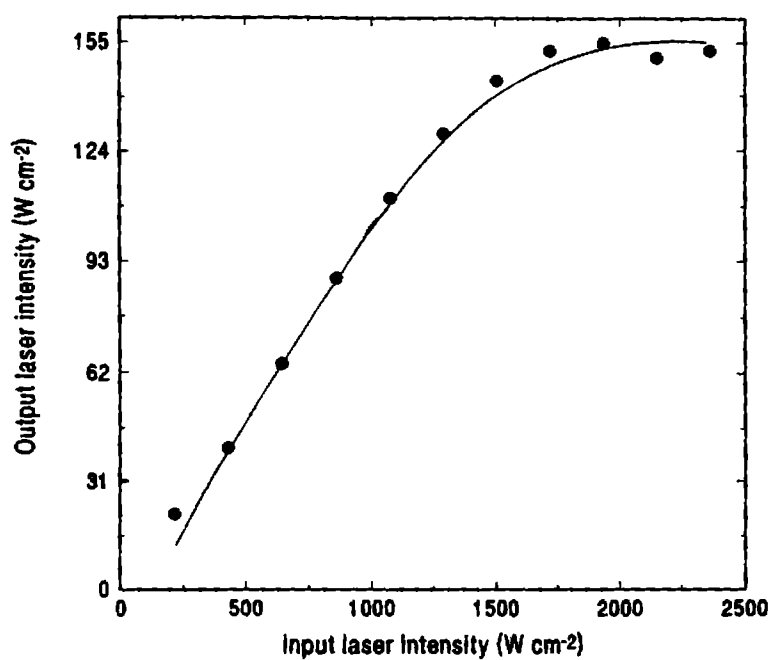Fig.5.14 Optical limiting characteristics obtained from Eu(Nc)$_2$ using 514.5 nm

Sample	Eu(Pc)$_2$		Eu(Nc)$_2$	
Wavelength	476.5 nm	514.5 nm	476.5 nm	514.5 nm
Input Power (W)	9.1×10^{-3}	14×10^{-3}	8.5×10^{-3}	8.3×10^3
α_0 (cm^{-1})	1	0.885	3.762	3.29
L_{eff} (cm)	0.39	0.4035	0.225	0.245
ω_0 (cm)	3.55×10^{-3}	3.84×10^{-3}	3.55×10^{-3}	3.84×10^{-3}
Z_0 (cm)	0.83	0.9	0.81	0.9
I_0 (W/cm^2)	458	604	428	258
β_0	125.1	187.03	901.03	787

Table 1: Experimental Parameters and open aperture Z-scan measurement results of Eu(Pc)$_2$ and Eu(Nc)$_2$

Sample	Eu(Pc)$_2$		Eu(Nc)$_2$	
Wavelength	476.5 nm	514.5 nm	476.5 nm	514.5 nm
Input Power (W)	3.5×10^{-3}	14×10^{-3}	3.9×10^{-3}	2×10^3
α_0 (cm^{-1})	1.178	1.178	3.17	3.32
L_{eff} (cm)	0.3773	0.3773	0.25	0.244
Δn	4.5×10^{-4}	6.8×10^{-4}	3.48×10^{-4}	1.1×10^{-4}

Table 2: Experimental Parameters and closed aperture Z-scan measurement results of Eu(Pc)$_2$ and Eu(Nc)$_2$

which is comparable to the reported values[29]. Since Eu(Nc)$_2$ has more absorption coefficient at the wavelengths studied, optical limiting was also observed in this sample at 514.5 nm and 476.5 nm. The optical nonlinearities in Eu(Pc)$_2$ and Eu(Nc)$_2$ are so large that it is prominent at comparatively low laser intensities of a CW laser.

In order to account for the experimental observations the excited state absorptions from the triplet level must also be included. A six level model must be used for the complete description of the observed phenomena. The fairly good heat conduction of the liquid solution distorts the Gaussian temperature distribution. Therefore, there is a necessity for a more detailed modelling, including the change of n with the temperature (dn/dT), the geometrical deformation of the solution due to thermal expansion and the deviation from the Gaussian nature of heat distribution in the sample.

References

[1] R Lina Yang, Dorsinville, Q Z Wang, P X Ye, and R R Alfano, Opt. Lett., **17**, 323, (1992).

[2] Alan Kost, Lee Tutt, Marvin B Klein, T Kirk and William E Elias, Opt. Lett., **18**, 334, (1993).

[3] Michael D Tocci, Mark J Bloemer, Michael Scalora, J P Dowling and Charles M Bowden, Appl. Phys. Lett., **66**, 2324, (1995).

[4] E W Van Stryland, Vanherzeele, M A Woodall, M J Soileau, A L Smiri, Shekhar Guha, Thomas F Boggess, Opt. Eng., **24**, 613, (1985).

[5] Fryad Z Henari, Karl H Cazzini, Declan N Weldon, and Werner J Blau, Appl. Phys. Lett., **68**, 619, (1996).

[6] R Priestly, A D Walser, R Dorsinville, W K Zou, D Y Xu, N L Yang, Opt. Commu., **131**, 347, (1996).

[7] H S Nalwa, Atsushi Kakuta, Akio Mukoh, Chem. Phys. Lett., **303**, 109, (1993).

[8] P P Ho, 'Semiconductors Probed by Ultrafast Laser Spectroscopy', Vol.II, Ed. R R Alfano, Academic, New York, (1984).

[9] M J Soileau, W E Williams, and E W Van Stryland, IEEE J. Quant. Electron., **QE-19**, 731, (1983).

[10] R F Wallis, and G I Stegmann (Eds.) 'Electromagnetic Surface Excitation' Springer-Verlag, Berlin (1986).

[11] M. Sheik-Bahae, Ali A. Said, E.W.Stryland, Opt. Lett., **14**, 955, (1989).

[12] M. Sheik-Bahae, Ali A. Said, Tai-Huei Wei, David J.Hagan, E.W.Stryland, IEEE J. Quant. Electron., **26**, 760, (1991).

[13] J S Shirk, et al. 'New Materials for Nonlinear Optics' S R Marder, J E Sohn, G D Stucky, (Eds.) ACS Symposium series 455, American Chemical Society, Washington, DC, p-626, (1991).

[14] Z Z Ho, C Y Ju, W M Heatherington, J. Appl. Phys, 62, 716, (1987).

[15] N Q Wang, Y M Cai, J R Helfin, A F Garito, Mol. Cryst. Liq. Cryst., 189, 39, (1990).

[16] J S Shirk, J R Lindle, F J Bartoli, Michael E Boyle, J. Phys.Chem., 96, 5847, (1992).

[17] J S Shirk, R C G S Pong, F J Bartoli, A W Snow, Appl. Phys. Lett., 63, 1880, (1993).

[18] S Venkatachalam, and V N Krishnamurthy, Indian J. of Chemistry, 33A, 506, (1994).

[19] D R Ulrich, 'Organic Materials for Nonlinear Optics', Ed. R A Hann and D Bloor, Royal Soc. Chem. London, (1989).

[20] H S Nalwa, A Kakuta and S Miyata, 'Nonlinear Optics of Organic Molecular and Polymeric Materials' (CRC press, Bocaraton).

[21] Xerox Corporation, US Patent No. 4492750, Jan.8, (1985).

[22] S Kobayashi, K Iwaski, H Sasaki, Oh-Hara, M Nishizawa and M Kateyyose, Jap. J. Appl. Phys., 30, L114, (1990).

[23] A Kakuta, and S Kobayashi, IInd International Symposium on Chemistry of Functional Dyes, Aug. 23-28, Kobe, Japan (1992).

[24] J W Perry, K Mansour, Seth R Marder, K J Perry, D Alvarez, Jr., Ingrid Choong, Opt. Lett., 19, 625, (1994).

[25] J S Shirk, J R Lindle, F J Bartoli, C A Hoffmann, Z K Kafafi, A W Snow, Appl. Phys. Lett., 55, 1287, (1989).

[26] I S Kirin, P N Moskalev, Y A Makashev, Russ. J. Inorg. Chem., **12**, 369, (1967).

[27] A DeCian, M Moussavi, J Fischer, R Weiss, Inorg.Chem., **24**, 3162, (1985).

[28] Chufei Li, Lei Zhang, Miao Yang, Hui Wang, and Yuxiao Wang, Phy. Rev. A, **49**, 1149, (1994).

[29] K Kandaswamy et al., Appl. Phys. B, **64**, 479, (1997).

[30] J J Andre, K Holczer, P Petit, M T Riou, C Clarisse, R Even, Fourmigue, M Simon, J.Chem. Phys. Lett., **115**, 463, (1985).

[31] M B Robin, P Day, Adv. Org. Radiochem., **10**, 267, (1967).

[32] N S Hush, Prog. Inorg. Chem., **8**, 391, (1967).

[33] K Y Wong, P N Schatz, Prog. Inorg. Chem., **21**, (1981).

[34] J S Shirk, J R Lindle, F J Bartoli and Michael E Boyle, J. Phys. Chem., **96**, 5847, (1992).

[35] M D Iturbe Castillo, J J Schez-Mondragon, S I Slepanov, Optik, **100**, 49, (1995).

[36] P A Firey, W E Ford, J R Sounik, M E Kenney, and MA Rodgers, J. Am. Chem. Soc. **110**, 7626, (1988).

[37] J H Brannon and D Magde, J. Am. Chem. Soc.,**102**, 62, (1980).

[38] T Wie et al. App. Phys. B, **54**, 46, (1992).

[39] R C C Leite, S P Porto, and T C Damen, Appl. Phys. Lett., **10**, 100.

[40] E W Van Stryland, Y Y Wu, D J Hagan, M J Soileau, J. Opt. Soc. America, **5**, 1980, (1988).

[41] F Z Henari, S MacNamara, O Stevenson, J Callaghan, D Weldon, and W Blau, Adv. Mater., **5**, 930, (1993).

[42] B I Justus, Z H Kafafi, and A L Huston, Opt.Lett., **18**, 1603, (1993).

[43] John Malowicki et al., Opt. Engg., **34**, 2248, (1995).

136

CHAPTER VI

STUDIES ON OPTICAL NONLINEARITIES OF CHLOROPHYLL AND FULLERENES

Abstract

In the first part of this chapter the nonlinear absorption mechanism of chlorophyll solution is studied employing different techniques, when pumped with the second harmonic radiation from an Nd:YAG laser. It was found that reverse saturable absorption plays an important role in the nonlinearity rather than two photon absorption. The second part deals with the measurement of thermo-optic coefficient of C_{70} in benzene solution using the Z-scan technique.

6.1 Introduction

Organic compounds are currently being studied intensively to identify materials of large third order nonlinearity. The application of nonlinear techniques like Z-scan, optical limiting, wave mixing and harmonic generation facilitates the understanding of the photophysics of these compounds. They also promise interesting applications in optical processing, switching and limiting. Materials with large third order nonlinearities can have an intensity-dependent index of refraction and/or absorption and exhibit nonlinear optical response. Many studies have been made on the organic and biological molecules having porphyrin like structures to understand their nonlinear optical properties[1-3]. One of the main members in the porphyrin family is the naturally occurring chlorophyll. Those in search of materials with large and fast optical nonlinearities have found that chlorophyll is a suitable candidate.

An interesting organic nonlinear material is green tea in which nonlinear studies have been reported. Using He-Ne laser, Hong -jin Zhang et al. have studied the nonlinearities of chinese tea in ethanol solution. The large nonlinearity observed was attributed to the pull of higher refractive index molecules into regions of high optical density by light pressure[4]. 532 nm, 70-ps pulses from a CW mode locked Nd:YAG laser were used by He et al.[5] to study the formation of transient multiple diffraction ring patterns in the solution of chinese green tea. They attributed the origin of optical nonlinearities to the reorientation and redistribution of the large and anisotropic molecules in tea solution.

In this chapter the different experiments performed to identify the origin of the absorptive nonlinearity of tea solution in chloroform are described and the results obtained are discussed. The open aperture Z-scan and optical limiting were used to measure the value of two-photon absorption coefficient. Photoacoustic measurements were also done to augment the argument that two photon absorption plays a negligible role in the nonlinearity of tea solution compared with reverse saturable absorption.

Discovery of fullerenes, the high molecular weight, stable allotropic form of carbon opened up a new and exciting field of research[6-9]especially after it became possible to synthesize and isolate them in macroscopic quantities using Krätschmer-Huffman

138

process[10,11]. These molecules have unique properties like relatively high temperature superconductivity, photovoltaic response and a high degree of hardness, persistent photoconductivity etc[12-16]. It has been found that fullerenes exhibit high optical nonlinearities which can be used for second harmonic generation, optical limiting, etc. in thin film and while embedded in matrices. Because of the high rate of intersystem crossing to the triplet level, the fluorescence emission spectra of these molecules are very weak with an extremely low fluorescent quantum yield of the order of 10^{-4} at room temperature[17-19]. In section 6.3 the thermal origin of nonlinearity of C_{70} in benzene solution is studied using Z-scan technique with He-Ne laser as the exciting source, from which the value of thermo optic coefficient, $(\partial n/\partial T)/k$, was evaluated.

6.2 Optical nonlinearity of tea solution in chloroform

6.2.1 Study using Z- scan technique

Purified tea powder was boiled in distilled water and the reddish brown solution was filtered off. This was repeated several times so that most of the water soluble pigments are washed off. The pigments in black tea (aqueous solution) are oxidized to polyphenolic compounds, mainly the aflavins and thearubigins, which are the oxidation products from the polymerization process in the tea fermentation. Theaflavins have a bright reddish color in solution while thearubigins are reddish-brown pigments with acidic properties. The tea leaves are then dried and dissolved in chloroform and the extract was used for the experiment. Chloroform was used as the solvent for chlorophyll, as it is a common solvent for dissolving polymers like PMMA so that doped polymers can be made for nonlinear applications.

The absorption spectrum of chlorophyll solution was recorded at room temperature and is given in Fig.6.1 it was concluded that the main component of the tea solution in chloroform is chlorophyll a. It has absorption peaks at 430 nm as well as 650 nm. While it is not possible to make detailed assignments, it seems fairly well established that the absorption bands at 430 nm and 660 nm in chlorophyll resulting from the $\pi \rightarrow \pi^*$ transition to the singlet states[20].

All the experiments reported here have used 10 ns pulses from a Q-switched frequency doubled Nd:YAG laser (Spectra Physics DCR-11) operating at 10 Hz repetition rate as the light source. The experimental arrangement for Z-scan is the same as that

given in Chapter II. The laser beam was tightly focussed using a lens, (f = 18 cm) so that the beam waist radius at the focus is calculated to be 9.5 μm. The laser irradiance at the focal point is 1.67 GWcm^{-2}. The solution was taken in a quartz cuvette of thickness 0.49 cm and the Rayleigh range was found to be 0.54 mm which is less than the thickness of the cuvette.
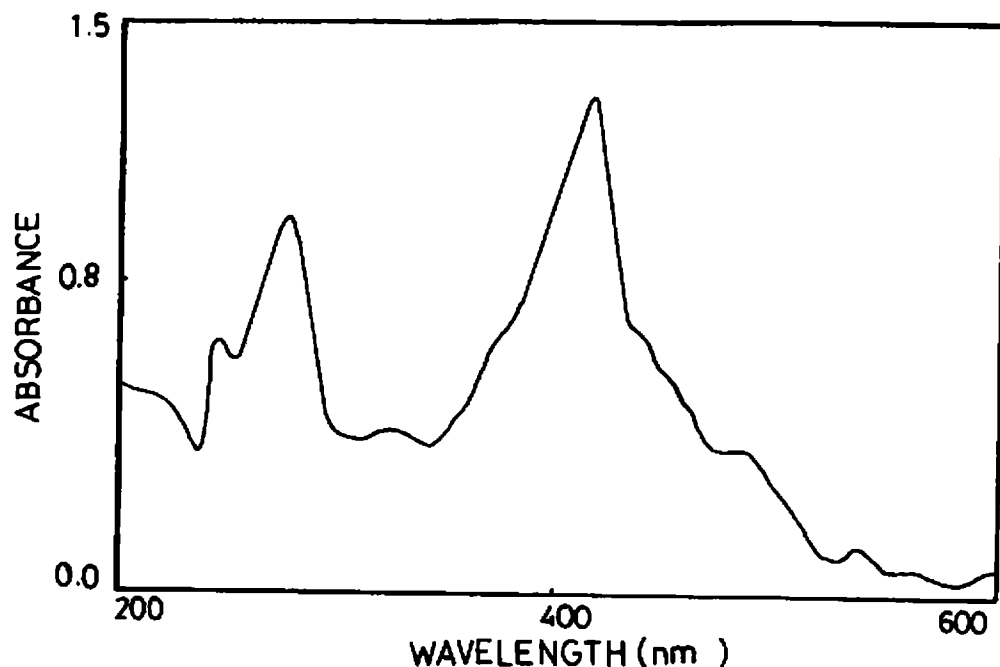

Fig.6.1 Absorption spectrum of chlorophyll

The transmitted light through the cuvette with the tea solution was detected by an open aperture configuration as a function of sample distance (z) from the focal plane. This allows the measurement of nonlinear absorption coefficient. The losses due to surface reflections were also taken into account during calculations. The incident energy is fixed for the entire duration of Z scan. The transmitted energy of the sample was measured after averaging for ten successive pulses. The incoming and the transmitted laser energy were measured by Scientech (Model No.362) laser power meter . To make sure that surface damage of the cuvette is not contributing to the nonlinear signal, it is necessary to translate the sample through the focus in one direction and then back

140

in the reverse direction. If surface damage occurs the two traces do not overlay. This was done for all Z-scans and no damage was observed. For clarity only the forward trace results are presented.

Intensity dependent transmission of laser beam can arise due to different mechanisms like nonlinear absorption, nonlinear refraction etc.. The nonlinear absorption may be due to two photon absorption, excited state absorption or free carrier absorption. Thermal nonlinear refractive and scattering processes may mask the effect of nonlinear absorptive process. These can be reduced by considering weakly concentrated solutions. Standard experimental results for the open aperture Z-scan is shown in Fig.6.2.

A three level molecular energy system with no saturation, diffusion or recombination during the pulse was considered for explaining the observed Z-scan plot. The equation for the intensity (I) of a laser beam propagating (in the z direction) through a nonlinear medium in which linear absorption, two photon absorption and excited state absorption are present can be written as[1]

$$\frac{dI}{dz} = -\alpha I - \beta I^2 - \sigma_{es} N(t) I \tag{1}$$

where α is the linear absorption coefficient, β is the two photon absorption coefficient, σ_{ex} is the excited state absorption cross section and N is the population density of the excited states created by the absorption process.

The population density N is governed by the eq.1.

$$\frac{dN}{dt} = \frac{\alpha\, I}{h\nu} - \frac{N(t)}{\tau} \tag{2}$$

where τ is the decay time for the excited state and $h\nu$ is the energy of a laser photon. The modified equation after combining eqs.1 and 2 is

$$\frac{dI}{dz} = -\alpha I - \frac{\sigma_{ex}\, \alpha\, I}{h\nu} \int_{-\infty}^{t} I(t')dt' \tag{3}$$

Solving this equation for the fluence and integrating over the spatial extent of the beam. we may write the normalized energy transmission T as
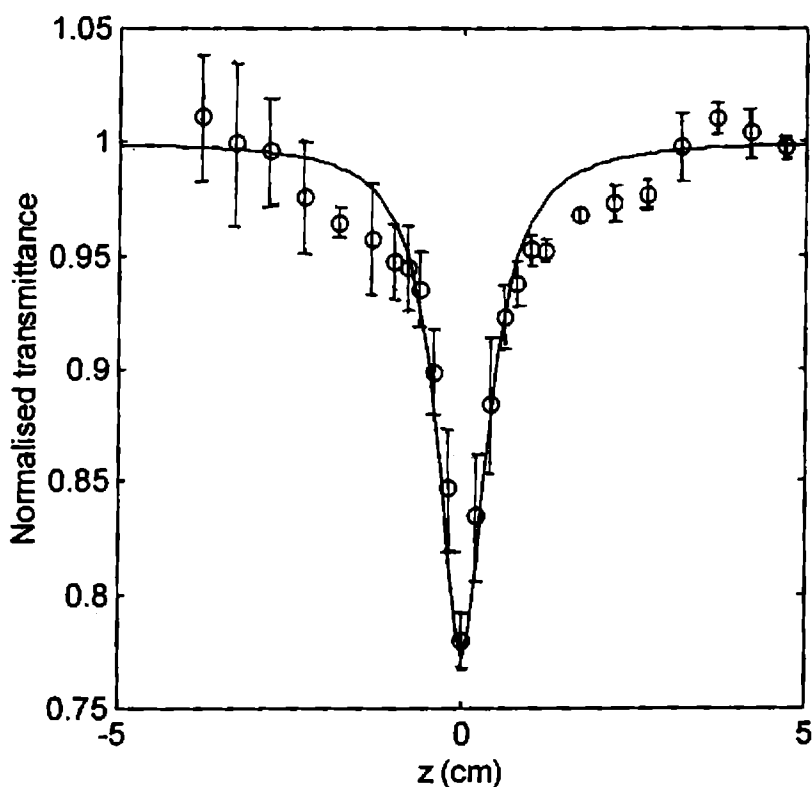
Fig.6.2 Open aperture Z-scan trace obtained from chlorophyll dissolved in chloroform, using 532 nm as the exciting source. From the theoretical fit the value of β was obtained as 1.53 cm/GW.

$$T = \ln\left[1 + \frac{q_0}{1 + x^2}\right] \Big/ \left[\frac{q_0}{1 + x^2}\right]$$

$$\text{where } q_0 = \frac{\sigma_{ex}\ \alpha\ F_0\ (r = 0)\ L_{eff}}{2h\nu} \tag{4}$$

$x = z/z_0$, z is the distance of the sample from the focus (with a positive value between the focus and the detector), $L_{eff} = [1-\exp(-\alpha L)]/\alpha$ and $F_0(r = 0)$ is the on-axis fluence at focus. The value of β was obtained by fitting the Z-scan nonlinear absorption curve (i.e. without aperture) using eq. 4.

The full curve in the figure represents the best fit to the data points utilizing eq. 4, giving a value for $\beta = 1.53\pm0.08$ cm/GW. The main uncertainties arise from the fluctuations in laser intensity and in the determination of the transmission at maximum intensities. Another uncertainty concerns with the beam waist parameter. The value found out in air will be different from that in solution. The variation can arise as

142

the beam has to traverse three media (air, quartz and solvent, i.e., chloroform) with different refractive indices. Hence experiment was repeated at the same input intensity and error bar was drawn.

6.2.2 Nonlinear absorption studies using optical limiting

Optical limiting is obtained by varying the input laser fluence and measuring both the input and output fluences[21]. The variation in the intensity of light as it passes through an absorbing medium is proportional to the intensity of light. The linear absorption of light through the specimen obeys Beer-Lambert's law.

$$I = I_0 \exp(-\alpha L) \qquad (5)$$

where I_0 is the input fluence, I the output fluence, α the absorption coefficient and L the length of the sample. At low input fluence, the transmittance (I/I_0) obeys Beer-Lambert's law. At high input fluence the transmittance decreases with input fluence and we observe an optical limiting property with saturated output fluence.

Optical limiting has been observed in many materials, but they all rely on the nonlinear mechanisms like nonlinear absorption, nonlinear refraction, induced scattering and even phase transition. The nonlinear absorption may be attributed to various processes like two photon absorption, excited state absorption, or free carrier absorption. Thus by studying the optical limiting property, the origin of absorptive nonlinearity can be found out.

The optical limiting studies were done in chlorophyll solution which has a low intensity transmittance of 68%. The 532 nm Nd:YAG laser beam was focussed using a lens of focal length 18 cm. The sample was taken in a cuvette of thickness 4.9 mm and kept close to the focal point. The input and output powers were measured using laser power meter (Scientech). The optical limiting curve obtained is as shown in Fig.6.3. The curve shows that the solution has a linear transmittance at low intensities and the curve deviated from linearity at 12 MWcm^{-1}, after which the output saturates. This optical limiting can be accounted by making use of reverse saturable absorption, two-photon absorption or both.
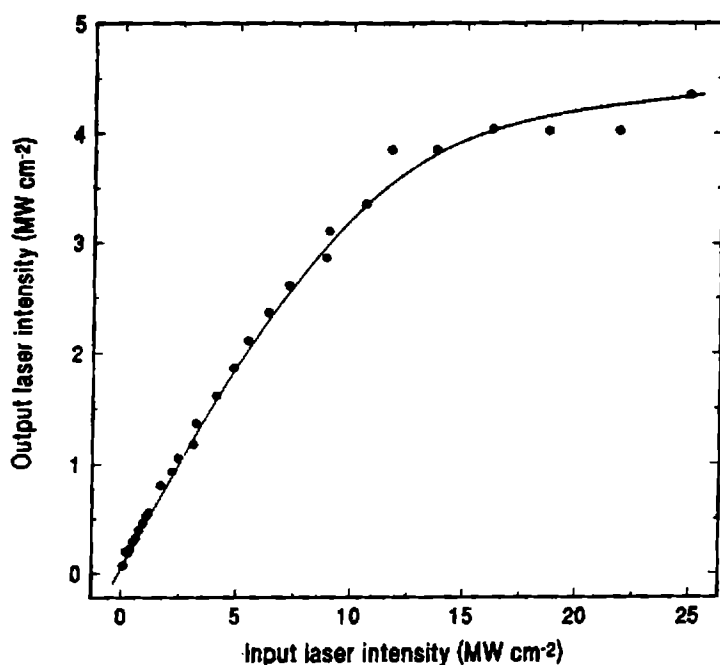
143

Fig.6.3 The optical limiting observed in tea solution. From the slopes at high and low intensity region the excited state cross section was found to have higher value, i.e., $\sigma_{ex}/\sigma_g = 7.3$.

Reverse saturable absorption arises in a molecular system when the excited state absorption cross-section is larger than the ground state cross-section. The process can be understood if three vibronically broadened electronic levels are considered as shown in Fig.6.4. The cross-section of absorption from the ground state 1 is σ_g and σ_{ex} is the cross section for absorption from the first excited state 2 to the second excited state 3. The life time of the first excited state is τ_2 (seconds).

As light is absorbed by the material, the molecules in the ground state are excited to the first excited level and the population in that level increases. If σ_{ex} is smaller than σ_g, then the material becomes more transparent or 'bleaches': i.e., it acts as a saturable absorber. But when σ_{ex} is higher than σ_g the material acts as reverse saturable absorber.
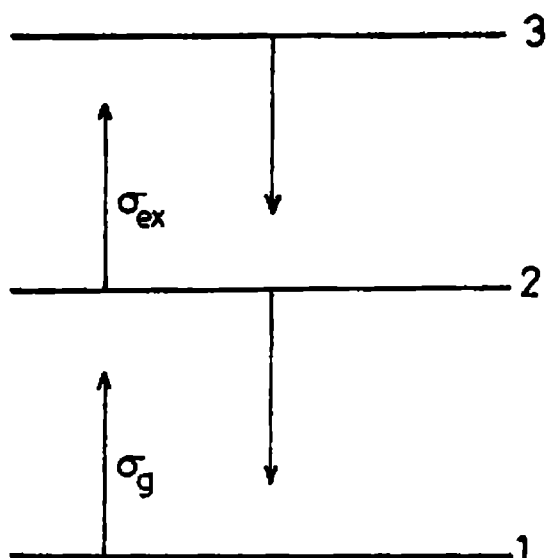
144

Fig.6.4 Three level model for reverse saturable absorption

The change in intensity of a beam as it propagates through the material is

$$dI/dz = -[N_T \sigma_g + N_2(\sigma_{ex} - \sigma_g)]I \tag{6}$$

where z is the direction traversed, N_T is the total number of active molecules per area in the slice dz, N_2 is the population of level 2 and the population in level 3 has been neglected. Initially the slope is given by $T = 10^{-\sigma_g N_T L}$, since the level 2 is empty. At sufficiently high fluence, however, the excited state 2 becomes substantially populated and in the limit of complete ground state depletion the slope again becomes constant at the new value of $10^{-\sigma_{ex} N_T L}$. The ratio σ_{ex}/σ_g will be sufficiently large for a reverse saturable absorber. From Fig.6.3 it can be seen that optical limiting is observed in tea solution. At low intensity region the slope is 0.68, while at high fluence region the slope decreases to 0.06. From this the ratio $K = \sigma_{ex}/\sigma_g$ was found to be 7.3. It is well known that a material with larger K will have stronger reverse saturable absorption (RSA) and hence better optical limiting[22]. It must be noted that C_{60}, which is considered a good optical limiter[23,24] has K~3.

145

A more effective model for reverse saturable absorbers with triplet absorption was proposed by Kojima et al.[25]. According to their five level model, the incident fluence I_0 and the transmitted laser fluence I obey the relation

$$\ln\left[\frac{I_0}{I}\right] = k(I_0 - I) + A_g \tag{7}$$

where k is a constant that depends on the absorption cross sections and life times of the ground, excited singlet and excited triplet states and A_g is the ground state absorbance. This equation implies that a plot of $\ln(I_0/I)$ versus (I_0-I) should be a straight line with a slope k and intercept A_g. Fig.6.5 shows one such plot and it is linear in the fluence range of interest. This is a clear indication that RSA plays the dominant role in the nonlinear absorption process in tea solution.
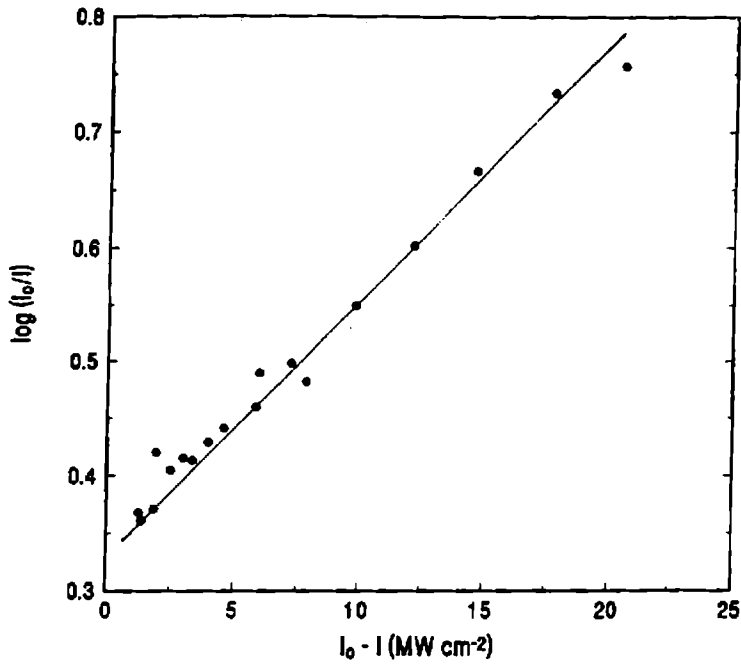

Fig.6.5 Plot of $\ln(I_0/I)$ versus $(I_0- I)$

Two photon absorption (TPA) may also contribute significantly to optical limiting in some cases. TPA is an optical nonlinearity that involves simultaneous absorption of two photons to promote an electron from its initial state to a state corresponding to two times the photon energy state. The mechanism of TPA can be thought of in

146

terms of the three level RSA model for the case where the lifetime of the intermediate state approaches zero and the ground state absorption is extremely low (highly transparent)[26]. The intensity of the beam as it traverses the material is

$$\partial I/\partial z = -(\alpha + \beta I)I \qquad (8)$$

where α is the linear absorption coefficient and β is the TPA coefficient. The solution to the propagation equation for negligibly $\alpha = 0$, is given by

$$I(L) = \frac{I_0}{(1 + I_0\beta\, L)} \qquad (9)$$

where L is the length of the sample. From this equation also the value of TPA coefficient was found to be 0.33 cm/GW and this shows that multiphoton absorption plays a minor role where as excited state absorption is the dominant cause of nonlinearity.

6.2.3 Pulsed photoacoustic technique

Pulsed photoacoustic (PA) technique can be effectively used to study multiphoton absorption in solutions.[27-30] Here, in order to confirm the results obtained by open aperture Z-scan and optical limiting experiments, PA technique was employed.

The schematic of the experimental setup for PA measurements is given in Fig.6.6 and it consists of a pulsed, second harmonic output from a Q-switched Nd:YAG laser, a fabricated PA cell that contains the sample chamber and a piezoelectric transducer, lead zirconate titanate (PZT) that detects the acoustic signals. The output from the PZT was observed in a storage oscilloscope (Tektronix TDS 220). The 532 nm, laser beam was focussed by a convex lens into the PA cell containing the tea solution, so that the focal point is at the center of the cell. The incident power was measured using Scientech (Model 362) laser power meter. The averaged amplitude of the first pulse in the PA signal trace is monitored as a function of laser power.

The PA cell is made up of stainless steel and for the entry and exit of the laser beam glass windows are provided, as shown in Fig.6.7. The PZT used is a disc of 4 mm thick and 15 mm diameter, firmly mounted on a stainless steel chamber to minimize external electrical pickup and to prevent sample contamination by PZT. This steel casing is screwed onto the PA cell. The diaphragm of the transducer chamber has a thickness of

0.5 mm and is finely polished. A lead disc followed by a copper disc forms the backing of the PZT which is spring loaded within the chamber.
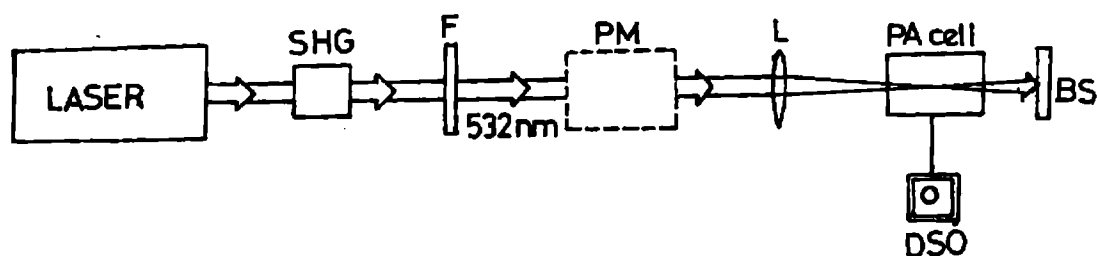

Fig.6.6 Schematic diagram of the experimental set up. SHG-Second harmonic generator, F-Filter, PM-Power meter, L-Lens, DSO-Digital storage oscilloscope, BS-Beam stopper

The PA signal amplitude q(ν) generated in an absorbing liquid medium at input laser frequency ν can be written as[30]

$$q(\nu) = \frac{A}{\pi\,\omega_0^2}\sigma\,(\nu)\,L_{eff}N\tau\eta(\nu_m)I^m(\nu) \tag{10}$$

i.e., q(ν) is proportional to the mth power of the incident intensity I(ν), m being the number of photons involved in the process. In the above equation, A is a constant determined by the calibration factor which include cell geometry, acoustic transducer property etc., $\sigma(\nu)$ the absorption cross section at a laser frequency ν, N the density of the absorbing molecules, L_{eff} the effective path length in the cell given by $L_{eff} = $ [1-exp($-\alpha L$)]/α, where α is the absorption coefficient in the units of cm^{-1} and ω_0 is the beam waist radius at the focal point. Therefore assuming the dominance of m photon

148

absorption, the slope of the plot of log q(ν) vs log I(ν) will give an indication of the number of photons involved in the process.
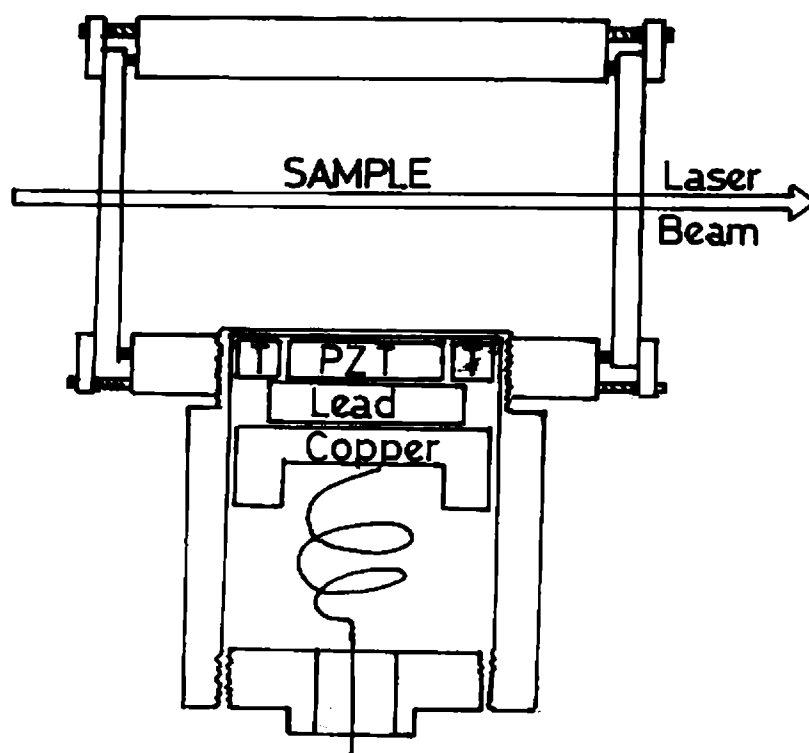

Fig.6.7 Photoacoustic cell and transaucer chamber

The chlorophyll solution is taken in the cell and 532 nm Nd:YAG beam is focussed into the cell. With varying input power the PA signal obtained is measured using the digital storage oscilloscope. Fig.6.8 shows the graph of PA signal as a function of laser power on a logarithmic scale. According to eq. 10, the slope of the curve yields the number of quanta absorbed. The intensity dependence of PA signal is found to be linear and there is no tendency for it to change over to higher order dependence greater than one, which clearly indicates that a multiphoton transition does not contribute to optical limiting in chlorophyll.

Since the radiative de-excitation cross section of the chlorophyll solution is comparatively small. Then one would expect an enhanced non-radiative relaxation and thereby a sudden jump in the PA signal in the higher laser fluence when optical limiting begins. But in the present case this is not observed. The graph obtained is linear indicating a slope equal to one.
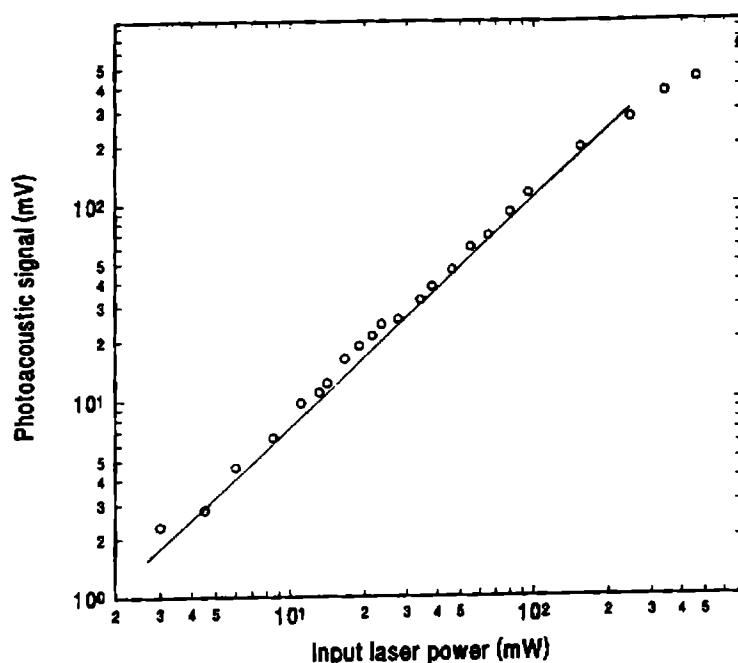
149

Fig.6.8 PA signal strength as a function of input laser power on a logarithmic scale for tea solution in chloroform. The graph is linear indicating that the contribution due to two photon process is negligible

In the high power region, the leading part of the laser pulse excites most of the molecules to the excited singlet state from which due to intersystem crossing, the molecules cross over to the triplet state, which has a longer life time. After resonantly absorbing a photon, the molecule in the triplet state excites to a higher energy state, whose lifetime is in the picosecond region due to fast internal conversion. The molecule can relax to the triplet level by collisional energy transfer to the surrounding solvent molecules.

6.3 Nonlinearity of C_{70} in benzene

The optical nonlinearity of fullerenes has attracted much attention because of its possible application as an optical limiter[18,31-34]. The nonlinear refractive index has been measured under different conditions. Thermal nonlinearity plays an important role in CW excitation. Using a CW laser at 633 nm Gu et al. obtained thermal nonlinearity in C_{60} films[35]. They have suggested that thermal effects play a major role in self focussing observed in films using CW lasers.

150

In order to understand the effects of temperature on nonlinearity the thermo-optic coefficient of the nonlinear solution must be known. Even though thermally induced nonlinearities have been known for many years during the last 30 years some extraordinary strong self focussing effects have come to light[36,37]. Spatially local Kerr nonlinearity was invoked to explain the experiments on spatial dark solitons using CW lasers, but steady state thermal nonlinearity must be utilized in those cases to explain the observed phenomena correctly.

A theoretical analysis for the estimation of the thermal nonlinear parameters was done by Castillo et al. in the case of dye dissolved in ethanol[38]. Using a similar analysis the thermo-optic coefficient, $(\partial n/\partial T)/k$, of the nonlinear solution of C_{70} in benzene was obtained.

6.3.1 Theoretical Analysis

The beam propagation analysis through the medium was done by ABCD Gaussian beam propagation technique. The focal length of the steady state thermal lens which was photoinduced in the volume of the cuvette is[39]

$$F_{th} = \frac{\pi \, k w^2}{P_{abs} \, (\partial n/\partial T)} \tag{11}$$

here k is the thermal conductivity of the liquid, w is the beam radius in the sample (since $d \ll z_0$, w is supposed to be constant through the cuvette thickness), P_{abs} is the total light power absorbed by the sample $P_{abs} = P_{in}(1-e^{-\alpha L})$ where P_{in} is the incident laser power and $(\partial n/\partial T)$ is the derivative of the liquid refractive index on temperature.

The final result for the Gaussian beam radius $(w(z'))$ at the output plane of the Z-scan configuration in the far field approximation $(z' \gg z_0, z)$ is given by

$$\frac{1}{w^2 \, (z')} = \left[\frac{\pi \, w_0}{\lambda \, z'} \right]^2 \left[\frac{F_{th}^2}{z_0^2 + (F_{th} - z)^2} \right] \tag{12}$$

It is clear that this value (i.e. $1/w^2(z')$), in the approximation of the Gaussian output form of the beam, is proportional to the light power detected by the photodiode at the output plane of the system. As a result, the final expression for the transmission coefficient T determined as the ratio of the output light intensity to that in the similar configuration without nonlinear sample (i.e., $F_{th} \to \infty$)

151

$$T = \frac{F_{th}^2}{z_0^2 + (F_{th} - z)^2} \tag{13}$$

Here it has been assumed that the focal length of the thermal lens F_{th} also depends on the beam radius $w(z)$, i.e., on the position of the cuvette, in the following way

$$F_{th} = F_0[1 + (z/z_0)^2] \tag{14}$$

where

$$F_0 = \frac{\pi k}{P_{abs} (\partial n/\partial T)} w_0^2 \tag{15}$$

is the minimal value for the focal length for a case when the sample is put in the waist of the beam i.e. at $z = 0$.

Substituting eq.14 into eq.13 gives the final expression for the transmittance coefficient of the Z-scan configuration in our case:

$$T = \frac{F_0^2 \left[1 + (z/z_0)^2\right]^2}{z_0^2 + \{F_0 [1 + (z/z_0)^2] - z\}^2} \tag{16}$$

As can be seen from eq.15, the ratio $F_0/w_0^2 = $ Constant (w_0), depends on the parameters of the liquid (k and $\partial n/\partial T$) the absorbed laser power P_{abs} only.

In the weak nonlinearity approximation ($F_0 \gg z_0$) and for $|z| \gg z_0$ eq. 8 takes the form

$$T = \left(1 + \frac{2z_0^2}{F_0 z}\right) \tag{17}$$

characterized by rather slow linear inverse dependence of the wings of the curve on z. Peak-to-valley transmittance difference is equal to

$$\Delta T_{p-v} = 2\frac{z_0}{F_0} = 2P_{abs} \frac{(\partial n/\partial T)}{k\lambda} \tag{18}$$

Eq.18 shows that if the absorbed light power is known, one can easily evaluate $(\partial n/\partial T)/$ k value of the liquid under investigation without exactly knowing the beam waist radius w_0.

6.3.2 Experimental details

The experimental arrangement is similar to that of Z-scan with an aperture. The Gaussian beam from a frequency stabilized 10 mW He-Ne laser is used as the excitation source. The focussing lens of focal length 10 cm was used and the C_{70} solution in benzene was taken in a quartz cuvette of thickness 6 mm. The input was chopped using a mechanical chopper whose frequency can be varied. The transmitted output was detected at far field through a narrow aperture of $S = 1.69 \times 10^{-3}$.
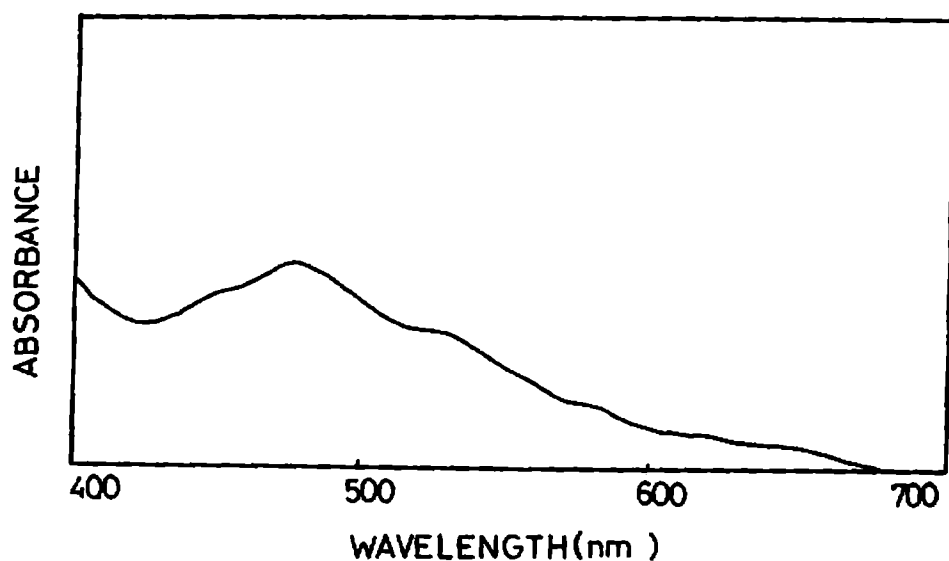

Fig.6.9 The absorption spectrum of C_{70} in benzene solution.

As the sample is moved across the focal point of the lens, i.e., through an intensity gradient, due to the intensity dependent refractive index the measured transmittance shows a variation. A PIN photodiode was used as the detector, the output of which is given to the lock-in amplifier. The experiment was repeated varying the chopping frequency.

The molecular structure of C_{70} molecule is given in Fig.1.9 and Fig.6.9 the absorption spectrum of C_{70} in benzene solution. C_{70} is a cage like molecule with large

153

de-localized π electron cloud responsible for the nonlinear behavior. From Fig.6.9 it can be seen that the wave length used in the study (632.8 nm) is in valley region of the absorption spectrum.

The normalized closed aperture Z-scan curves obtained when the input beam is chopped at different frequencies are given in Fig.6.10.
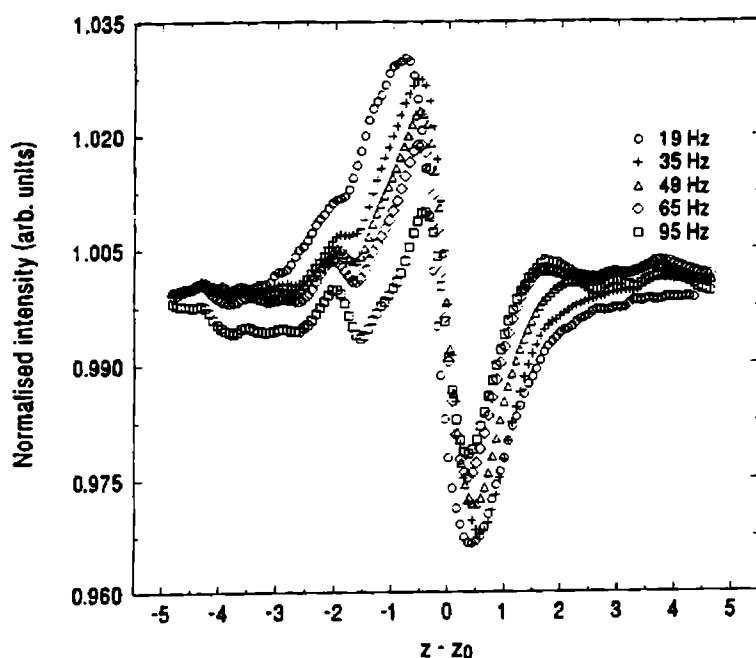

Fig.6.10 Closed aperture Z-scan curve with varying chopping frequency.

From the Z-scan curve the sign as well as the magnitude of nonlinearity can be evaluated. Since a peak is followed by a valley the sign of the nonlinearity is negative. The dependence of the peak to valley transmittance ΔT_{p-v}, on the chopping frequency shows that the nonlinearities exhibited by the molecules have thermal origin. The rise time of a thermal signal in a liquid is determined by the acoustic transit time $T = w_0/v_s$, where v_s is the velocity of the sound in liquid. Furthermore, the relaxation of the thermal lens, governed by the thermal diffusion, is of the order of 100 ms[40]. At higher chopping frequencies the effect of the previous pulse will not vanish by the time of the arrival of second pulse, which is about 10 ms. Hence the cumulative effect of the

pulses causes a decrease in the nonlinearity as shown in Fig. 6.11. Here the nonlinear refractive index was calculated using the well known Z-scan eq.

$$\Delta n = \frac{\Delta T_{p-v} \, \lambda}{2.5(1-S)^{0.25} \, L_{eff}} \tag{19}$$

The effective strength of the nonlinear signal decreases, causing weaker focussing resulting in the formation of a less negative lens in the C_{70} solution. Before the focus, it causes a decrease in collimation i.e., increased thermal blooming, with a consequent decrease in aperture transmittance. And after the focus, the defocussing decreases and the transmittance in the valley increases. This causes a decrease in ΔT_{p-v} value with increasing chopping frequency as observed in Fig.6.10.
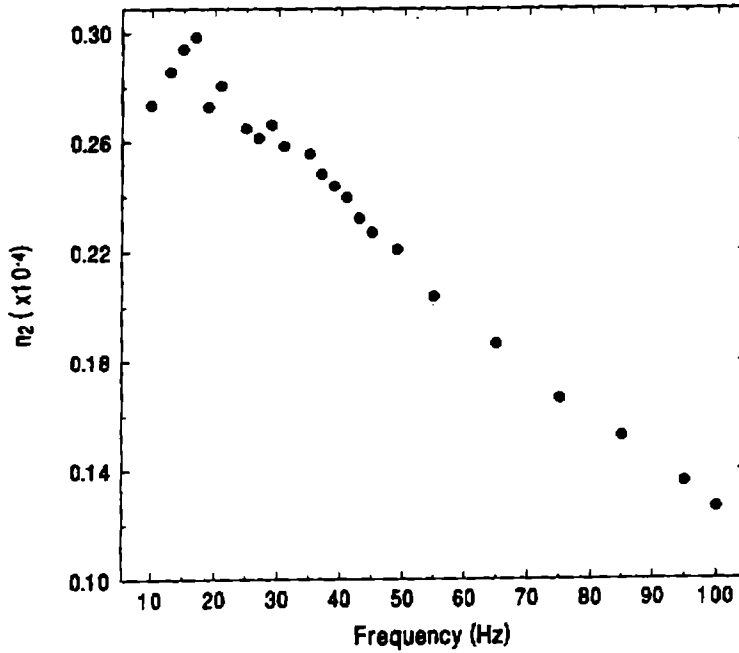
Fig.6.11 The variation in Δn with chopping frequency. As the chopping frequency increases the Δn value decreases.

The nonlinear refraction can also be expressed as[40]

$$\Delta n = \frac{dn}{dT}\Delta T \simeq \frac{dn}{dT} I \tau \alpha / \rho C \tag{20}$$

where τ satisfies the relationship: $\tau^{-1} = t^{-1} + t_c^{-1}$, t is the time exposed to the laser, $t_c = w^2 \rho C / 4k$ is the thermal relaxation time, k is the thermal conductivity, ρ is the

155

density, and C is the specific heat. When the chopping frequency is increased the time exposed decreases, i.e., when f = 10 Hz, t=100 ms, when f = 100Hz, t = 10 ms, and correspondingly the nonlinear refractive index also decreases. The value of thermo-optic coefficient is obtained using the eq. 18. At a particular chopping frequency of 10 Hz, the value of the thermo-optic coefficient was calculated as 0.011 cm/W. The value obtained according to literature[42] is 0.4434 cm/W. This may be due to the less heating up of the sample solution, due to different heat losses in the medium. Hence eq.11 must be modified adequately. Fig.6.11 shows the variation of Δn with chopping frequency. As the chopping frequency is increased, the value of Δn decreases, indicating the thermal origin of the nonlinearities.

6.4 Conclusion

Using the Z-scan, optical limiting and pulsed photoacoustic measurements it was found that simultaneous absorption of two photons is an unlikely process for explaining non-linearity of chlorophyll. Excited state absorption plays the major role in the nonlinearity. In the second part using the Z-scan technique thermooptic parameter of C_{70} in benzene was calculated. The role played by the solvent in which the nonlinear material is dissolved is very important, particularly in the case of thermal nonlinearity.

References

[1] Gary L Wood, Mary J Miller, and Andrew G Mott, Opt. Lett., **20**, 973, (1995).

[2] Armen Sevian, M Ravikath, G Ravindra kumar, Chem. Phy. Lett., **263**, 241, (1996).

[3] Shekhar Guha, Keith Kang, Pamela Porter, J F Roach, David E R, Franscico J Aranda, D V G L N Rao, Opt. Lett., **17**, 264, (1992).

[4] H J Zhang, J H Dai, P Y Wang, and L A Wu, Opt. Lett., **14**, 695, (1989).

[5] K X He, H Abdeldayem, P Chandra Sekhar, P Venkateswaralu, and M C George, Opt. Comm., **81**, 101, (1991).

[6] K L Akers, C Duketis, T L Haslett and M Moskovities, J. Phys. Chem., **98**, 10824, (1994).

[7] E Kolodney, B Tsipnyuk, and A Budrevich, J. Phys. Chem., **100**, 8542, (1994).

[8] F Z Cui, D X Liao, and H D Li, Phys. Lett. A, **195**, 156, (1995).

[9] S Matsuura, T Tsuzuki T Ishigaro, H Endo, K Kikuchi, Y Achiba, and Ikemoto, J. Phys. Chem. Solids, **55**, 835, (1994).

[10] W. Krtschmer, L D Lamb, K Fostriopopoulos, and D R Huffman, Nature, **347**, 354, (1990).

[11] J P Hare, H W Kroto and R Taylor, Chem Phys. Lett., **117**, 394, (1991).

[12] M J Rosseinsky, A P Ramirez, S H Glarum, D W Murphy, R C Haddon, A F Hebbard, T T M Palstra, A R Kortan, S M Zahurak and A V Makhija, Phys. Rev. Lett., **66**, 2830 (1991).

[13] C H Lee, G G Yu, D Mosses, and A J Heeger, Appl. Phys. Lett., **65**, 664, (1994).

[14] V Blank, M Popov, S Buga, S Davydov, V N Denisov, A N Ivlev, B N Mavrin, V Agatonov, R Ceolin, H Szawarc and A Rassat, Phys. Lett. A, **188**, 281, (1994).

[15] A Hamed, H Rasmusa, and P H Hor, Appl. Phys. Lett., **64**, 526, (1994).

[16] L Zhu, S Wang, Y Li, Z Zhang, H Hou and Q Qin, Appl. Phys. Lett., **65**, 702, (1994).

[17] L B Gan, D J Zhou, C P Luo, C H Huang, T K Li, J Bai, X S Zhao and X H Xia, J. Phys. Chem., **98**, 12459, (1994).

[18] Tutt L W, Kost A, Nature, 356, 225, (1992).

[19] J Castalan and J Elguero, J. Am. Chem. Soc., **115**, 9249, (1993).

[20] H vanderLaan, H E Smorenburg, Th. Schmidt and S Völker, J. Opt. Soc. Am. B, **9**, 931, (1992).

[21] Soileau M J, W E Willaims, E W Vanstryland, IEEE J. Quant. Electron., **19**, 731, (1983).

[22] C Li, Lei Zhang, Miao Yang, Hui Wang, and Yuxiao Wang, Phy. Rev. A, **49**, 1149, (1994).

[23] T W Ebbcsen, K Tanigaki, and S. Kuroshima, Chem. Phys. Lett., **181**, 501, (1991).

[24] Chun-Fei, Yu Xiao Wang, F Guo, R Wang, Lei Zhang, Acta Phy. Sin., **42**, 1236, (1993).

[25] Y Kojima, T Matsuoka, N Sato, and H Takahashi, Macromolecules, **28**, 2893, (1995).

[26] L W Tutt and T F Boggess, Prog. Quant. Electr., **17**, 299, (1993).

[27] A M Bonch-Bruevich, T K Razumova, and I O Starbogatov, Opt. Spectro., **42**, 45, (1977).

[28] D A Huchins, Can J Phys. ,**64**, 1247, (1986).

[29] S S Harilal, R C Issac, C V Bindhu, G K Varier, V P N Nampoori, and C P G Vallabhan, Mod. Phys. Lett. B, 9, 871, (1995).

[30] A C Tam, C K N Patel, Nature, **280**, 304, (1979).

[31] A Kost, Tutt L W, Klein M B, Dougherty T K, and Elias W E, Opt. Lett., **18**, 334, (1993). ,

[32] B L Justus, Kafafi Z H, Huston A L, Opt. Lett., **18**, 1603, (1993).

[33] M Cha, N S Sariciftci, A J Heeger, J C Hummelen and F Wudl, Appl. Phys. Lett., 67, 3850, (1995).

[34] Riju C Issac, S S Harilal, Geetha K Varier, C V Bindhu, V P N Nampoori, and C P G Vallabhan, Opt. Eng., **36**, 332, (1997).

[35] Gu G, Zhang Wen, Zen H, Du Y, Han Y, Zhang Wei, Dong F, and Xia Y, J. Phys, B: At. Mol. Opt.Phys., **26**, L451, (1993).

[36] H H Lin, A Korpel, D Mehri and D R Anderson, Opt. News, **15**, 55, (1989).

[37] P P Banerjee, R M Misra, and M Maghranoui, J. Opt. Soc. Am. B, **8**, 1072, (1991).

[38] M D Iturbe Castillo, J J Snchez-Mondragon, S l Stepanov, Optik, **100**, 49, (1995).

[39] H L Fang, R L Swafford, In D Kliger (Ed.): 'Ultra Sensitive Laser Spectroscopy', Academic Press, New York, pp 175-232, (1983).

[40] J N Hayes, Appl. Opt., **2**, 455, (1972).

[41] R L Carman, A Mooradian, P L Kelly, and A Tufts, Appl. Phys. Lett., **14**, 136, (1969).

[42] D Solimini, J. Appl. Phys., **37**, 3314, (1966).

CHAPTER VII

APPLICATIONS OF PHOTONIC MATERIALS

Abstract

Some of the applications of the photonic materials mentioned in the previous chapters are described here. The nonlinear optical properties of Europium phthalocyanine, is made use of in the construction of an optical limiter and Europium naphthalocyanine is used for the construction of an optical inverter. The feasibility of a molecular spatial light modulator was checked making use of reverse saturable absorption of rhodamine 6G doped polyacrylamide at 457.9 nm. The usefulness of dye doped polymer as a luminescent solar concentrator was also studied.

7.1 Introduction

Photonics has emerged as the technology of 21st century and the field of nonlinear optics is being increasingly exploited for the development of a variety of optoelectronic and photonic devices. By making use of the nonlinear optical phenomena, light modulators for controlling the phase or amplitude of a light beam, optical switches, optical limiters etc. have been developed. The present chapter deals with the study of photonic devices like optical limiters, optical switch, spatial light modulator etc. by making use of the nonlinear properties of Europium phthalocyanine and rhodamine 6G doped polyacrylamide matrix. Also attempt was made to study the use of rhodamine 6G doped polyacrylamide as a luminescent solar concentrator.

Considerable effort has been expended to devise passive means for protecting sensitive detection systems from damage caused by high-power laser beams[1-3]. Limiting devices protect sensitive optical elements and sensors from laser-induced damage. In passive devices focussing optics is used to concentrate the light through a nonlinear optical (NLO) element to reduce the limiting threshold. Unfortunately, these NLO elements may themselves undergo laser induced damage for high inputs, restricting the useful dynamic range. To date no materials have exhibited strong enough nonlinear response to show limiting without optical gain, i.e., focusing to concentrate the light in the material. Although the strongest nonlinear response will be obtained by placing the nonlinear material at the focus, the material is also likely to undergo laser-induced damage at this position. Molecules exhibiting reverse saturable absorption have received considerable attention as promising candidates for use in passive optical limiters. Liquid-based limiters are sometime more helpful because the plasma formed in liquid by the focussed beam block the incoming light more efficiently at very high intensities[2].

The high speed processing of data is essential to numerous technologies like computing and telecommunication systems. It is predicted that in the future photonic-switching devices for telecommunications will operate 10,000 channels producing a combined bit rate of 1 terabps or 10^{12} bps[4]. In contrast, the current electronic devices handle a combined bit rate of less than 15×10^9 bps[4]. All-optical architectures have been

161

designed that are well-suited for the serial and parallel processing of high bit-rate data streams[5,6]. It is obvious that the efficiencies of these nonlinear optical processes are dependent upon the material employed to couple the given combination of electrical and/or optical signals. The implementation of all optical signal processing has been slow because of the lack of materials needed for the components in an optics-based signal processor[7].

Most of the nonlinear optical materials currently used in the fabrication of passive and active photonic devices are ferroelectric inorganic crystals[8-10]. The third-order nonlinear optical phenomenon of an optically-induced change in refractive index is fundamental to all optical switching and computing as well as phase conjugate adaptive optics[11-13]. New nonlinear optical materials are needed to widen the range of photonic technology. Phthalocyanines (Pc) are a class of stable, robust materials that have recently been shown to be attractive candidates for NLO applications[14-16]. Especially when heavy metal atoms are substituted in the phthalocyanine molecule the nonlinearity shows a marked increase. The case of Europium phthalocyanine [Eu(Pc)$_2$], with two phthalocyanine molecules coupled by the Europium atom and Europium naphthalocyanine [Eu(Nc)$_2$], with two napthalocyanine molecules connected via an Europium atom are special since the number of conjugated double bonds are large and they have a heavy central metal atom.

Another area of application which has been studied is spatial light modulators. Spatial light modulator (SLM) is a device for transferring the information content of one beam to another beam. They are useful in a variety of applications, including optical processing, computing and beam steering and control·functions. In the present case a molecular SLM was constructed using rhodamine 6G doped polymer matrix. The use of luminescent solar concentrators (LSC) in solar energy conversion is also a promising field. The feasibility of constructing LSC with the dye impregnated polyacrylamide matrix was checked.

7.2 Optical limiting in Eu(Pc)$_2$ solution

The desire to protect eyes and sensors from optical damage resulting from exposure to intense laser sources has led to the development of a number of passive optical limiting devices[2,17-20]. Optical limiters are devices that strongly attenuate intense

optical beams beyond a desired power level while exhibiting high transmittance for low intensity beams. Most efforts to develop optical-limiting devices based on various mechanisms including nonlinear absorption and refraction in semiconductors, optical breakdown-induced scattering in particle suspension, thermal refractive beam spreading, and excited state absorption has fallen short of the blocking level needed (attenuation of 10 mJ pulses by a factor of 10^4 or higher) to protect the human eye by two orders of magnitude or more[19-27].

Recent works suggest that high levels of blocking at a reasonable linear transmittance, even in highly convergent optical systems may be possible with high performance, excited-state absorber materials[28,29]. Perry et al[27]. have shown that metallophthalocyanine (MPc) complexes containing heavy metal atoms exhibit enhanced excited-state absorption and optical limiting of nanosecond-duration laser pulses at a wavelength of 532 nm because of an increased rate of intersystem crossing from the lowest excited singlet state (S_1) to the triplet state (T_1) and the concomitant increase in the population of the strongly absorbing T_1 states during the laser pulse. Moreover, analysis of the performance of optical-limiting devices that utilize excited state absorbers indicate that large enhancements are possible in designs where the excited-state absorption is inhomogenously distributed so as to achieve maximal excited-state population along the beam path[30-31]. Molecules with weak ground-state absorption that has strongly absorbing excited states can be used in optical limiters. Phthalocyanine complexes bearing heavy atoms or paramagnetic groups show optical limiting enhanced by excited triplet state absorption.

7.2.1 Experimental details

The optical limiting studies were performed on $Eu(Pc)_2$ dissolved in dimethyl formamide. The solution was taken in a cuvette of thickness 0.49 cm. The transmission in the linear region was measured to be 45%. And the absorption coefficient 1.62 cm^{-1}. The absorption spectrum of $Eu(Pc)_2$ is given in Fig.5.3.

The experimental setup for optical limiter consists of a laser beam from the frequency doubled Nd:YAG laser with pulse width 10 ns, and frequency 532 nm as the pumping beam. It was focussed using a lens of focal length 10 cm. The cuvette with $Eu(Pc)_2$ solution was kept at a distance of 7.5 cm from the focussing lens. The high

power density at the focal point will cause the optical breakdown and damage of the cuvette if kept at the focal point. The incident and transmitted powers were measured using a calibrated laser power meter (Scientech).

7.2.2 Results and discussion

The plot of transmitted laser intensity as a function of input intensity is given in Fig.7.1a. As the input intensity is increased the output also increases showing a low intensity transmission of about 45% upto about 2.1 $MWcm^{-2}$ beyond which the output intensity levels off. On the other hand the percentage transmission decreases as the laser intensity is increased as shown in Fig.7.1b. This can be attributed to excited state absorption which is explained by a five level model of Kojiama et al.[34].
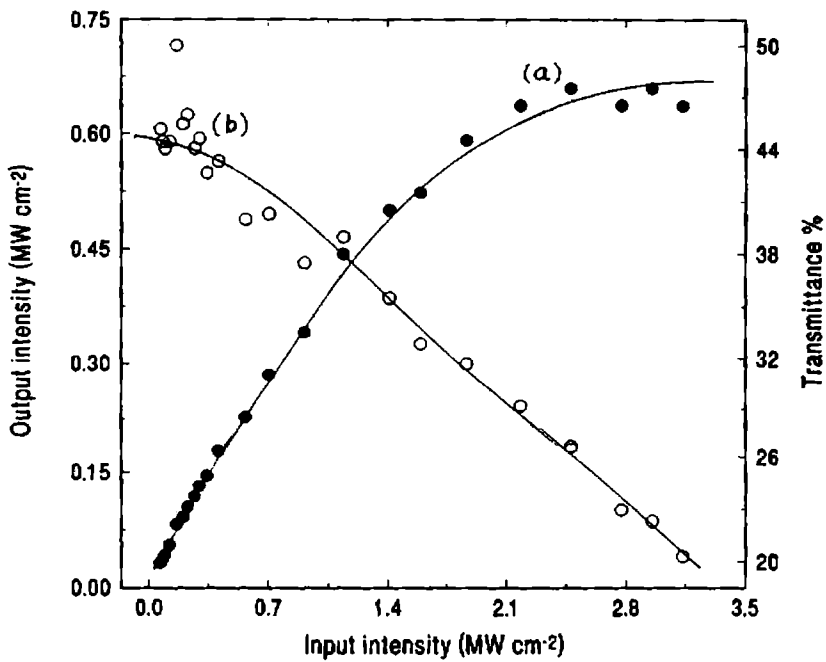

Fig.7.1 Plot of optical limiting observed in $Eu(Pc)_2$ along with the transmittance curve

A pure reverse saturable absorber obeys the relation

$$\ln \left[\frac{I_0}{I}\right] = k(I_0 - I) + A_g,$$

where I is the incident laser intensity, I_0 the transmitted laser intensity, k is a constant that depends on the absorption cross-sections and lifetimes of the ground, excited

164

singlet and excited triplet states and A_g is the ground state absorbance. This equations implies that a plot of $\ln(I_0/I)$ versus $(I_0\text{-}I)$ will be a straight line for a reverse saturable absorber. The plot of $\ln(I_0/I)$ versus $(I_0\text{-}I)$ is as given in Fig.7.2, which fits into a straight line.
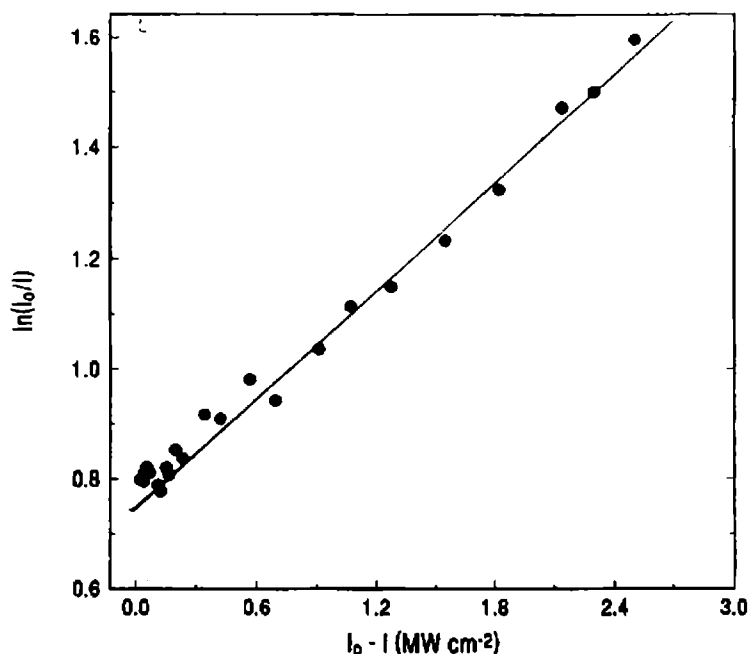

Fig.7.2 The plot of $\ln(I_0/I)$ versus $(I_0\text{-}I)$. The graph is linear showing that reverse saturable absorption is the main cause of optical limiting.

The performance of excited state absorbers can be characterized by the ratio of the excited-state (σ_{ex}) to ground-state (σ_g) absorption cross-sections, σ_{ex}/σ_g, where σ_{ex} includes the weighed average of σ_s and σ_t for S_1 and T_1 states respectively. The ratio of σ_{ex}/σ_g must be larger than one for effective optical limiting. In the present case, the value obtained is ≈ 8.2, which is much greater than that of C_{60} solution which is widely studied as an optical limiter. The high value of σ_{ex}/σ_g can be explained as follows. From the time resolved spectroscopic measurements of MPc complexes, it is seen that T-T absorption is actually larger by a factor of 2 than the S-S excited state absorption[32]. The well known heavy-atom effect enhances the triplet population, wherein the large spin-orbit coupling for the metal orbitals and their mixing with the orbitals of the conjugated ring leads to an increased rate of S to T intersystem crossing

165

and thus to an increased T_1 population during short laser pulses[33]and thus to reverse saturable absorption. The interesting consequence of Europium as a central atom is its unique optical properties as the molecule occurs as phthalocyanines. Attachment of heavy atoms to the conjugated ring provides a synthetically flexible way of maintaining close proximity between the heavy atoms and the ring. This is important to sustain the triplet enhancement for larger ring molecules[35].

7.3 Optical switching

All-optical devices use light either in the form of the signal itself or as a separate control beam to influence some operating characteristics, typically the transmission of light through the device. Initial work on all-optical devices was directed primarily toward bistable optical devices. These devices, which exhibit two output states for a given optical input state, have been proposed for a variety of optical signal-processing and logic operations[11].

The electronic all optical nonlinearity can be classified into two groups. The first category involves nonlinear effects that occur for light energies significantly less than the band gap of the nonlinear material. Such nonlinearities can be described as arising from virtual transitions and are referred to as bound electron or nonresonant effects in nonlinear refractive index changes. These are related to the change in the two-photon absorption spectrum through nondegenerate Kramer-Kronig relationships[36]. Such nonlinearities are small, but have femtosecond response times. The second category of nonlinearity corresponds to the induced changes in absorption. These changes are due to light with energy near or above the band gap which is then referred to as resonant nonlinearities. The light induced absorption changes, result in change in the refractive index of the material. Resonant nonlinearities tend to be large with significant contribution from thermal nonlinearities, but they have relatively slow response times of the order of nanoseconds.

For most all-optical device applications, a large nonlinearity and rapid response is desirable. Other desirable properties include low loss (high transparency) and absence of competing nonlinear effects that would affect the device operation. Such an ideal material does not exist, but there can always be a trade-off for device applications. Hence in recent times, there have been much investigations on several new nonlinear

optical materials. Phthalocyanines have been identified as promising materials for nonlinear optical applications[37-39]. In particular, the intensity dependent absorption makes these materials interesting candidates as optical limiters as shown above and in literature[2,17,18,40]. They are also suitable for the fabrication of optical switches and optical bistable devices[41]. Napthalocyanines are also being reported as nonlinear materials, but these materials are not very easily sythesized in bulk.

By making use of the nonlinear absorption of Europium napthalocyanine $Eu(Nc)_2$, an optical inverter was constructed. Under CW excitation thermal contribution arises from heating of the solvent due to the absorption of the laser light. It has been shown that this heating increases the excited state absorption, which enhances the nonlinear properties .

7.3.1 Experimental details

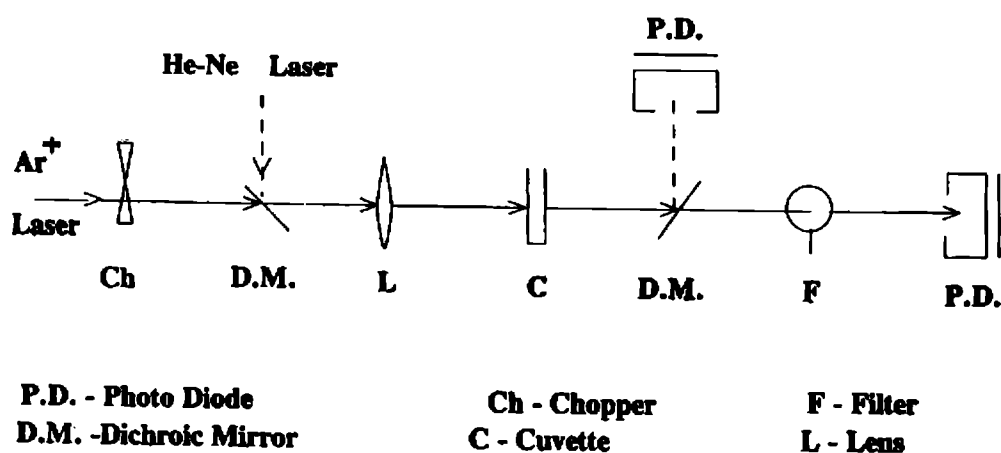The schematic of the experimental setup is shown in Fig. 7.3.

Fig.7.3 Experimental setup demonstrating an optical inverter using $Eu(Pc)_2$

The 514.5 nm of the Ar^+ laser was used as the pumping beam (writing beam) and it was focused by a lens (focal length 18 cm) to a beam waist of 5-8 μm. A weak laser

167

beam of wavelength 632.8 nm from a He-Ne laser was used as the probe beam (reading beam) which passes collinearly with the pump beam, but without being chopped. The pump beam was chopped at a frequency of 25 Hz.
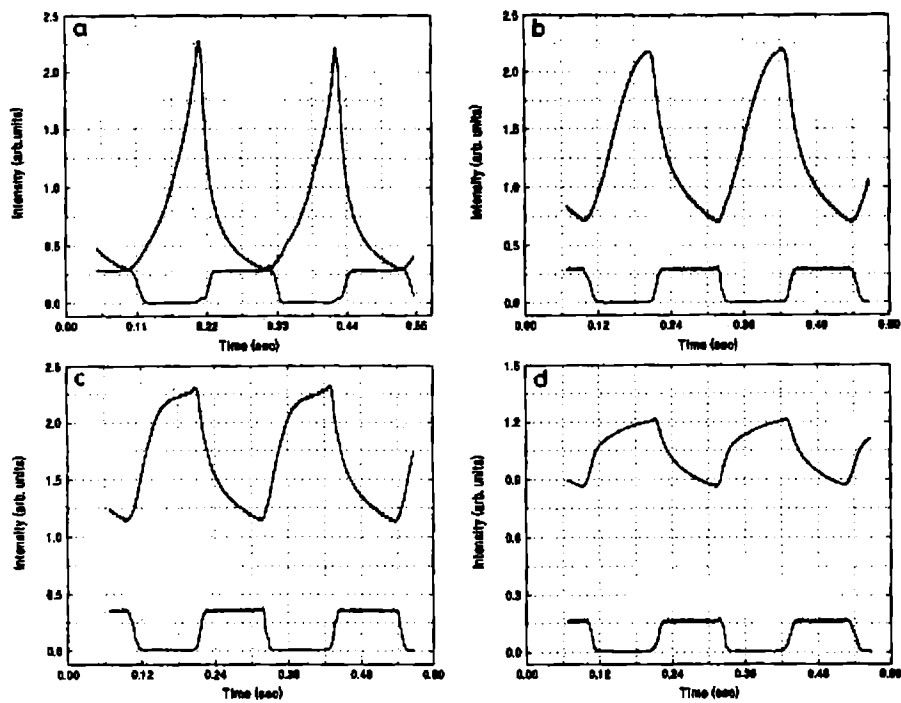

Fig.7.4 All optical logic signal from an optical inverter with varying input laser intensities (a) 74.5 W cm^{-2}, (b) 34.8 W cm^{-2}, (c) 13.4 W cm^{-2}, (d) 8.3 W cm^{-2}.The upper curves show the signal shape of the He-Ne laser beam, whereas the lower curves shows the signal shape of the incoming Ar^+ laser beam.

The transmitted probe beam was allowed to fall completely on to a PIN photodiode and the photodiode output was displayed on an oscilloscope which is connected to a computer for data acquisition and storage. The photodiode actually measures the absorption changes in the He-Ne laser beam since the whole beam is focussed on the diode after proper intensity attenuation.

The oscilloscope signals of the on-off states observed with varying the pump laser intensity are shown in Fig.7.4. The pump beam intensities were (a) 74.5 W cm^{-2} (b) 34.8 W cm^{-2} (c) 13.4 W $cm^{-2}$and (d) 8.3 W cm^{-2} at the focal point. The upper curves are the signal shape in the He-Ne laser output where as the lower curves show the

168

pump laser input pulse shapes at all intensities. The input signal is almost square waves whereas the He-Ne laser signal shape varies according to the laser intensity. The switching action observed at low laser intensity has the ideal behavior and reflects exact input signal shape. At higher laser intensities the increased population of the excited level causes decrease in the probe beam transmission and thus affect the signal shape considerably as described below.

The optical switching action was based primarily on reverse saturable absorption. From the ground state absorption spectrum of napthalocyanine, given in Fig.5.8., and from studies done by Chufei Li et al.[42] it can be seen that the ground state and the excited states have different absorption coefficient in the visible and near infrared region. Usually in the valley of the ground state absorption the excited state absorption exhibits a peak.[42] The probe beam of wavelength 632.8 nm is sufficiently away from the absorption band of the ground state, but at this wavelength there exists considerable excited state absorption cross-section. The output intensity in this case is in the 'ON' state, because of the low linear absorption of 632.8 nm. When the sample is exposed to the pump beam, the population of the excited state molecules is greatly enhanced, thereby strongly absorbing the probe beam. The probe beam in this case is in the 'OFF' state and the sample behaves as an optical inverter.

Usually the thermal effects also contribute substantially to nonlinearity as predicted by Sutherland[43]. The nonlinear index change due to a temperature rise of ΔT is $\Delta n = (dn/dT)\ \Delta T$. It is due to the density change with temperature and the medium acts as a negative lens, causing thermal blooming of the probe beam passing through it. Here the contribution due to thermal effects are reduced since the diverged probe beam is focussed and whole of the transmitted intensity detected. Hence the main contributor is reverse saturable absorption of the probe beam.

7.4 Spatial light modulators

Materials used for nonlinear optical applications include atomic/molecular vapors, photorefractive crystals, semiconductor glasses, dye doped polymers, etc.[44-46]. Strong absorption of dyes in the visible region makes them particularly suited for nonlinear optical applications. The nanosecond lifetime of the S_1 state may be an important consideration for fast processing of optical information but such devices are unlikely

to be realized owing to other phenomena[47]. The radiative lifetime of the lowest triplet state in organic dyes is quite long, but quenching mechanism in liquid state lead to considerable shortening of this lifetime. In rigid environment of solids, the triplet state regains its lifetime. This allows the observation of nonlinear effects in the dye doped polymers at incredibly low power levels. This dye doped polymers are being used in phase conjugation, four wave mixing, etc.[48-49]. The nonlinear properties are being made use of in the construction of a spatial light modulator (SLM). Optically addressed spatial light modulators are a class of electro-optical device used to spatially modulate the amplitude, phase or polarization of an optical beam in response to an input optical signal.

The SLMs can be used for many applications like image amplification, time/space transformation, scratch pad memory, programmable detector masking and page composition for holographic memories. In recent years this field has advanced tremendously. Organic materials were shown to be ideal media for such optical hardware. It is already known that such materials exhibit high nonlinear susceptibilities that is necessary for optical data processing. A detailed study of the possibility of constructing molecular SLM using a nonlinear absorber has been reported by Spesier et al[51]. Using a steady-state kinetic analysis it has been shown that a probe light can be modulated by propagating through a medium excited by another light.

Intensity dependent refractive index change can be made use of in the construction of molecular SLMs. Reverse saturable absorbers with excited state absorption cross section much larger than the ground-state absorption cross-section are being used in the construction of SLMs. Organic dye molecules such as rhodamine 6G exhibit RSA characteristics at wavelengths between 400 and 470 nm[52].

In this section the possibility of using rhodamine 6G impregnated in polyacrylamide is explored for the construction of a molecular SLM. The kinetic analysis of Speiser and Dantsker is extended to study the SLM characteristics of rhodamine 6G molecule[51].

7.4.1 Analysis of molecular SLM using dye impregnated polymers

In the SLM configuration the write beam of intensity I_W (x,t) excites the rhodamine 6G impregnated in polyacrylamide matrix. At the wavelength of write beam it acts as a reverse saturable absorber which in turn modulates a probing read light of intensity

I_R (x,t).

The read and write beams propagate in the same direction and $I_W \gg I_R$. The schematic diagram of the vibrational levels of the reverse saturable absorber is given in Fig.7.5. It is assumed that the transition from level 3 to 2 and 4 to 2 are extremely fast. Thus the effective population of the levels 3 and 4 are negligible and only levels 1 and 2 are appreciably populated. Thus the total population is $n = n_1 + n_2$ where n_1 and n_2 are the populations in levels 1 and 2 respectively. The dynamics of this system propagating in the x direction is described by the following rate equations

$$\frac{\partial n_1}{\partial t} = -I_W(x,t)\sigma_{13}(W)n_1 + \frac{n_2}{\tau_r} \tag{1}$$
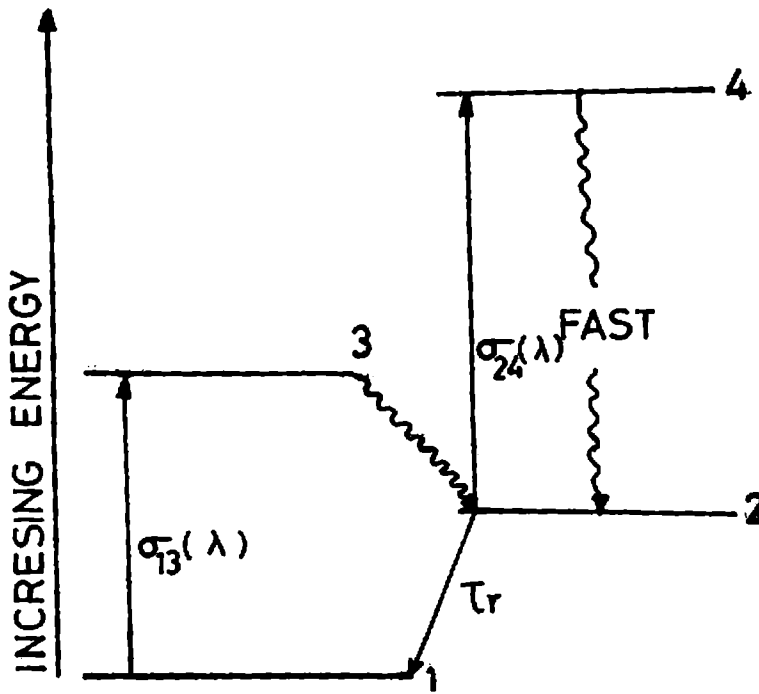

Fig.7.5 Schematic energy level diagram showing RSA in rhodamine 6G molecule

$$\frac{\partial n_2}{\partial t} = -I_W(x,t)\sigma_{24}(W)n_2 - \frac{n_2}{\tau_r} \tag{2}$$

$$\frac{\partial I_W(x,t)}{\partial t} + c\frac{\partial I_W(x,t)}{\partial x} = -\alpha_W I_W(x,t) \tag{3}$$

171

where $\alpha_{13}(W)$ and $\alpha_{24}(W)$ are the ground state and excited state absorption cross-section respectively, τ_r the life time of the excited level 2 and α_W is the absorption coefficient given by,

$$\alpha_w = n_1\sigma_{13}(W) + n_2\sigma_{24}(W) \tag{4}$$

Eqs. (1) - (4) yield a steady state equation of the form

$$\frac{dI_w(x)}{dx} = -\alpha_w^0 \left[\frac{1 + \beta(W)\ (I_w/I_S)}{1 + (I_w/I_S)}\right] I_w(x) \tag{5}$$

where the small signal absorption coefficient $\alpha_W^0 = n\ \sigma_{13}(W)$, $\beta(W) = \sigma_{24}(W)/\ \sigma_{13}(W)$ and the saturation intensity $I_s = (\sigma_{13}(W)\ \tau_r)^{-1}$. Assuming that the length of the doped polymer is L, the intensity equation can be integrated to yield,

$$Y = \frac{I_w(L)}{I_w(0)} = \exp(-\alpha_W^0 L) \left[\frac{1 + \gamma\ I_w(0)\ Y}{1 + (I_w/I_S)}\right]^\delta \tag{6}$$

where $I_w(o)$ is the intensity at $x = 0$, $I_w(L)$ is the intensity at $x = L$, $\gamma = \sigma_{24}(W)\tau$, and $\delta = (\beta(W)-1)/\beta(W)$.

Similarly for the read beam intensity

$$\frac{dI_R(x)}{dx} = -\alpha_R^0 I_R(x) \tag{7}$$

where $= n_1(R)\ \sigma_{13}(R) + n_2\sigma_{24}(R)$ is the absorption coefficient for the read beam. Substituting the values of n_1 and n_2 obtained from eqs. (1) and (2) for the steady state,

$$\alpha_R = -\alpha_R^0 \left[\frac{1 + \beta(R)\ (I_w/I_S)}{1 + (I_w/I_S)}\right] \tag{8}$$

$\alpha_R^0 = n\sigma_{13}(R)$ and $\beta(R) = \sigma_{24}(R)/\ \sigma_{13}(R)$

From eqs. (7) and (8),

$$\frac{dI_R^0(x)}{I_{R(x)}} = \left[\frac{\alpha_R}{\alpha_W}\right]\frac{dI_w(x)}{I_w\ (x)} = \left[\frac{\alpha_R}{\alpha_W^0}\right]\left[\frac{1 + \beta(R)\ (I_w/I_S)}{1 + \beta\ (W)\ (I_w/I_S)}\right]\frac{dI_w}{I_w}$$

This equation yields, after integration over the medium length L

172

$$\frac{I_R^0(L)}{I_R(0)} = \left[\frac{\alpha_R}{\alpha_W^0}\right] \left\{ \ln\frac{I_W(L)}{I_W(0)} + \ln\left[\frac{1 + \beta(R)\ (I_W\ [L]\ /I_S)}{1 + \beta\ (W)\ (I_W\ [0]\ /I_S)}\right] \left[\frac{\beta(R)}{\beta(W)} - 1\right] \right\}$$

Defining $\Gamma = \beta(R)/\beta(W) -1$ and $\zeta \equiv \alpha_R^0/\alpha_W^0 = \sigma_{13}(R)/\sigma_{13}(W)$ and using (6), the above equation can be rewritten as,

$$Z = \frac{I_R(L)}{I_R(0)} = \left\{ Y\left[\frac{1 + \gamma\ I_W(0)\ Y}{1 + \gamma I_W(0)}\right]^\Gamma \right\}^\zeta \tag{9}$$

7.4.2 Construction of SLM

A polyacrylamide slab of dimension (20x9x1) mm^3 was doped with rhodamine 6G so that the concentration of dye in the polymer is $\approx 10^{-3}$ M. This sample was used for constructing the SLM. The 457.9 nm wavelength from the Ar$^+$ laser was used as the write beam. The read beam was 632.8 nm from a He-Ne laser. This exemplifies the case of an open SLM medium. The write and the read beams propagate in the same direction. The experimental setup for the SLM operation is shown in Fig.7.6.
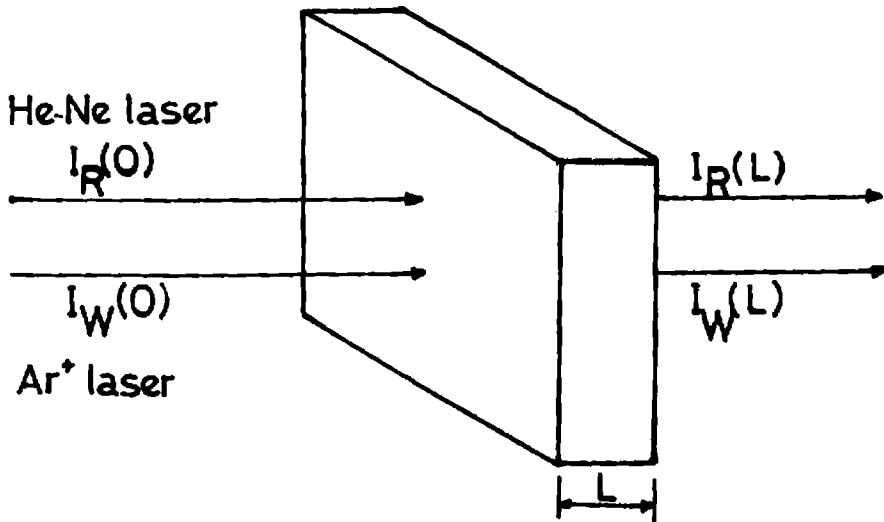

Fig.7.6 Experimental setup for SLM

Eq. 9 is the basic equation for the discussion of molecular SLM performance due to RSA. For the rhodamine 6G molecule it was found that $\sigma_{24} > \sigma_{13}$ over the wavelength range of 400-465 nm[53]. The experimentally obtained curve for variations of Z for different write beam intensity values I_W (0) are shown in Fig.7.7. This curve qualitatively agrees with the theoretical curve obtained by K P J Reddy et al.[54] while studying the characteristics of rhodamine 6G solution as an open SLM.

7.4.3 Sensitivity and contrast ratio

The main drawback of a molecular SLM seems to be the lack of a wide linear range, i.e., a range for which Z varies linearly with I_W . The sensitivity range is given by,

$$S = \frac{\partial Z}{\partial I_W (0)} \tag{10}$$

For the SLM constructed using dye impregnated polyacrylamide, over the range $I_W(0)$ of 0.12-0.28 $\times 10^{18}$ photons/cm^{2}s, S = 2.3 cm^2/W at 457.9 nm.
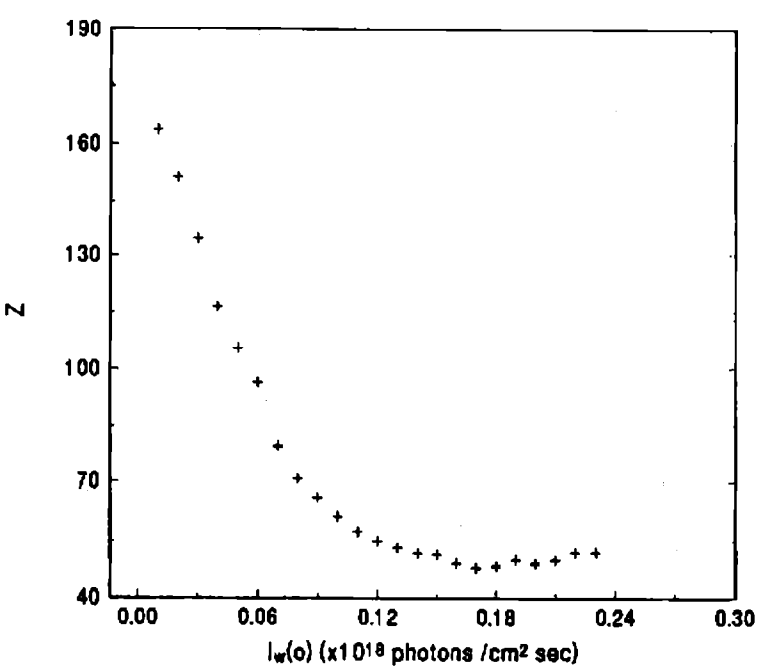

Fig.7.7 Characteristic curve for the read beam transmission Z for rhodamine 6G doped polyacrylamide which acts as open SLM

Contrast ratio is computed using the expression $R = \exp[\sigma_{24} (R)nL]$. With the read beam absorption coefficient $\sigma_{24} = 0.34 \times 10^{17}$ cm^2 and length 1 mm and $n = 6 \times 10^{17}$cm^{-3}, the contrast ratio is 7.69. It is evident that by proper manipulation of the exponent parameters, one can achieve very high contrast ratios. The present study on the characteristics of SLM provides a new and efficient material for SLM whose efficiency can be further modified for device applications.

7.5 Luminescent solar concentrators

The luminescent solar concentrators (LSC) offers the promise of reducing the cost of photovoltaic energy conversion by the use of high gain concentrators which do not require tracking. The conceptual design and operation of LSC is described in Chapter I.

An LSC operates on the basis of light pipe trapping of luminescence induced by the absorption of solar radiation. The photon flux at the edge of an idealized LSC is the product of the absorbed flux, the fraction of the resulting luminescence that is trapped and the geometric ratio of the area of the face directly exposed to the sunlight divided by the area of the edge covered by solar cells. But in a practical LSC there will be many parasitic losses. These are inadequate absorption bandwidth, imperfect quantum efficiency, self absorption of the luminescence, absorption by the matrix material, reflective mismatches, geometrical trapping effects and lifetime of the materials used, etc.

It has been shown by Batchelder et al.[55] that by using suitable combination of dyes with successively overlapping absorption and emission bands, solar photons can be absorbed over the integrated absorption spectrum of all the dyes with a cascade being formed by excitations being transferred from one dye to the next. In this section some experimental techniques are described to show the efficacy of rhodamine 6G doped polyacrylamide as an LSC. The absorption and the emission spectra under different conditions are used to understand the self absorption and photobleaching of dyes in polymer matrix.

7.5.1 Self absorption effect

Method of preparation of rhodamine 6G doped polymer was the same as that given

in Chapter III. The absorption spectra were recorded using Perkin-Elmer spectrophotometer. For recording the emission spectrum, 476.5 and 514.5 nm emission lines from an Ar$^+$laser was used as pump source. The excitation beam was chopped using a mechanical chopper to enable signal detection using a lock-in amplifier. The fluorescence output was taken at 90^0 to the exciting beam and the collimated light was allowed to incident on the entrance slit of a one meter monochromator (Spex Model No. 1704) coupled to a photomultiplier tube (Thorn EMI, Model KQB 9863). The output of this is given to a lock-in amplifier for data analysis and storage.

Fig.7.8 (a) shows the absorption as well as emission spectrum of rhodamine 6G in methanol where as Fig.7.8 (b) that of the dye in polyacrylamide. There is some overlap between the absorption and emission spectra for most of the dyes. In this solid matrix the overlap is comparatively less than in solution phase. The observed overlap allows the fluorescent photon to be self-absorbed by another dye molecule of the same type. Self-absorption is actually a dominant effect over the long path lengths travelled by light trapped in an LSC.
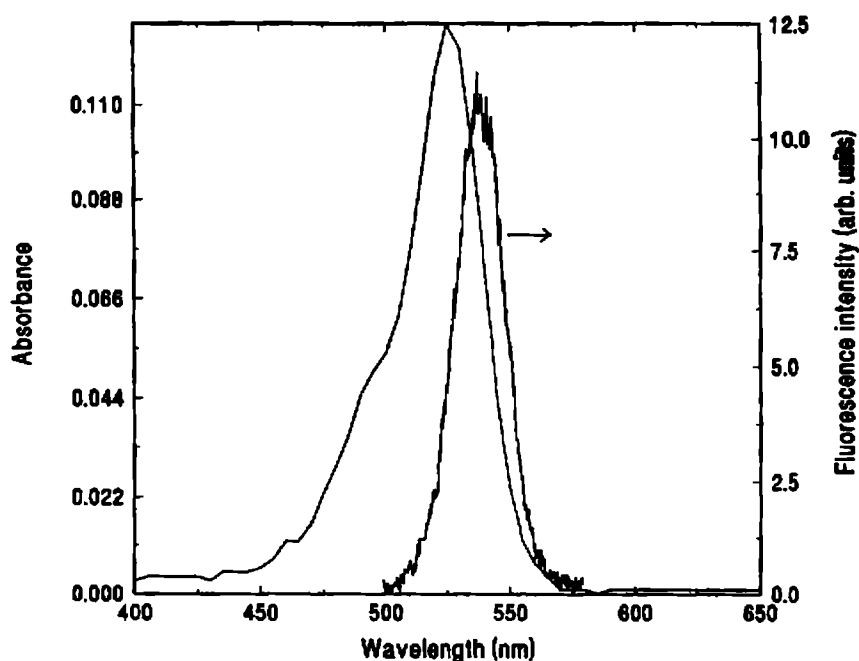

Fig.7.8a Absorption and emission spectra of rhodamine 6G in methanol solution.

Hence the probability of self absorption will be reduced if there is a large stokes shift.

176

From the emission spectra in methanol and in polymer matrix, it was found that in the case of emission from polymer sample, peak is shifted towards the long wavelength side and also the fluorescence band was broadened. The same effect was observed by Lo et al.[56], in sol-gels doped with rhodamine and it was attributed to the increase in the polarity of the solvent and defined as solvatochromic effect[57]. When there is considerable amount of self absorption, the LSC plate acts as a filter that attenuates the luminescence resulting from the absorption of solar photons. The LSC is a particular sort of filter in which the light that is absorbed can then be reluminescensed in an arbitrary direction, most of which will again be trapped in the plate. This results in a number of different generations of luminescence which will be inhomogeneous except the first generation. An absorbed photon can be re-emitted with an energy less than or equal to its initial energy so that each generation is progressively red shifted with respect to the preceding generation.
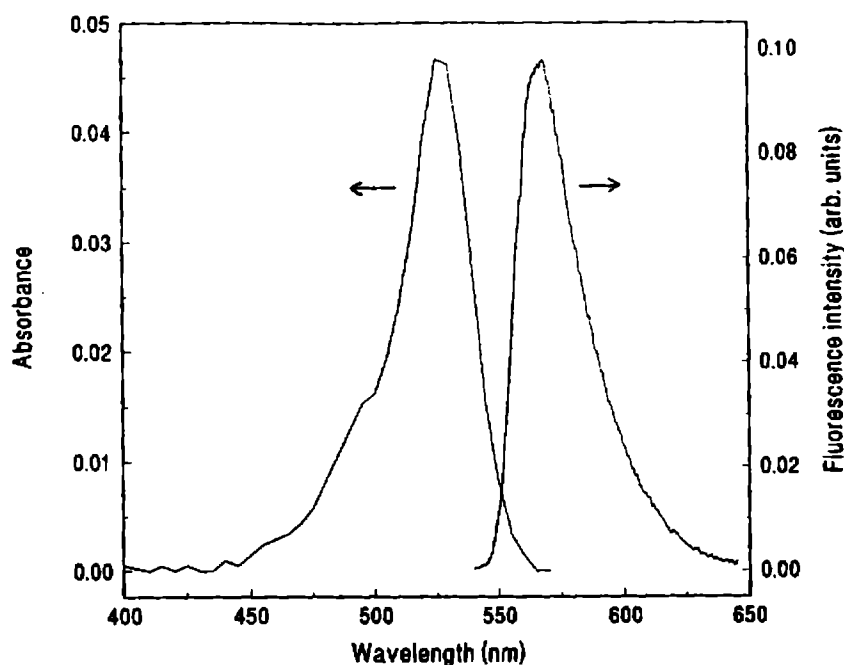

Fig.7.8b Absorption and emission spectra of rhodamine 6G in polyacrylamide matrix. Notice the red shift of the emission peak in polymer matrix compared with that in methanol solution

Hence higher self absorption results in spatial nonuniformity. Reduction in self ab-

177

sorption can be insured by requiring the possible emission frequencies to be exclusively less than all possible absorption frequencies. This is possible by using dyes doped in polymer matrices rather than in solution phase.

7.5.2 Studies on spectral homogeneities

One of the primary aim of the work was the determination of the homogeneity of the absorption and emission spectra in the dye doped polymer. Fig.7.9 (a) and (b), show the emission spectrum obtained when excited using 514.5 and 476.5 nm respectively of Ar^+ laser radiation. Note that the peak of the emission for the lower excitation wavelength is at the same wavelength as that of the higher excitation wavelength. This is useful when solar radiation of different wavelengths are causing the emission. The edge mounted array of solar cells can be arranged so as to have maximum efficiency in the range of optimal emission output. A desirable change in the peak wavelength of the dye emission can be obtained by varying the path length of the dye, which is shown in Fig.7.10.
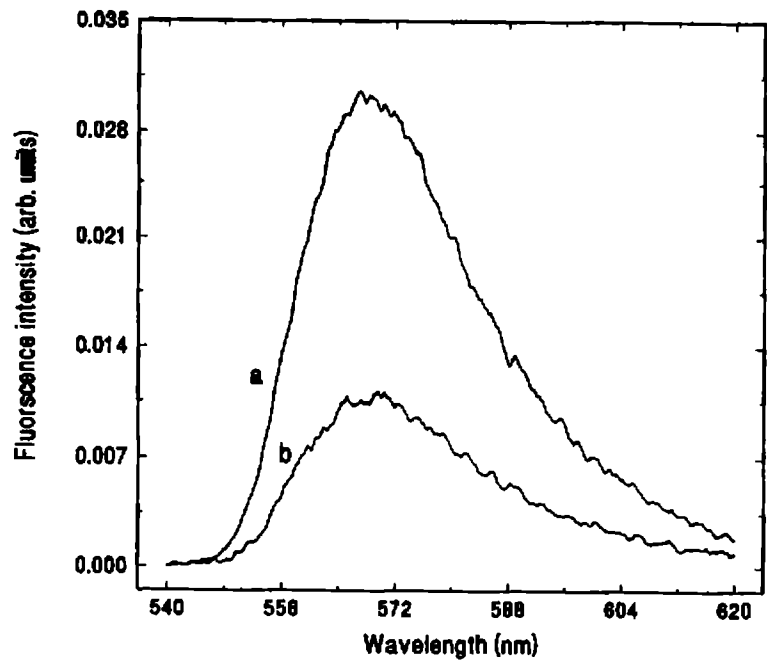
Fig.7.9 The emission spectra of dyes impregnated in polymer hosts at (a) 514.5 nm, (b) 476.5 nm wavelengths.
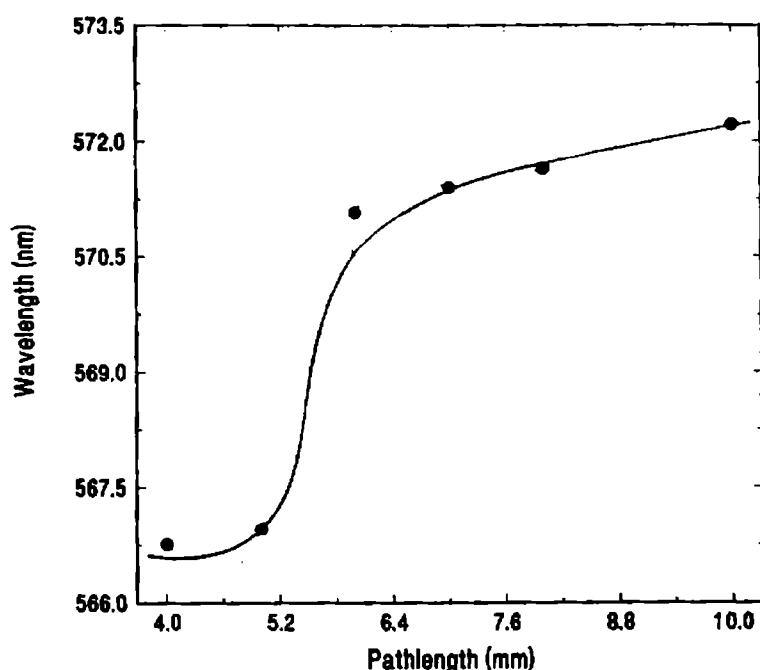
178

Fig.7.10 Peak wavelength of observed emission spectra at different path lengths

7.5.3 Photobleaching of the dye

The most important question in the implementation of LSC technology is the stability and operation life time of the dyes under the conditions found in an exposed environment.

Photobleaching occurs at room temperature whereby the absorption of the light by the sample leads to deterioration of the dyes. In the case of rhodamine 6G doped polyacrylamide, the dye bleaching when kept in room temperature was very slow against the reported time scales in other solid hosts like PMMA. Even after 6 months absorption and emission spectra of the samples remain the same. This extremely high resistance to photobleaching is due to the lack of bond formation between the dye and the polymer molecules[58]. The dye is not firmly linked to the polymer chain and the matrices seldom influence the characteristics of the dye molecules.

It has been suggested that one of the mechanisms of photodestruction in xanthene dyes in polymeric matrices is radical formation[59]. In this a neutral radical is formed as a result of combination of excited dye molecule with the electron derived from the

179

free radical. These free radicals were formed by the interaction of the dye molecules with the surrounding polymeric macromolecules which causes radiationless deactivation of excited states through the highly excited state of the matrix. In this case some additives will significantly improve the photoresistance of the dye through resonance vibrational cross relaxation which hampers the formation of macroradicals[60].Another reason for the long life span of rhodamine 6G in polyacrylamide matrix may be the addition of methanol, which was used to dissolve the dye properly. It also acts as a retarder for the generation and branching of radical chains. This is because the addition of methanol (which acts as a low molecular weight additive) induce cross relaxation between the vibrational levels of the polymer macromolecules and those impregnated additive compounds.

7.6 Conclusion

The development of various photonic devices are described in this chapter. Organic nonlinear optical materials are considered to be the materials of the future because their molecular nature combined with the versatility of synthetic chemistry can alter and optimize molecular structure to maximize nonlinear responses and other properties. This has been made use of in the construction of optical limiter and switches.

The performance of a heavy-atom phthalocyanines during optical limiting process has been investigated. And it was demonstrated that the europium phthalocyanine, which acts as a reverse saturable absorber at 532 nm can be used as an efficient optical limiter. Results show that it is a better reverse saturable absorber than C_{60} or C_{70} solution. More efficiency can be achieved by using $Eu(Pc)_2$ in tandem or graded density for optical limiting applications. Using Ar^+ as the pump laser beam reverse saturable absorption can be observed due to triplet transitions even at low intensities. The working of the optical inverter can be explained on the basis of excited state absorption of the probe beam. Hence all-optical switching can also be achieved in the $Eu(Nc)_2$ solution. This has been demonstrated and discussed in this chapter.

The dye impregnated solid matrices with their low threshold for nonlinearity has been used to make a spatial light modulators. SLM was constructed using the rhodamine 6G doped polyacrylamide matrix. The RSA property of the rhodamine 6G at the write beam wavelength has been utilized for the purpose. The theory developed by

K P J Reddy et al.[54] has been used to explain the observed result. The sensitivity of rhodamine 6G doped polyacrylamide was calculated as 2.3 cm^2 /W at 457.9 nm and the contrast ratio as R = 7.69. Since the thermal conductivity of organic materials is low, it will be important to design devices with careful attention to heat sinking and dissipation to take full advantage of their potentials[61]. The results presented here indicate that a molecular SLM can be constructed using rhodamine 6G dye in polymer matrix. Preliminary studies were conducted on doped polyacrylamide to check its usefulness as a luminescent solar concentrator. And it has been concluded that polyacrylamide, because of its low cost and high photostability, can be efficiently used as a luminescent solar concentrator.

References

[1] G L Wood, W W Clark, M J Miller, G J Salamo and E J Sharp, 'Materials for Optical Switches, Isolators, and Limiters', M J Soileau, Ed., Proc. SPIE 1105, 154, (1989).

[2] L W Tutt and T F Boggess, Prog. Quatum. Electron., 17, 299, (1993).

[3] K Mansour, E W Van Stryland, and M J Soileau, J. Opt. Soc. Am. B 9, 1100, (1992).

[4] H S Hinton, 'IEEE Spectrum' 42, (Feb., 1992).

[5] G I Stegman, E M Wright, Opt. Quant. Electron., 22, 95,

[6] G I Stegman, A Miller, 'Physics of All-Optical Switching Devices', Midwinter, J E; Ed. Academic, Orlando.

[7] J L Bredas, C Adant, P Tackx, and A Persoons, Chem.Rev, 94, 243, (1994).

[8] F Zernike, J E Midwinter, 'Applied Nonlinear Optics' Wiley, NewYork, (1973).

[9] R S Weis, T K Gaylord, Appl.Phys. A, 37, 191 (1985).

[10] M E Lines, A M Glass, 'Principles and Applications of Ferroelectrics and Related Materials' Claderon: Oxford,(1975).

[11] H M Gibbs, 'Optical Bistability: Controlling Light with Light', Academic Press: New York, (1985).

[12] Bowden, C M; Giftan, M; Robl, H R; 'Optical Bistability', Plenum, New York, (1981).

[13] R Fisher, 'Optical Phase Conjugation', Academic Press: New York, (1985).

182

[14] J S Shirk, J R Lindle, et al. 'New Materials for Nonlinear Optics' , S R Marder, J E Sohn, G D Stucky, Eds. ACS Symposium Series 455, American Chemical Society, Washington, DC, p-626, (1991).

[15] Z Z Ho, C Y Ju, W M Heatherington, J. Appl. Phys, 62, 716, (1987).

[16] N Q Wang, Y M Cai, J R Helfin, A F Garito Mol. Cryst. Liq.Cryst. 189, 39, (1990).

[17] L W Tutt and A Kost, Nature 356, 225, (1992).

[18] A Kost, L Tutt, M B Klein, T K Dougtherty, and W E Elias, Opt. Lett., 18, 334, (1993).

[19] M J Soileau, Ed., Proc. SPIE 1105, (1989).

[20] R Crane, K Lewis, E Van Stryland, M Koshnevisan, Eds., Materials for Optical Limiting , Vol. 374, (Materials Research Society, Pittsburgh, PA, (1995).

[21] E W Van Stryland et al., J Opt. Soc. Am. B, 5, 1980 (1988).

[22] K Mansoor, M J Soileau, E W Van Stryland, J Opt. Soc. Am. B, 9, 1100, (1992).

[23] B L Justus, A J Campillo, A L Huston, Opt. Lett., 19, 673 (1994).

[24] B L Justus, Z H Kafafi, A L Huston, Opt. Lett., 18, 1603 (1993)

[25] D R Coulter et al. Proc. SPIE, 1105, 42, (1989).

[26] J S Shirk, R G S Pong, F J Bartoli, A W Snow, Appl. Phys. Lett., 63, 1880, (1993).

[27] J W Perry et al. Opt. Lett., 19, 625, (1994).

[28] D J Hagan, T Xia, A A Said, T H Wei, E W Van Stryland, Int. J.Nonlinear Opt. Phys. 2, 483, (1993).

[29] K Mansour C T Chen, S R Marder, J W Perry, and P Miles, 'Conference on Lasers and Electroptics' Vol.8 of 1994 OSA Technical Digest series, P-418, (Optical Society of America, Washington, DC. (1994).

[30] S W McCahon and L W Tutt, U S patent 5,080, 469, (1992).

[31] P Miles, Appl. Phys. B, 33, 6965, (1994).

[32] T Wie, D J Hagan, M J Sence, E W Van Stryland, J W Perry, and D R Coulter, App. Phys. B, 54, 46, (1992).

[33] N J Turro, 'Molecular Photochemistry' (Benjamin, Reading, PA, (1977).

[34] Y Kojiama, T Matsuoka, N Sato, and H Takahashi, Macromolecules, 28, 2893, (1995).

[35] W E Ford et al., Inorg. Chem.31, 3371, (1992).

[36] D C Hutchings, M Sheik-Bahae et al. Opt. Quantum. Electron., 24, 1 (1992).

[37] D J Hagan, et al. 'Materials for Optical Limiting', Eds. R Crane, K Lewis, E Van Stryland, and M Khoshnevisan, MRS Symp. Proc. 374, 161, Materials Research Society, Boston, (1995).

[38] P A Miles, Appl. Opt., 33, 6965, (1994).

[39] J W Perry et al. Science 273, 1533, (1996).

[40] F Henari, J Callaghan, H Stiel, W Blau and D J Cardin, Chem. Phys. Lett., 199, 144 (1992).

[41] F Lin, J Zhao, T Luo, M Jian, Z Wu, Y Xie, Q Qian, and H Zeng, J Appl. Phys., 74, 2140, (1993).

[42] Chufei Li, Lei Zhang, Miao Yang, Hui Wang, and Yuxiao Wang, Phy. Rev. A, 49, 1149, (1994).

[43] Richard L Sutherland, 'Handbook of Nonlinear Optics', R A Fischer (Ed.), 'Optical Phase Conjugation' (Academic press, New York, (1983), Marcel Dekker, (NY), (1996).

[44] D C Hanna, M A Yuratich, and D Cotter, 'Nonlinear Optics of Free Atoms and Molecules' Springer-Verlag, Berlin (1979).

184

[45] P Gnter and J P Huignard (Ed.), 'Photorefractive Materials and Applications I & II' Springer-Verlag, Berlin (1988).

[46] T A Shankoff, Appl. Opt., 8, 2282 (1969).

[47] B I Greene, J Orestein, and A Schmitt Rink, Science, 247, 679, (1990).

[48] Y Silberg, and I Bar Joseph, Opt. Commu., 39, 265, (1981).

[49] H Fujiwara and K Nakagawa, Opt. Commun. 55, 386, (1985).

[50] H Fei, Y Yang, Z Wei, L Han, Y Che, P Wu, G Sun, Appl. Phys. B, 62, 299, (1996).

[51] S Speiser and D J Dantsker, Appl. Phys. 66, 61, (1989).

[52] D J Harter, M L Shand, and Y B Band, J. Appl. Phys., 56, 865, (1984)

[53] P R Hammond, IEEE J. Quantum. Electron., QE-16, 1157, (1980).

[54] K P J Reddy and P K Barhai, Pramana J. Phys., 35, 527, (1990).

[55] J S Batchelder, A H Zewail, and T Cole, Appl. Opt., 20, 3733, (1981).

[56] D Lo, J E Paris, J L Lawless, Applied Physics B, 56, 385, (1993).

[57] K H Drexhage 'Dye Lasers', Ed. F P Schaffer (Springer Berlin, Heidelberg, (1990).

[58] B D Hames, and D Rickwood 'Gel Electrophoresis: A Practical Approach', IRL press, Oxford, (1990).

[59] Gromov D A, Dyumaev K M, Manenkov A A et al., AN USSR Phys. Series, 7, 1364, (1984).

[60] K M Dyumaev, A A Manenkov et al. Izv. Akad. Nauk SSSR Ser. Fiz. 49, 1084, (1985).

[61] Paras N Prasad, David J Willams, 'Introduction to Nonlinear Optical Effects in Molecules and Polymers', John Wiley, New York, (1990).

CHAPTER VIII

GENERAL CONCLUSIONS

8.1 Introduction

Organic molecules and polymeric systems have emerged as a class of promising photonics materials because they offer the flexibility, both at the molecular and bulk levels, to optimize the nonlinearity required for device applications. In the present case, we have mainly studied the amplified spontaneous emission from dye impregnated polymeric matrices and explored the nonlinear optical properties of certain organic materials. Also the feasibility of these materials in actual devices such as optical limiters, optical switches, spatial light modulators, luminiscent solar concentrators etc. have been analysed.

8.2 Work already carried out

Polymers are being used worldwide in various optical applications. We have used a polymeric matrix, viz. polyacrylamide impregnated with the laser dye rhodamine 6G to study the lasing efficiency of these doped solid matrices. The amplified spontaneous emission was used to evaluate the lasing characteristics of this matrix. The evaluation of single pass gain coefficient and the conversion efficiency were done and it seems that this has promising radiative properties with negligible aging effects which is prominent in other matrices like PMMA. The present studies show that, by properly controlling the pump intensity and concentration of the dye molecules, this system can be used as the active medium for solid state lasers. It has been found that there is an optimum pump intensity above which nonlinear phenomena like multiphoton processes causes decrease in the gain coefficient. Maximum single pass gain coefficient and conversion efficiency obtained in the present sample was about 8 cm^{-1} and 36% respectively. These are reasonably good values when compared to dye solutions in organic solvents.

In the application of polymers as host matrices, the resistance to laser damage is of special importance. Photothermal phase shift spectroscopy was used to study the damage threshold of the polymeric matrices. It has been observed that plasticizers like ethanol increases the optical strength of these polymers.

186

Phthalocyanines (Pc) are now emerging as a suitable candidates for optical, electronic and photovoltaic applications. The nonlinear properties of some members of this class of materials such as Europium phthalocyanine [Eu(Pc)$_2$] and Europium naphthalocyanine [Eu(Nc)$_2$] were investigated using Z-scan technique with Ar$^+$ laser emission at 476.5 nm and 514.5 nm as the excitation source. At these wavelengths low power optical limiting was observed in Eu(Nc)$_2$ solution. Such studies were also done on chlorophyll at 532 nm emission from an Nd:YAG laser. Transmission measurements and pulsed photoacoustics were used to ascertain the origin of the nonlinearity. It was found that the prominent nonlinear process occurring is excited state absorption rather than two photon absorption. In order to find the thermal contribution to nonlinearity in C$_{70}$ solutions, Z-scan technique with He-Ne laser output as the pump beam was performed and the thermo-optic coefficient was calculated from it.

Nonlinear optical processes are increasingly being used in a variety of photonic applications like optical limiters, light modulators for controlling the phase or amplitude of a light beam, optical switches, etc. Considerable effort has been expended to devise passive means of protecting sensitive detection systems from damage caused by high-power laser beams. A liquid-based optical limiter was constructed using Eu(Pc)$_2$ dissolved in dimethyl formamide. Good optical limiting action was found at 532 nm from a frequency doubled pulsed Nd:YAG laser.

Third-order nonlinear optical phenomenon causing an optically induced change in refractive index is fundamental to all optical switching techniques. A low power optical inverter has been demonstrated using Eu(Nc)$_2$ solution, utilizing its excited state absorption at 632.8 nm and with the 514.5 nm radiation from the Ar$^+$ laser as the pump radiation.

Spatial light modulator (SLM) is a device for transferring the information content of one beam to another beam. They are useful in a variety of applications, including optical processing, computing beam steering and control functions. Here a molecular SLM was constructed using rhodamine 6G doped polymer matrix. Sensitivity as well as contrast ratio of this system was measured. Even though the performance is not upto the desired level, by proper manipulation of molecular parameters and molecular concentration, a more efficient spatial light modulator can be realised.

The luminescent solar concentrators (LSC) offer the promise of reducing the cost of photovoltaic energy conversion by the use of high gain concentrators which do not require tracking. A qualitative study of some of the properties of an LSC, was done using Ar^+ radiation on rhodamine 6G doped polyacrylamide. The high photostability of the dye in the matrix suggest its usefulness as a LSC.

8.3 Outlay for future studies

Due to the complexity and richness of the higher-order nonlinear optical processes, investigations into the fundamental physics of electromagnetic interactions in various media reveals new physical insights and perhaps new effects of interest. Much more work is needed to understand the third-order nonlinear response, particularly at the microscopic level. Even though theoretical models predict their values, the experimentally determined values do not exhibit very good agreement. This is partially due to computational inefficiencies and also due to the inadequacy of these models. Currently, one has to rely on semiempirical methods, which are not foolproof . More fundamental investigations are necessary in the following fields in order to develop useful photonic materials.

8.3.1 Theoretical modelling:

Since nonlinear optics contributes much to the field of photonics, more work should be devoted to that area. At present, accurate calculations of third order polarizabilities can be performed only on atoms or very small molecules. For the macromolecules and polymers, their inability of predicting absolute hyperpolarisability values. Hence much more work has to be done in this direction so as to enable the prediction of structure and other functional requirements that might be useful in synthesising molecules of desirable properties .

8.3.2 Molecular engineering:

For studying the effect of electronic and structural features, it must be possible to fabricate molecules with systematically varied structures. For fabrication of devices with varied structure, a detailed understanding to manipulate properties like refractive index is a must. Hence progresses in the field of synthetic and polymeric chemistry and chemical engineering are important.

188

8.3.3 Device fabrication:

Considerable opportunities exist in the development and fabrication of devices. With the development of new materials having desirable properties, devices possessing improved performances can be realised.

In conclusion, one can say that the field of device engineering based on photonic materials and nonlinear optical phenomena is a fertile area of research which will yield important results both in the understanding of basic phenomena as well as in realizing useful all optic and hybrid gadgets.